Structure Elucidation and the Antimalarial Activity of Indole Alkaloids from *Tabernaemontana macrocarpa* Jack

2021 年 9 月

星薬科大学大学院生薬学教室

Puteri Amelia

Table of Contents

Abbreviations

$[\alpha]_D$	Specific rotation
^{1}H-NMR	Proton nuclear magnetic resonance
^{1}H-^{1}H COSY	Proton-proton correlation spectroscopy
^{13}C-NMR	Carbon-13 nuclear magnetic resonance
2D-NMR	Two-dimensional nuclear magnetic resonance
AC	Absolute configuration
aq.	Aqueous solution
CD	Circular dichroism
CE	Cotton effect
COSY	Correlated spectroscopy
CQR	Chloroquine-resistant strain
DFT	Density functional theory
ECD	Electronic circular dichroism
ESIMS	Electrospray ionization mass spectrometry
ext.	Extract
GI	Growth inhibition
HMBC	Heteronuclear multiple bond correlation
HPLC	High performance liquid chromatography
HRESIMS	High-resolution electrospray ionization mass spectrometry
HSQC	Heteronuclear single quantum coherence
IC_{50}	50% Inhibitory concentration
IR	Infrared
J	Coupling constant
MS	Mass spectrometry
m/z	Mass-to-charge ratio
NMR	Nuclear magnetic resonance
NOESY	Nuclear Overhauser effect spectroscopy
ODS	Octadesylsilane
partit.	Partition
ROESY	Rotating frame Overhauser effect spectroscopy
sat.	Saturated

TDDFT	Time dependent density functional theory
TFA	Trifluoroacetic acid
TLC	Thin layer chromatography
rt.	Room temperature
UV	Ultraviolet

Solvents

$CHCl_3$	Chloroform
DMSO	Dimethyl sulfoxide
MeOH	Methanol
EtOAc	Ethyl acetate

Chapter I Introduction

For centuries, natural products and their derivatives have played an important role as a source of medicinal agents. They are produced by living cells, either as primary metabolites, which are used by the cells for their basic life function, or biosynthesized as secondary metabolites, which do not participate directly in the growth, development, and production of an organism.[1,2]

Most of the interesting molecules that are considered as drug leads are secondary metabolites that are naturally produced by plants, microorganisms, and marine organisms. Generally, but not always, it occurs in relatively low quantities in specific cells or tissues of an organism.[3] Several types of natural product compounds are often differentially distributed among limited taxonomic groups of plants. Their unique carbon skeleton structures are the basic properties in exhibited significant biological activities.[4]

The biological activities of the plant's secondary metabolites are beneficial to the organism that produces it as they contribute to the characteristic of specific odors, tastes, and colors in plants, serving as attractants for pollinators and seed-dispersing animals.[3,5] On the other hand, these chemicals can also provide lead compounds such as glycoside, alkaloids, flavonoids, and so on for the production of medication for various diseases in humans.

According to the World Health Organization (WHO), about 65% of the population of the world depends on plant-derived medicines for their primary health care[5], and behind the efficacies of nature-derived traditional medicines are natural product compounds. The contributions of natural products to modern medicine are abundantly clear. Nowadays, modern medicines are modified versions of natural products or completely synthetic versions based upon models of the natural origin.

Some important examples of drug development from plant origin are vinblastine and vincristine which were isolated from the Madagascar periwinkle, *Catharanthus roseus* G. Don., which was used as an antitumor therapy. An isolated compound from *Galega officinalis* L., galegine, has been used as a model for the synthesis of metformin and other biguanides-type for antidiabetic drugs. Khellin, a furanochromone derivative, from *Ammi visnaga* (L.) Lam., was led the development of sodium cromoglycate (cromolyn) as a bronchodilator.[5]

Examples of other drug development from some traditional medicinal plants including podophyllotoxin which was first isolated 141 years ago by Podwyssotzki. This anticancer agent

was obtained from *Podophyllum peltatum* (Berberidaceae) and has been used as a synthetic precursor for etoposide, a chemotherapeutic drug.[6] Purple foxglove or *Digitalis purpurea* L (Plantaginaceae) is a source of phytosteroid digitoxin that has cardiotonic activity.[7]

Some alkaloid-containing plants also manifest significant pharmacological activities such as the antihypertensive alkaloid reserpine isolated from *Rauwolfia serpentina* (Apocynaceae) which have been used for the treatment of snakebite and other ailments in traditional Ayurveda medicine.[5] Ephedrine alkaloid, which is used for the synthesis of the antiasthmatic agent salbutamol and salmeterol, has been used in traditional Chinese medicinal from the plant *Ephedra sinica* (Ephedraceae). And even now, after decades of advances in drug discovery and development, natural products are still an essential part of the discovery of new drugs.[5]

Malaria is a life-threatening disease caused by *Plasmodium* parasites and transmitted by the bite of a female Anopheles mosquito. Four species of *Plasmodium* that infect humans are *P. vivax, P. ovale, P. malariae,* and *P. falciparum.* Human cases of lethal or febrile malaria have also occurred recently with *P. knowlesi,* a parasite usually found in macaques in certain forested areas of Southeast Asia, making *P. knowlesi* the fifth species known to cause malaria in humans. *P. falciparum and P. vivax* are the most common strains infecting humans, *P. falciparum* being responsible for the most severe malignant malaria, leading to coma and death.[8]

A WHO malaria report showed that malaria remains a serious parasitic disease in the world with an estimated 229 million malaria cases and 409,000 deaths in 2019 cited in the latest World Malaria Report 2020.[9] This parasitic disease widespread in all tropical and subtropical areas. Although effective plant-derived antiplasmodial compounds such as quinine and artemisinin are currently available and have been known as two important currently used antimalarial drugs, but the potential emergence of resistance to artemisinin and its derivatives[8] make finding alternative and more effective parent compounds for drug development as an antimalarial is a necessity.

Due to structural characteristics such as multiple stereocenters, flexible conformations, and presence of heteroatoms, natural products are more likely than synthetic compounds to have multiple targets and/or new targets. The antiplasmodial natural products are organized into seven classes, i.e., endoperoxides, alkaloids, terpenes, polyphenols, quinones and polyketides, macrocycles, and cyclic phosphotriesters, with subclasses where applicable. In their review published in Malaria Journal, Tajuddeen and Van Heerden[10] found that 39% of the 1524 compounds that tested against at least one strain of *Plasmodium* were described as new natural

products, and 29% of the compounds had an $IC_{50} \leq 3.0$ µM against at least one strain of *Plasmodium*. Some of these natural compounds could be developed into effective anti-malarial drugs.[10]

Alkaloid derivatives have occupied a special position as anti-malarial agents. Some indole and bisindole alkaloids isolated from plants have been reported for their antimalarial activity. Chemical investigation of the Apocynaceae family led to the isolation of alstoniaphyllines A-C together with alstonisine, a known compound that exhibits antiplasmodial activity against *P. falciparum,* with an IC_{50} value of 7.6 µM. Some of aspidosperma-alkaloids including aspidocarpine, ellipticine, and olivacine which have been isolated from the bark of *Aspidospermae desmanthum, Aspidospermae vargasii,* and *Aspidospermae olivaceum* exhibited significant *in vitro* antiplasmodial activity against the K1 strain of *P. falciparum.*[11]

Some bisindole alkaloids also showed antimalarial activity. Chemical investigations of *Flindersia amboinensis* (Rutaceae) from Papua New Guinea led to the isolations of flinderole A-C, isoborreverine, and dimethylisoborreverine. These indole alkaloids have been reported as selective antiplasmodial activity against a wide panel of drug-sensitive and drug-resistant parasites.[10]

Two new bisindole alkaloids, 12-*O*-demethyl-vobtusine-5-lactam and isovobtusine-*N*-oxide isolated from the leaves of *Voacanga grandifolia* (Apocynaceae) were exhibited potent antimalarial activity against *P. falciparum* 3D7 with the IC_{50} value of 5.1 and 3.3 µM, respectively.[12] Also, Tang *et al.*, reported the isolation of two new eburnane and quebrachamine-type skeletons from the bark of *Leuconotis eugeniifolia*, leucophyllinines A and B, which exhibited antiplasmodial activities against *Plasmodium falciparum* 3D7 with the IC_{50} value of 32.7 and 2.6 µM, respectively.[13]

Indonesia is known as a mega-diversity country. The richness of Indonesian flora provides opportunities for the discovery of many novel compounds. Plants of the genus *Tabernaemontana* (Apocynaceae) are known as one of a storehouse of indole and bisindole alkaloids that possess antimalarial agents.[14,15] In order to search for more bioactive indole alkaloids with antimalarial activity from this family of plants, the chemical investigation on the bark of *Tabernaemontana macrocarpa* Jack was carried out.

Chapter II The Alkaloids

Alkaloids are a diverse group of natural products derived from secondary metabolism that contain a nitrogen atom or atoms (amino or amide in some cases) as part of the heterocyclic system. These nitrogen atoms give these compounds their alkalinity, and they can react with acids to form salts.

Generally, alkaloids are produced by many plants' species, mainly by flowering plants, but also can be found in microorganisms (bacteria, fungi), marine animals (sponges, slugs, worms, bryozoa), arthropods, amphibians (toads, frogs, salamanders), and also in a few birds, and mammals. Alkaloid-containing plants have been traditionally used since ancient times in folk medicines for the treatment of sedatives, antitussives, and a variety of ailments.[16]

The study of alkaloids began when morphine was successfully isolated from the opium plant (*Papaver somniferum*) by a young German pharmacist, Friedrich Wilhelm Adam Sertürner. Following the initial discoveries, there were gradual investigations that led to the number of known and pharmacologically used alkaloids either as medicines or poisons including xanthine, strychnine, atropine, quinine, and caffeine in 1817-1820.[17]

Most alkaloids are water-soluble under acid conditions. Free bases alkaloids are usually soluble in an organic solvent such as chloroform and ether. Alkaloids are often found as optical active substances, colorless, crystalline, or liquid at room temperature, and quite often they have a bitter taste that can form salts when being united to acids. In the plants, they can hide in a free state, like salts or like *N*-oxides.[16]

Some alkaloids are sufficiently toxic to animals to cause death if eaten. Several alkaloids such as nicotine and anabasine are used as insecticides. In humans, many alkaloids exhibit a wide range of pharmacological activities and have been used as major therapeutic agents as an antibacterial, antimitotic, anti-inflammatory, analgesic, local anesthetic, hypnotic, psychotropic, and antitumor activity, and many others.[18]

The alkaloidal drug, quinine, is the first antimalarial drug isolated from Cinchona bark. This drug is still quite useful in the treatment of multidrug-resistant malaria. Other plant-derived alkaloidal drugs have also been used as medicines such as atropine, an anticholinergic alkaloid from *Atropa belladonna* (Solanaceae); morphine an opioid analgesic from *Papaver somniferum* (Papaveraceae); theophylline from *Camellia sinensis* (Theaceae) which exhibits relaxes smooth muscles; cocaine from the leaves of *Erythroxylon coca* (Erythroxylaceae) which is a local

anesthetic; strychnine, a potent cerebellum stimulator from *Strychnos nux-vomica* (Loganiaceae),[18,19] and many others.

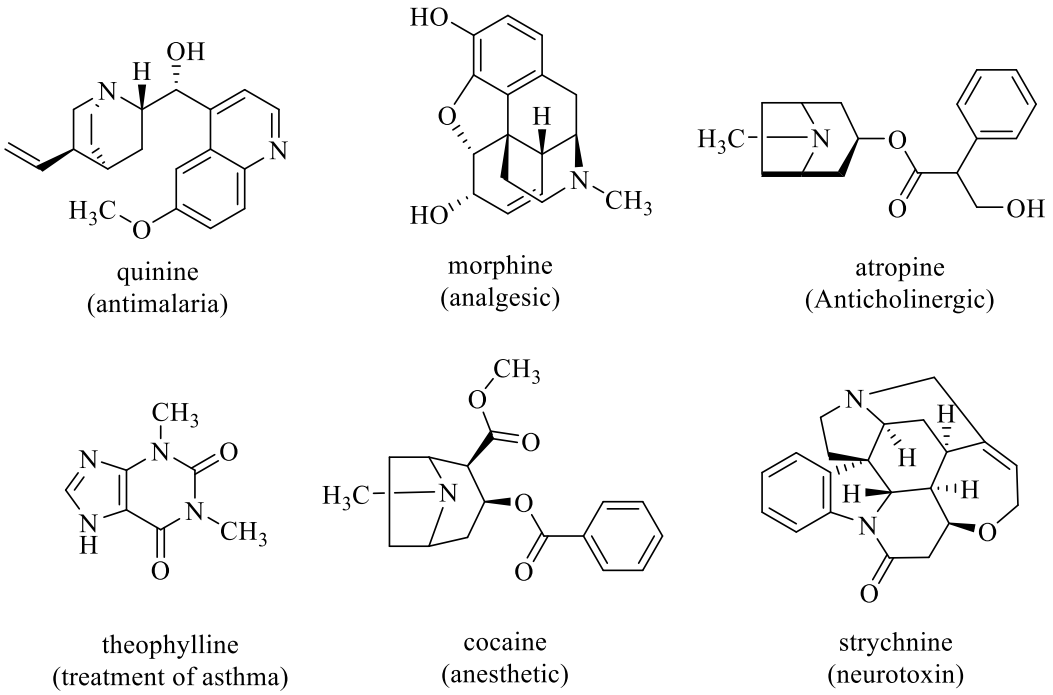

Figure II–1. Some alkaloids and their pharmacological activities[18,19]

II.1 Indole Alkaloids

Indole alkaloids represent the biggest single class of all alkaloids by more than 4000 known compounds have been reported and mostly produced by plants of the families Apocynaceae, Rubiaceae, Annonaceae, and Loganiaceae.[20]

Indole alkaloids have a bicyclic structure consisting of a benzene ring fused to a five-membered pyrrole ring and many of these class alkaloids include isoprene groups and are thus called terpene indole. The major groups under investigation are the ones with monoterpene (C_{10}) or *nor*-monoterpene (C_9) moieties joined to the tryptamine. The building blocks of their chemical structures are also recognized to have apparent uniformity and it may provide novel promising bioactive natural products.[21]

Generally, there are three hypothetical building blocks of indole alkaloids, Types I, II, and III based on their sub-architecture. Since the type I alkaloids are more abundant, they may be the origin of types II and III. LeMen and Tylor had proposed to extend the agreement to type

alkaloids and by these hypothetical bases that the MIAs are categorized into three main groups based on their biological pathway: corynanthe, aspidosperma, and iboga (Fig. II-2).[22]

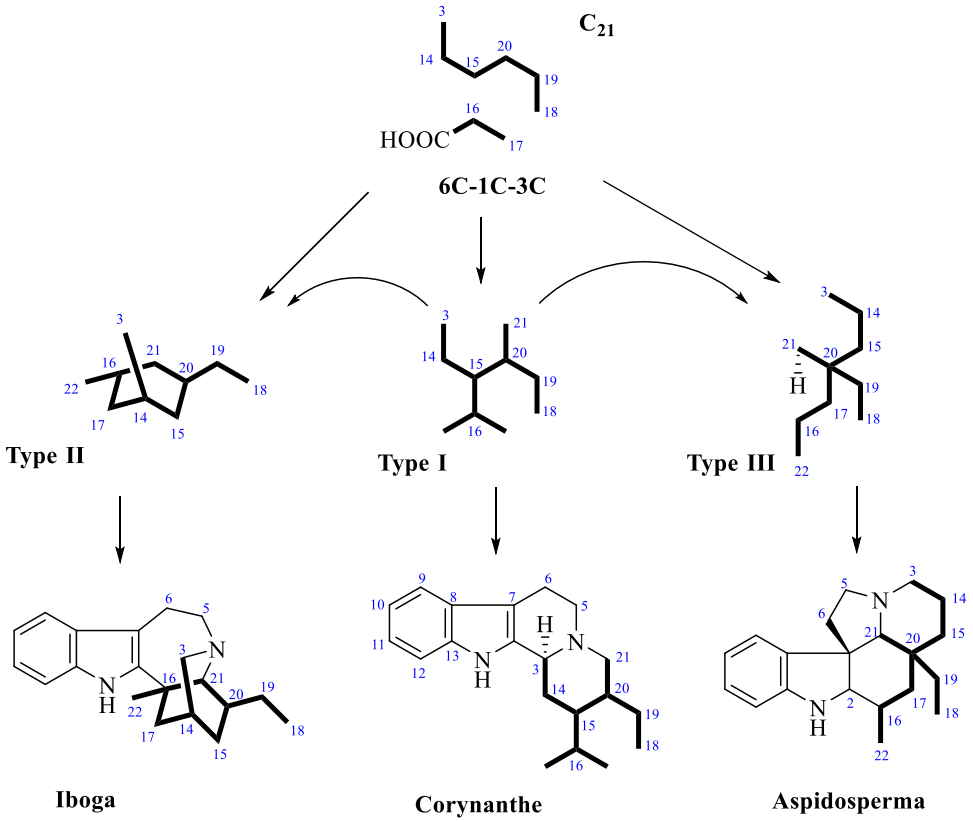

Figure II–2. Biogenetic numbering rule as adopted from LeMen and Tylor[22]

Furthermore, following Hesse, eight main types of indole alkaloids have been defined as vincosan, vallesiachotaman, corynanthean, strychnan, aspidospermatan (class I skeleton with an intact secologanin); plumeran, eburnan (class II skeleton, corresponding to a rearranged secologanin), and ibogan (class III skeleton, corresponding to a further rearranged monoterpene). A ninth type, tacaman (with class III skeleton) was added by Verpoorte and Van Beek to account for the isolation of a few tacamines.[23,24] The nine main skeletal types are given in Fig. II-3 – Fig. II-4.

Alkaloid Type	Skeleton	Example
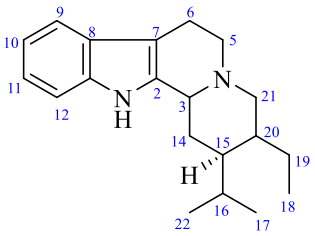 Corynanthean (C)-type	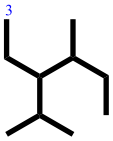 Class I	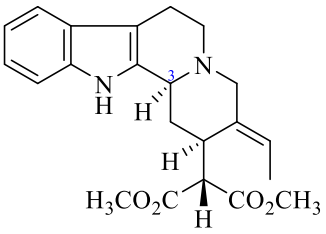 isositsirikine
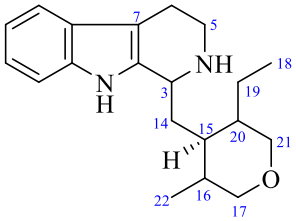 Vincosan (D)-type	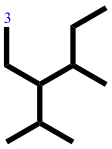 Class I	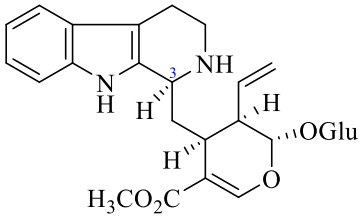 strictosidine
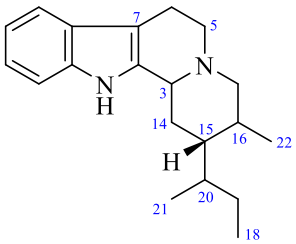 Vallesiachotaman (V)-type	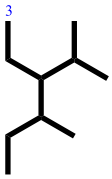 Class I	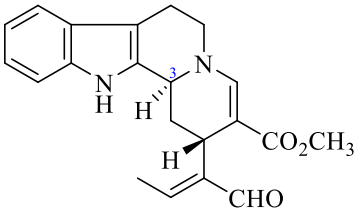 vallesiachotamine
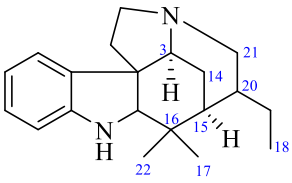 Strychnan (S)-type	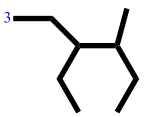 Class I	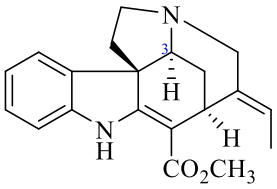 akuammicine
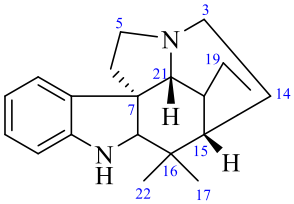 Aspidospermatan (A)-type	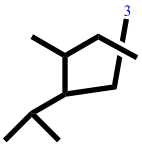 Class I	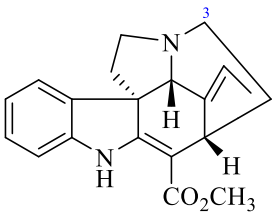 condylocarpine

Figure II–3. Classification of indole alkaloids[23,24]

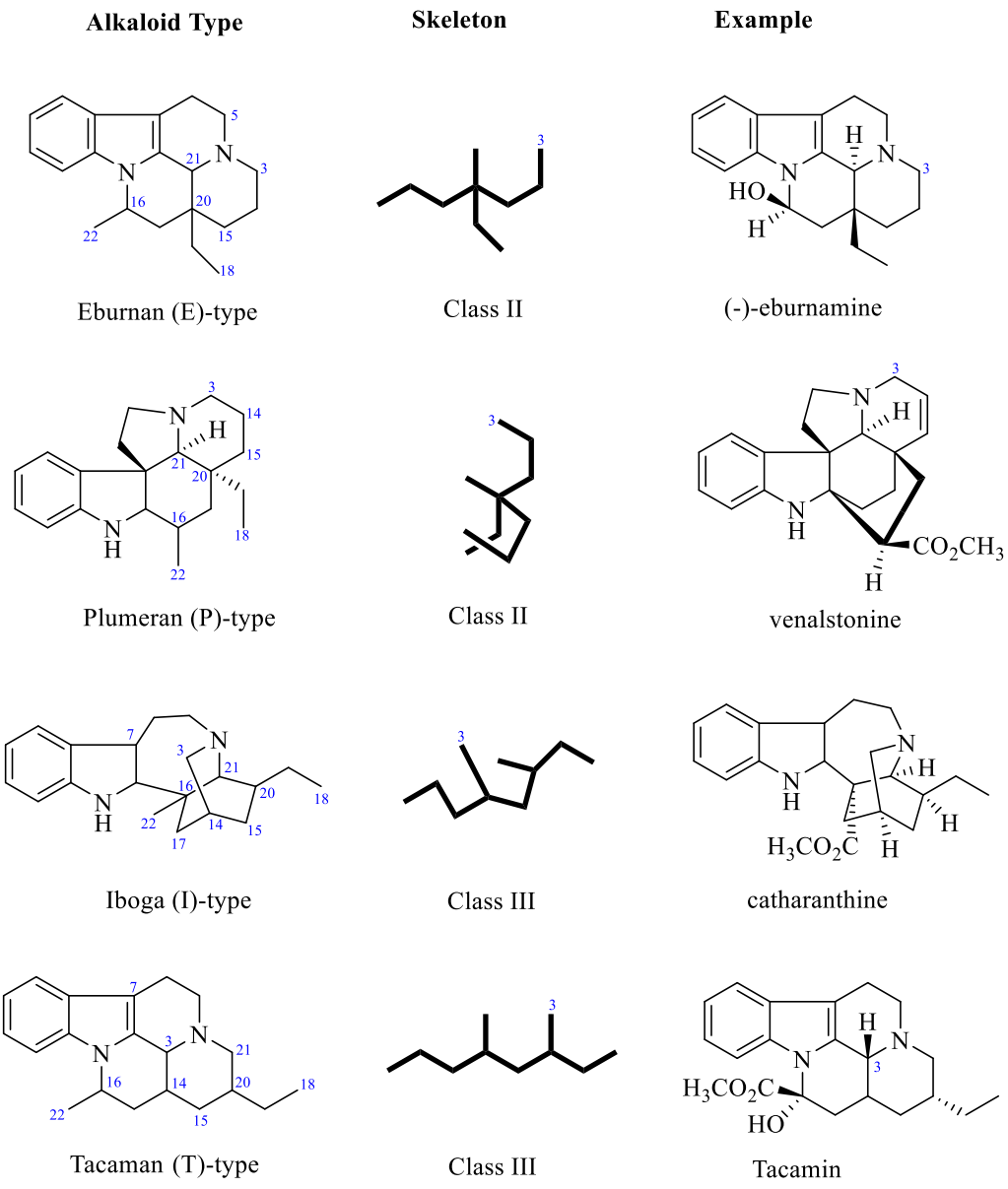

Figure II–4. Classification of indole alkaloids (cont')[23,24]

II.2 Bioactivity of Indole alkaloids

Indole containing compounds leading to the development of novel bioactive drugs[25] such as antidepressant alkaloids, mytraginine, which has been isolated from *Mytragina speciosa* (Rubiaceae)[26]; vinblastine and vincristine, anticancer alkaloids from the periwinkle plant *Catharanthus roseus* (Apocynaceae); vallesiachotamine, an anticancer alkaloid isolated from the fruits of *Anthocephalus cadamba* (Rubiaceae)[27]; reserpine, the antihypertensive alkaloid from the plant *Rauvolfia serpentina* (Apocynaceae); and the cardio-arrhythmic alkaloid, ajmalicine, from *Catharanthus sp* (Apocynaceae)[28,21].

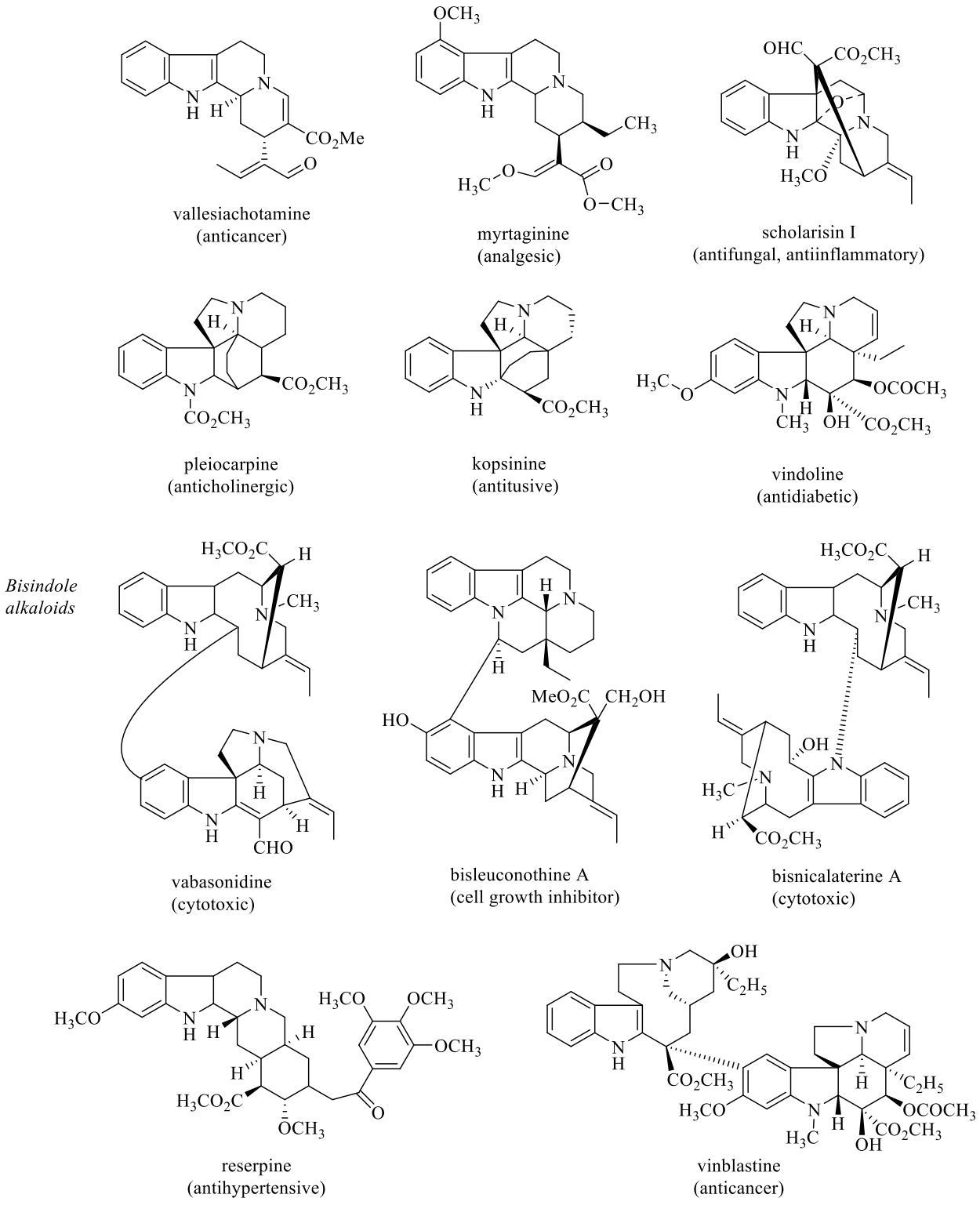

Figure II-5. Bioactive indole alkaloids[12,20,21,29]

Some indole alkaloids also have been investigated and shown to possess potent antiplasmodial activity against *P. falciparum*, many of which are bisindole alkaloids. [10,12,13,30,31] Indole-based antiplasmodial compounds are endowed with multiple modes of action, of which

inhibition of hemozoin formation is the major mechanism of action reported for compounds such as cryptolepine, flinderoles, and isosungucine. Indole-based compounds exert their potent activity against chloroquine-resistant *Plasmodium* strains by inhibiting hemozoin formation in a mode of action different from that of chloroquine or through a novel mechanism of action.[32]

An aspidosperma alkaloid, ulein, isolated from *Aspidosperma parvifolium* was reported to have antimalarial properties via inhibiting *P. falciparum* with the IC_{50} value of 0.98-0.20 μM. Aspidoscarpine, an indole alkaloid isolated from *Ochrosia moorei*, was assayed for *in vitro* antimalarial activity against multidrug-resistant *P. falciparum* K1 strain with the IC_{50} value of 0.007 μM. Furthermore, indole alkaloid ellipticine from the bark of *Aspidosperma vargasii* displayed antiplasmodial properties via inhibiting CQ-resistant strain of *P. falciparum* FcM29-Cameroon with IC_{50} values of 0.28 μg/mL.[33]

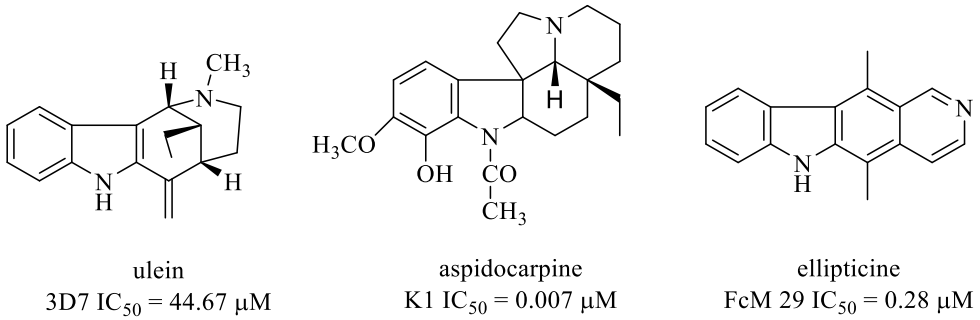

ulein
3D7 IC_{50} = 44.67 μM

aspidocarpine
K1 IC_{50} = 0.007 μM

ellipticine
FcM 29 IC_{50} = 0.28 μM

Figure II–6. Some antimalarial indole alkaloids

Many bisindole alkaloids have also shown potent antimalarial activity including voacamine, a vobasine-iboga type bisindole alkaloid isolated from the plant *Voacanga africana* which also can be found in *Tabernaemontana spp* and *Pescheria fuchsiae*. In many African countries, voacamine has been approved for the treatment of malaria (IC_{50} 411 nM).[34] The *in vivo* antiplasmodial activity of voacamine was shown to have 25.4% and 43.4% inhibition of parasitaemia with 2.5 and 10 mg/kg, respectively.[34]

Bioguided fractionation of some bisindole alkaloids from *Strychnos* species showed some promising antimalarial activity including isosungucine (IC_{50} = 168 nM, CQR) and 18-hydroxyisosungucine (IC_{50} = 85 nM, CQR). The antimalarial action of these compounds may explain the traditional use of *S. icaja* by the Pygmies from Cameroon to treat malaria fever. Some bisindole alkaloids such as flinderole A-C, isoborreverine, and dimethylisoborreverine isolated from the bark of Flindersia plant were also reported to exhibit selective antiplasmodial activity against a wide panel of drug-sensitive and -resistant parasites.[10]

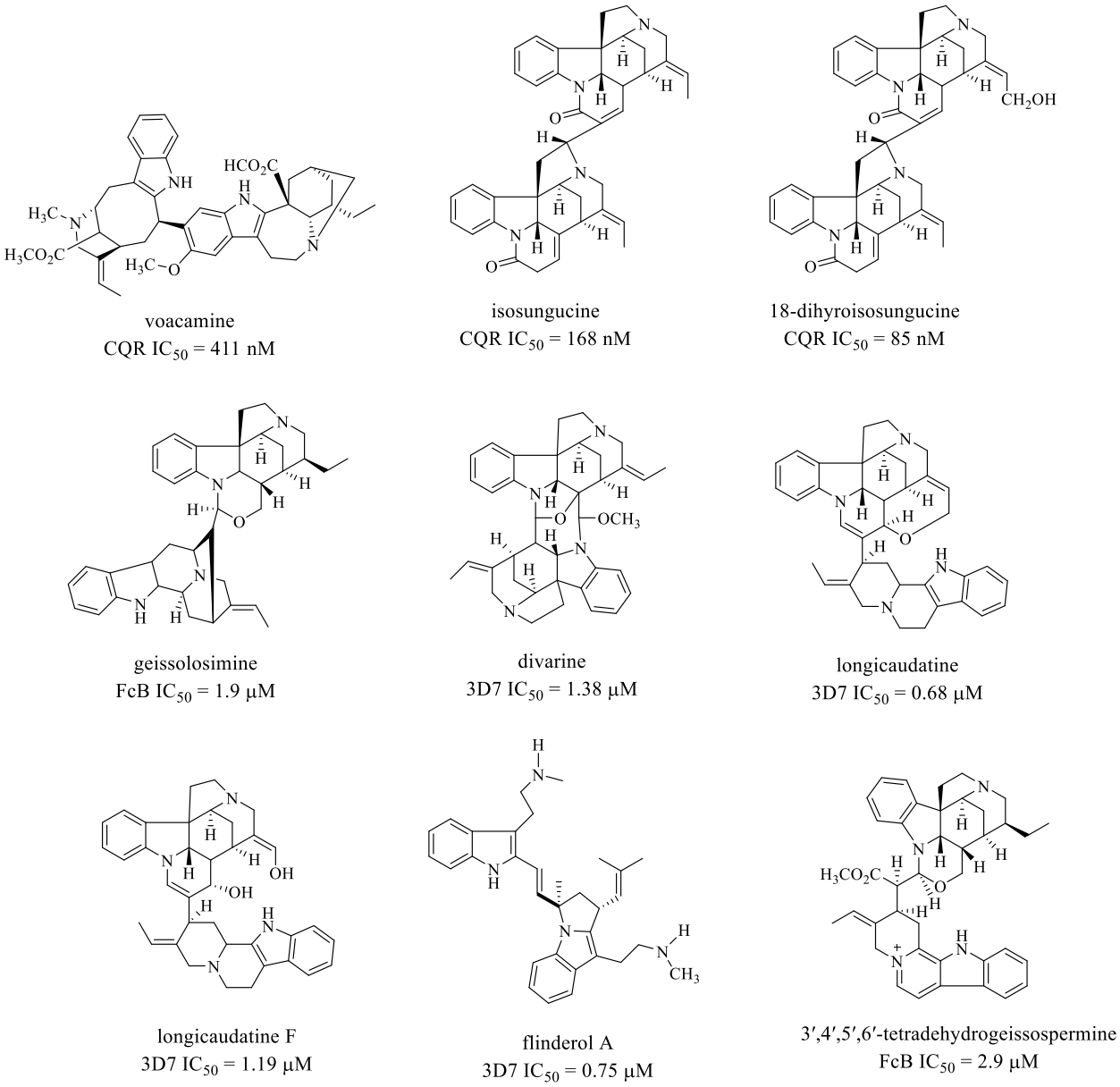

Figure II–7. Some antimalarial bisindole alkaloids

II. 3 Biosynthesis of Indole Alkaloids

The biosynthesis of monoterpene indole alkaloids (MIAs) was derived from a Mannich condensation of tryptamine as the indole nucleus and a C-9 or C-10 monoterpene moiety from secologanin leads to strictosidine, which was the precursor for a large number of terpenoid indole alkaloids, such as strychnine, vinblastine, and some related quinoline alkaloids.[35] Wenkert suggested the transformation of strictosidine to ajmalicine, geissoschizine, preakuammicine, and eventually to stemmadenine by the isomerization and collapse *via* enamine provides didehydrosecodine, from which the aspidosperma, iboga, and vinca/eburnea alkaloids are successively derived as described in Fig. II-8.[36]

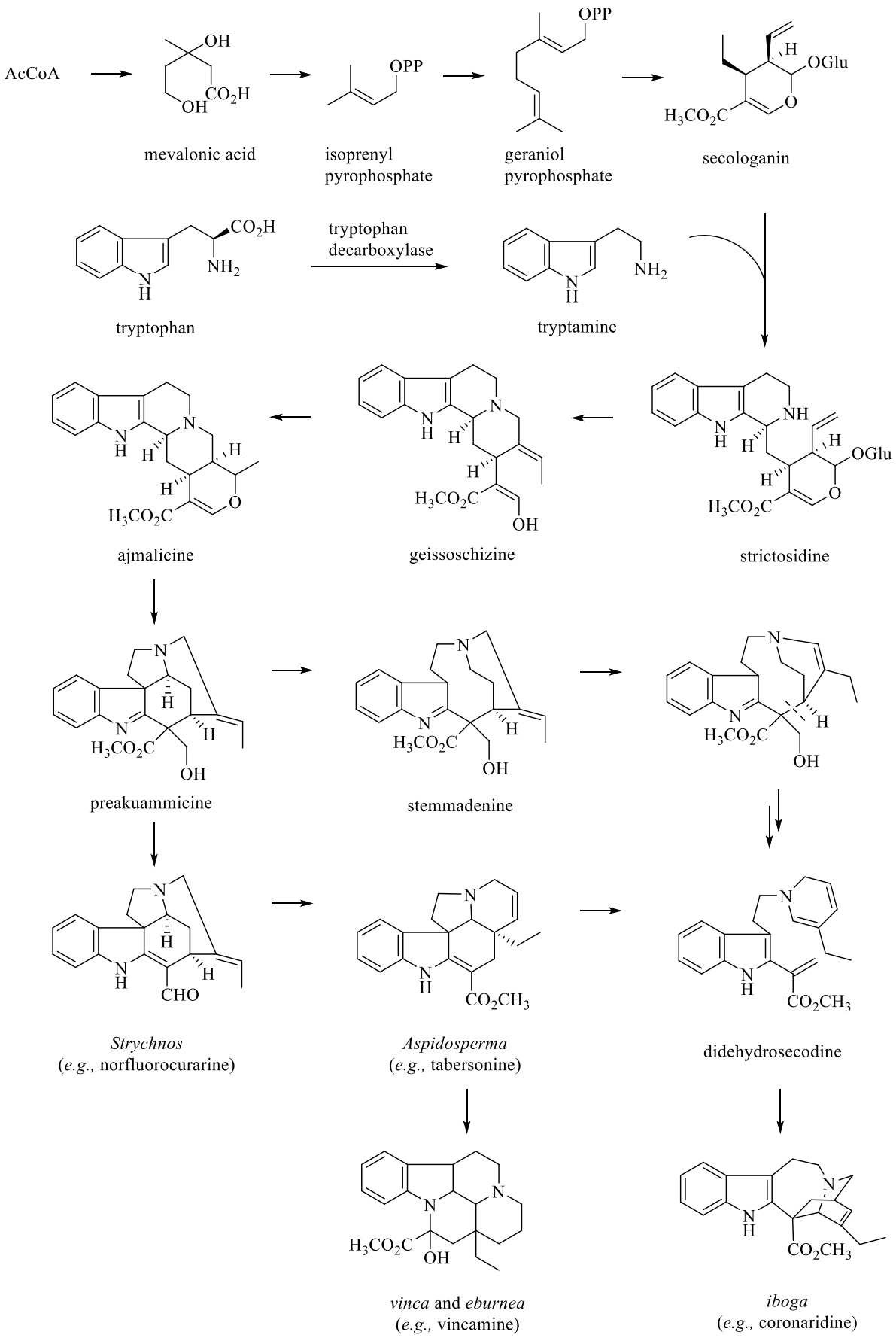

Figure II–8. Biosynthesis of indole alkaloids[24,36]

II. 4 Apocynaceae Family

Apocynaceae is a family of plants comprising of woody climbers, vines, perennial herbs, trees, or shrubs, and more rarely annuals distributed mainly in the tropical and subtropical area. The plants are typically laticiferous with the latex usually milky, sometimes clear, and rarely yellow or red. Many species of the family are used for both non-medicinal (ornamental, poison, timber, fiber, perfume, dye, etc.) and medicinal purposes.[33]

Traditionally, many species of the Apocynaceae in the Asia- Pacific region are used in the treatment of skin diseases, abdominal diseases, fever, malaria, dysmenorrheal, epilepsy, and asthma[37]. A variety of alkaloids have been isolated from this family and have been reported to possess anticancer, anti-hypertensive, and antimalarial properties, such as vinblastine (anticancer), vincristine (anticancer), reserpine (anti-hypertensive), and voacamine (antimalaria). Dey *et al.*,[33] have been reviewed some Apocynaceaeous alkaloids and their pharmacological activities, including anticancer from indole alkaloid catharanthine, ajmalicine, tabersonine, and lochnericine that have been isolated from *C. roseus* (L.) G. Don leaves.

Some studies from this family of plants also reported its antimalarial activity. Chemical investigation of *Aspidosperma ulei* Markgr. (Apocynaceae) led to the isolation of 20-*epi*-dasycarpidone which exhibited potent antimalarial activity against multidrug-resistant K1 strain of *P. falciparum* with the IC_{50} value of 16.7 μM.[11] The monoterpenoid indole alkaloid uleine was reported as the major antiplasmodial alkaloid from the trunk bark of *Aspidosperma parvifolium* (Apocynaceae) and was more active against the W2 than the 3D7 strain, with low cytotoxicity against the Hep G2A16 and Vero cell lines.[10]

Some of the bisindole alkaloids which consist of two monomeric indole alkaloids also exhibited diverse bioactivity since they have a diverse molecular skeleton. Two bisindole alkaloids with a vobasinyl-iboga skeleton, tabernaelegantines B and D, were isolated from the stem bark of *Muntafara sessilifolia* (Apocynaceae) and inhibited the FcB1 plasmodial strain but these compounds were also cytotoxic against L6 and MRC-5 cells.[10] Also, Tachinda *et al.* reported the isolation of a new bisindole alkaloid, strychnobaillonine, which has potent activity against the chloroquine-sensitive 3D7 strain of *P. falciparum* with an IC_{50} value of 1.1 μM.[30]

II.4.1 Classification of Apocynaceae

Apocynaceae can be divided into Plumerioideae subfamily, which is further divided into a few tribes (Fig. II-9). Each tribe comprises several genera. The genus *Tabernaemonatana* is classified as a member of the tribe Tabernaemontaneae.[23]

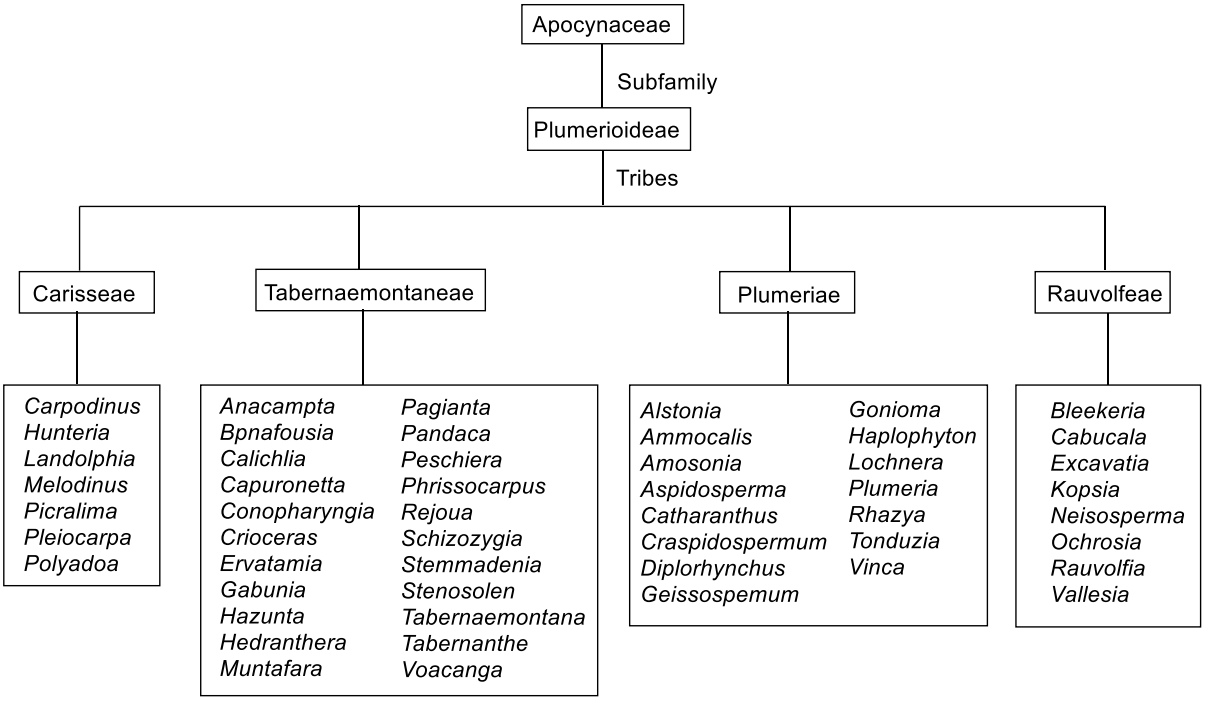

Figure II-9. Classification of Apocynaceae[23]

II.4.2 Genus *Tarbenaemontana*

The name of the genus *Tabernaemontana* is referred to Tabermaemontanus, the birthplace of J. Th. Müller, a German physician, and botanist, who was born in Bergzabern and died in Heidelberg, Pfalz in 1590.[38,39] *Tabernaemontana* is a genus belonging to the Apocynaceae family (also known as Dogbane family) and composing about 110 species which are distributed in tropical and partial subtropical regions of the world. Forty-four species of this genus are grown in America, whereas 30 species were grown in Brazil, and the rest were distributed in different places around the world.[21] Many plants of the *Tabernaemontana* species are used in traditional medicine and for other purposes to treat sore throats, high blood pressure, and abdominal pain.[21,39]

Plants of *Tabernaemontana* genus are a prolific source of the monoterpene indole alkaloids. These alkaloids are a diverse class of natural products, comprising over 2000 members and possessing a range of chemical structures such as corynanthean alkaloids (*e.g.*, tabernaemontanine), bisindole alkaloids (*e.g.*, voacamine), iboga alkaloids (*e.g.*, coronaridine), plumeran alkaloids (*e.g.*, ervatanine), and aspidospermatan alkaloids (*e.g.*, conolidine).[38,39]

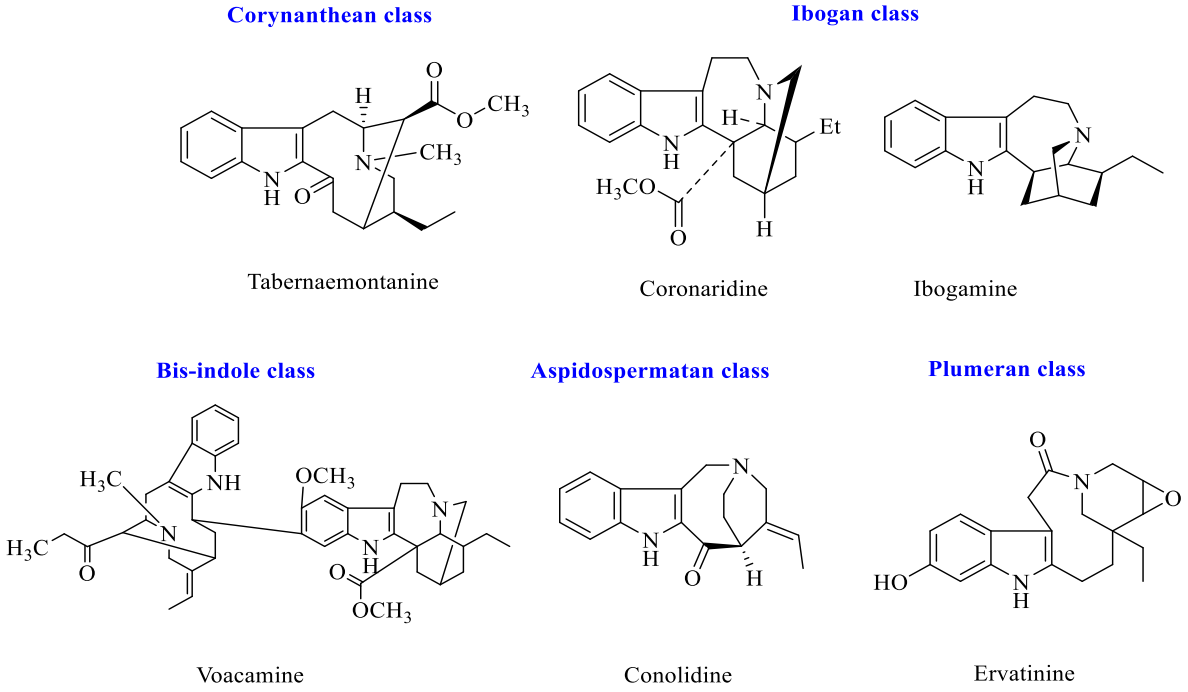

Figure II–10. Some alkaloids from *Tabernaemontana*

More than three hundred indole and bisindole alkaloids have been isolated from *Tabernaemontana* species with various skeletal types including iboga-type alkaloids, aspidospermatan-type alkaloids, and corynanthean or vobasinyl-type alkaloids.[23] Most of bisindoles are of the vobasinyl-iboga, vobasinyl-aspidosperma, or iboga-plumeran types. An example of vobasine-vobasine and vobasine-strychnan bisindoles namely vobasonidine and vobatricine has been also reported by Kam in 2002.[40]

A journal review by Mohammed *et al.* reported some indole alkaloids *from T. corymbosa*, a Malaysian plant, including tabernamine, 19′(*S*)-hydroxytabernamine, 19′(*R*)-hydroxytabernamine, and 16′-decarbomethoxyvoacamine which exhibited growth inhibitory effects against drug-sensitive KB/S with an IC_{50} value < 4.7 μM[21], and these compounds were shown to exhibit a wide array of biological activities including anticancer, antimalarial, and anti-arhythmic.[24,39]

In 2009, Zaima *et al.* reported two new bisindole alkaloids, biscarpamontamine A (aspidosperma-iboga-type skeleton), and biscarpamontamine B (aspidosperma-aspidosperma-type skeleton) which have been isolated from the stems of *T. sphaerocarpa*. These dimeric alkaloids showed potent cytotoxicity against various human cancer cell lines, including human blood premyelocytic Leukemia (HL60), multiple myeloma (RPMI8226), non-small cell lung

carcinoma (NCI-H226), human colon cancer (HCT116), and human breast adenocarcinoma (MCF-7) cells with the IC_{50} value in the range of 0.5–1.9 μM.[41]

II.4.3 *Tabernaemontana macrocarpa* Jack

T. macrocarpa Jack is distributed in Indonesia, Malaysia, Brunei, and the Philippines. In eastern Malaysia, Sabah, the fruit of this plant is used to relieve the pain of toothache. Whereas in Indonesia, its abundant sticky latex serves as birdlime, while the fine, whitish, very softwood is used for making kris scabbards.[38] Traditionally, the exudate of this plant has been used in Borneo, Indonesia, for the treatment of dental disease, herpes, and eczema.[42,43]

a. b. c. d.

Fig. II-11. Plant of *T. macrocarpa* Jack

a. Trees c. Flowers

b. Leaves d. Fruit

Preliminary studies of the *n*-hexane, ethyl acetate, ethanol, and water extracts from the stem of *T. macrocarpa* Jack were reported to have antioxidant and anticancer activities.[42] Some alkaloids compounds have been isolated from its roots, including 3-oxo-coronaridine, 19-*R*-heyneanine, coronaridine, pseudoindoxyl, and voacangine pseudoindoxyl.[43] Also, Van Beek has been reported indole alkaloids voaphylline, coronaridine, voacangine, and voacangine hydroxyindolenine from the seeds of this plant.[38]

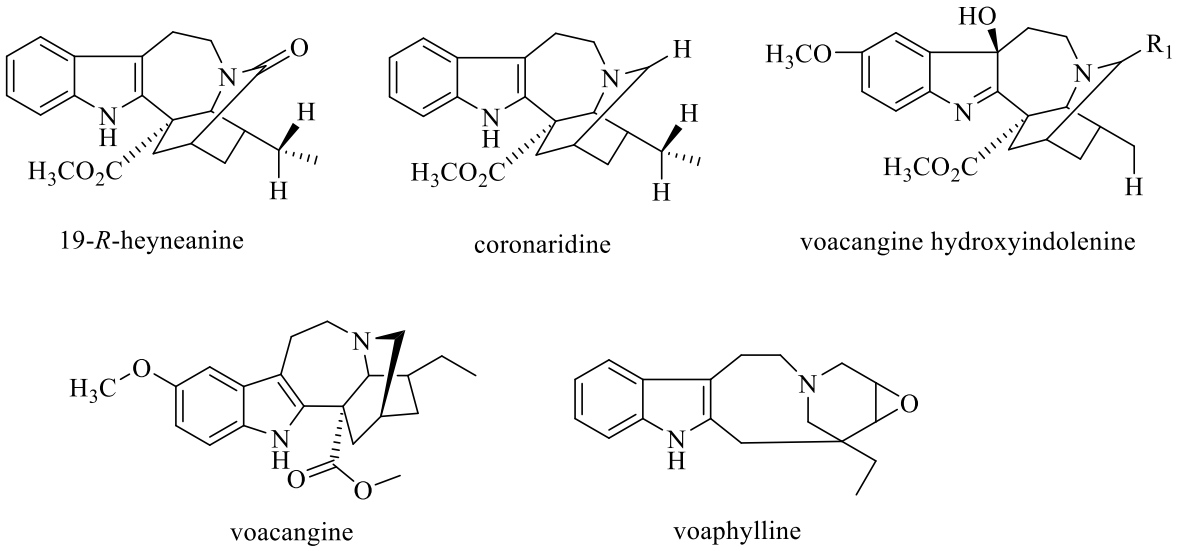

Figure II–12. Some alkaloids from *T. macrocarpa Jack*[38]

Chapter III Antimalarial Bioassay-guided Fractionation of *T. macrocarpa* Jack Metabolites

III.1 New Monomeric Indole Alkaloids

III.1.1 Separation and Purification

The barks of *T. macrocarpa* Jack (550 g) were extracted with MeOH, and part of the extract (8 g) was partitioned between EtOAc and 3% tartaric acid. The aqueous layer was adjusted at pH 9 with saturated Na_2CO_3 (aq). and extracted with $CHCl_3$ to give $CHCl_3$ fraction (1.5g) and continued by a partition with BuOH to give BuOH fraction (3.7 g).

The collected fractions were screened for antimalarial activity *in vitro* against *P. falciparum* laboratorium strain 3D7 by flow cytometric analysis using an automated hematology analyzer, XN-30. The $CHCl_3$ and BuOH fractions were selected for further separation by column chromatography since it considered to be highly active with growth inhibition (GI) of 128.9% and 107.8%, respectively.

The $CHCl_3$ fraction was chosen to be further purified by being subjected to column chromatography (CC) over silica gel and eluted with *n-hexane*/ethyl acetate (49:1 to 1:1, v/v) continued by $CHCl_3$/methanol (49:1 to 100%) to give 16 fractions. Each fraction (1‑16) obtained was tested *in vitro* against CQ-sensitive strain (3D7) of *P. falciparum*, and those fractions showing 50% parasite inhibition in 48 h were selected for further column chromatographic separation. Among the fractions tested, fractions 9 and 11 were selected to further purification due to their GI of 99.7% and 110%, respectively. Fraction 9 was the first selected for separation by Sephadex LH-20 with $CHCl_3$/MeOH (1:1, v/v) to afford 16-demethoxycarbonylvoacamine (**4**, 3.4 mg, 0.0425%), isositsirikine (**5**, 0.6 mg, 0.0075%), affinisine (**6**, 3.1 mg, 0.0388%), and affinine (**7**, 13.0 mg, 0.1625%). Fraction 11 was purified by amino silica CC and eluted with $CHCl_3$/MeOH (1:1, v/v) yielded 12-methoxy-4-methylvoachalotine (**3**, 151.0 mg, 1.8875%).

The butanol fraction was continued to purified by subjected to HP-20 Diaion CC with $CHCl_3$/MeOH (20-100%, v/v) to afford 15 fractions. Fraction 15 was selected for further purified based on its antimalarial activity against *P. falciparum* laboratory strain 3D7 (GI 122.2%) using Sephadex LH-20 with $CHCl_3$/MeOH (1:1, v/v) and HPLC (Cholester 10 x 250 mm, 50% MeOH at 2.4 mL/min, UV detection at 254 nm) to yield **1** (6.3 mg, 0.0788%, t_R 11.3 min), and **2** (3.1 mg, 0.0388%, t_R 23.2 min).

The two new compounds **1** and **2**, together with five known compounds; 12-methoxy-4-methylvoachalotine (**3**), 16-demethoxycarbonylvoacamine (**4**), isositsirikine (**5**), affinisine (**6**), and affinine (**7**) were tested for the antimalarial activity against *P. falciparum* 3D7 strain. The result showed only the dimeric alkaloid, 16-demethoxycarbonylvoacamine (**4**), possessed moderate *in vitro* antimalarial activity (the half-maximal (50%) inhibitory concentration (IC_{50}) = 28.8 μM) while the others did not show activity even at 50 μM.

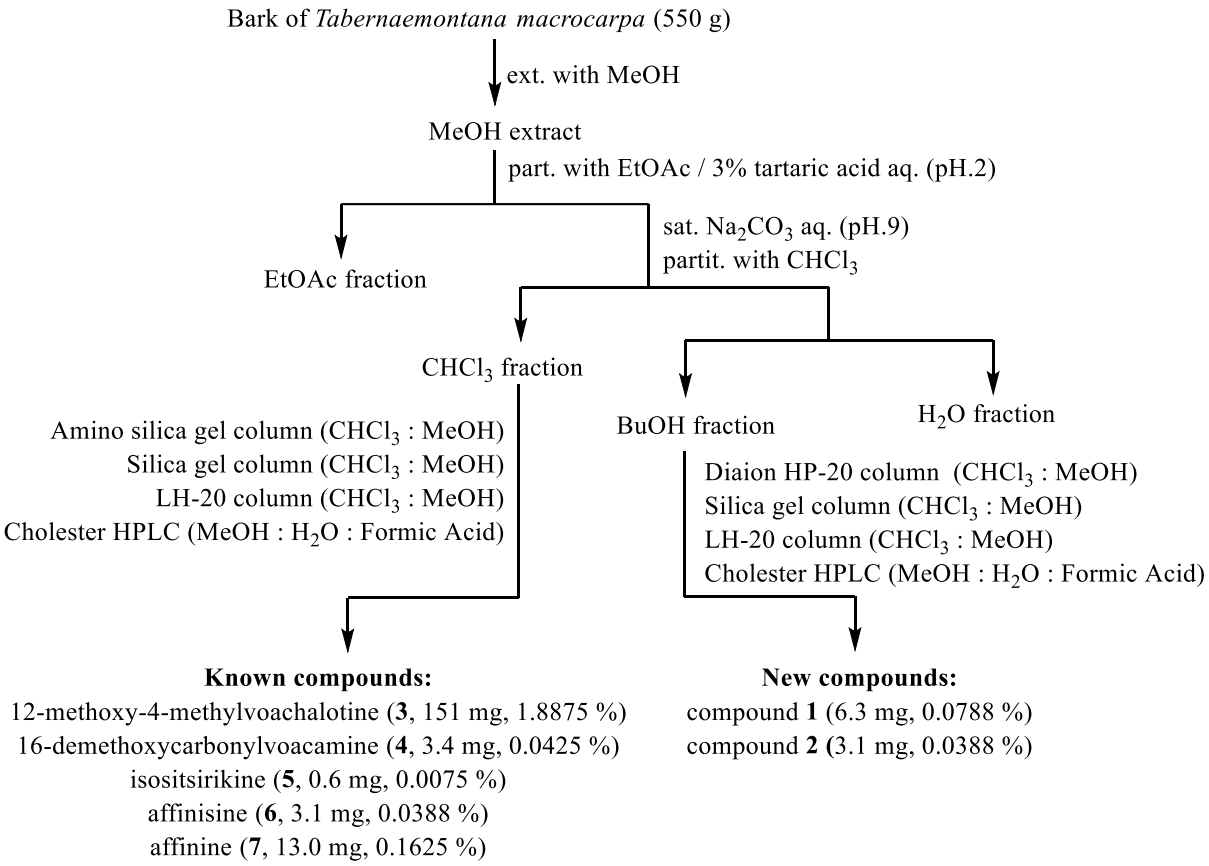

Figure III–1. Isolation scheme of **1**–**7** from *T. macrocarpa* Bark

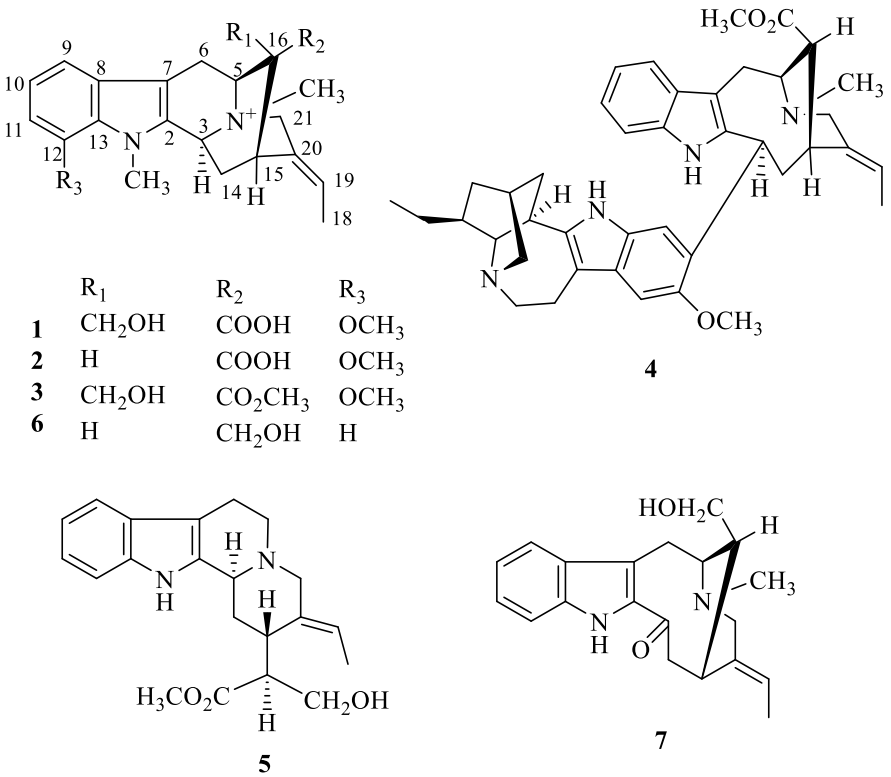

Figure III–2. Structure of **1-7**

III.1.2 Structure Elucidation

III.1.2.1 Compound 1

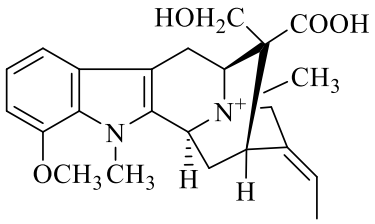

1

Compound **1** was obtained as an optically active brownish amorphous solid, $[\alpha]^{25}_{D}$ -45 (*c* 1.0, MeOH). The IR spectrum showed two important absorptions at 3382 and 1678 cm^{-1} for hydroxyl and carbonyl groups respectively, while the UV absorption bands at λ_{max} 225 and 271 nm indicated an indole chromophore. The ESIMS (pos.) of **1** showed a molecular ion peak at *m/z* 397 and the molecular formula of **1** was established as $C_{23}H_{29}N_2O_4$ from HRESIMS.

Analysis of the ^{1}H NMR data (Table 1) suggested the presence of one substituted indole moiety from three aromatic resonances at δ_H 6.77 (1H, d, J = 8.0 Hz), 7.02 (1H, t, J = 8.0 Hz), and 7.11 (1H, d, J = 8.0 Hz), three *N*-methyl or methoxy (δ_H 3.97, 3.19 and, 3.94), and one olefinic proton (δ_H 5.50, 1H, q, J = 6.0 Hz). The ^{13}C NMR data revealed 23 resonances, comprising seven sp^2 quarternary carbons, four sp^2 methines, four methyls, four sp^3 methylenes, three sp^3 methines, and one sp^3 quarternary carbon.

The structure of **1** was deduced from extensive analysis of the two-dimensional NMR data, including the ^{1}H-^{1}H COSY, HSQC, and HMBC. In particular, the HMBC cross-peaks of H_2-17 (δ_H 3.72 and δ_H 3.58) to C-22 (Fig. III-3) provides additional support for the presence of a carboxyl moiety at C-22. Furthermore, the HMBC correlations of methyl signals at δ_H 3.94 to C-12, δ_H 3.97 to C-2 and C-13, and δ_H 3.19 to C-3, C-5, and C-21, revealed the presence of a methoxy group at C-12 and two *N*-methyl groups. Moreover, an ethylidene side-chain at C-20 was confirmed by HMBC cross-peaks from H_3-18 (δ_H 1.72) to C-20, H-19 (δ_H 5.50) to C-15 and C-21 (Fig. III-3).

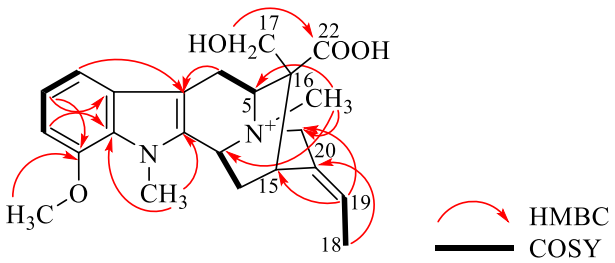

Figure III-3. Selected 2D NMR correlations of **1**.

The relative configuration of **1** was elucidated by NOESY correlation to be similar to that of 12-methoxy-4-methylvoachalotine (MMV) (**3**).[44] First, H-3 and H-5/*N*4-CH_3 were assigned to be *α*-axially oriented from the NOESY correlations of H-3 and H-5/*N*4-CH_3 while CH_2-17 were deduced to possess β-orientation from the NOESY correlations of H-17a/H-14a. Furthermore, the *α* configuration of H-15 and the *E* configuration of the ethylidene group was confirmed by the NOE correlation of H-15 to H_3-18 and H-14b (Fig. III-4).

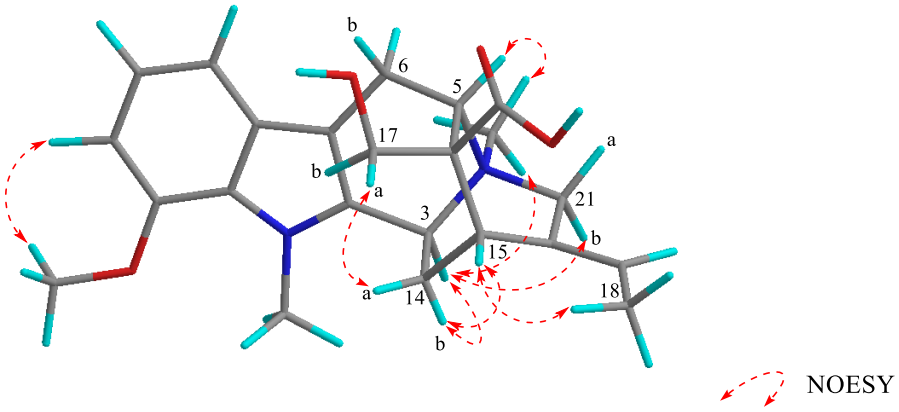

Figure III-4. Selected NOESY correlations of **1**.

Further analysis of ^{1}H and ^{13}C NMR showed that **1** is very similar to MMV, except for the signal of the methyl ester at C-22 in MMV which was not observed in **1**. Thus, **1** was assumed to be a 22-demethyl derivative of MMV. Finally, the stereochemistry of **1** was confirmed by a methyl esterification reaction of **1** using TMS-diazomethane to form a product with identical spectroscopic data to that of MMV.

Methyl esterification reaction. The preparation of methyl esters from carboxylic acids can be achieved with trimethylsilyldiazomethane ($TMSCHN_2$) in methanolic benzene. Compound **1** (0.1 mg) was dissolved in MeOH (100 µl) and $TMSCHN_2$ (50 µl) added. The reaction was easily monitored by the disappearance of the yellow color of $TMSCHN_2$ to form a product with identical spectroscopic data to that of MMV.

III.1.2.2 Compound 2

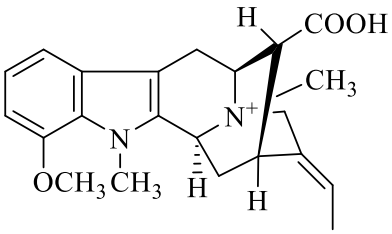

2

Compound **2** was isolated as an optically active brownish amorphous solid, $[\alpha]^{25}_{D}$ -5 (*c* 1.0, MeOH). The UV spectrum showed two absorption bands at λ_{max} 225 and 280 nm as characteristic of an indole chromophore. The IR absorptions bands at 3383 and 1685 cm^{-1} resulted from the hydroxyl and carbonyl groups respectively. The ESIMS mass spectrum displayed a molecular ion peak at *m/z* 367 and the molecular formula of **2** was established as $C_{22}H_{27}N_2O_3$ from HRESIMS.

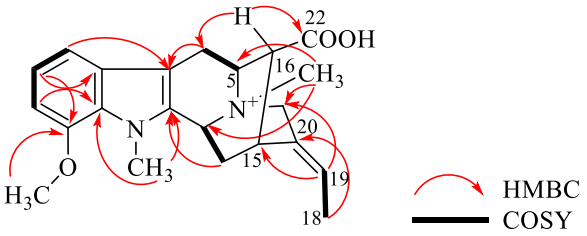

Figure III-5. Selected 2D NMR correlations of **2**

The NMR spectra of **2** and **1** exhibited similar resonances, differing by the presence of a doublet signal of methine (δ_H 2.48) in **2** instead of a methyl alcohol signal at (δ_H 3.58 and δ_H 3.72) in **1** linkage at C-22 (Fig. III-5), indicating the structure of **2** as a 22-deethylate of fuchsiaefoline [45] (Figure III-6).

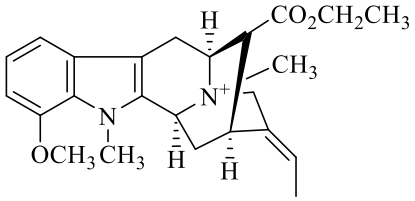

Figure III-6. Fuchsiaefoline

The relative configuration of **2** was assigned by analyses of the ^{1}H-^{1}H coupling constant data and the NOESY correlations to be similar to **1**. In particular, the observed H-16/H-6b NOE indicated that the configuration of C-16 is *R**.

Table 1. ^{1}H and ^{13}C NMR data of **1** and **2** in CD_3OD[a)]

Position	**1**[a]		**2**[b]	
	δ_H	δ_C	δ_H	δ_C
2		133.3		133.9[c)]
3	5.04 (1H, br d, 10.4)	59.4	4.99 (1H, br d, 10.4)	60.6 [c)]
5	5.01 (1H, br d, 6.1)	65.8	4.39 (1H, br d, 4.8)	66.0
6a	3.79 (1H, br d, 18.0)	20.1	2.93 (1H, dd, 17.6, 4.8)	25.2
6b	3.25 (1H, dd, 18.0, 6.1)		3.27 (1H, br d, 17.6)	
7		103.4		102.2
8		129.0		129.1
9	7.11 (1H, d, 8.0)	112.6	7.09 (1H, d, 8.0)	112.3
10	7.02 (1H, t, 8.0)	121.8	7.02 (1H, t, 8.0)	121.8
11	6.77 (1H, d 8.0)	105.2	6.75 (1H, d, 8.0)	105.0
12		149.3		149.3 [c)]
13		128.3		129.0
14a	2.06 (1H, br d, 13.2)	29.4	2.17 (1H, br d, 13.7)	32.5
14b	2.49 (1H, dd, 13.2, 10.4)		2.51 (1H, dd, 13.7, 10.4)	
15	3.35 (1H, br s)	31.1	3.52 (1H, br d, 6.0)	29.5
16		49.9	2.48 (1H, d, 6.0)	50.8 [c)]
17a	3.58 (1H, d, 10.4)	63.8		
17b	3.72 (1H, d, 10.4)			
18	1.72 (3H, d, 6.0)	12.9	1.71 (3H, d, 6.0)	13.1
19	5.50 (1H, q, 6.0)	120.9	5.52 (1H, q, 6.0)	121.4
20		128.7		129.1
21a	4.29 (1H, d, 16.0)	65.9	4.24 (1H, d, 15.6)	66.2
21b	4.39 (1H, d, 16.0)		4.32 (1H, d, 15.6)	
22		175.1		176.4[c)]
N1-Me	3.97 (3H, s)	33.1	3.97 (3H, s)	33.3
N4-Me	3.19 (3H, s)	50.1	3.10 (3H, s)	49.6
OMe-12	3.94 (3H, s)	56.0	3.94 (3H, s)	56.0

a) ^{1}H NMR spectrum was measured on 400 MHz spectrometer, while ^{13}C NMR spectrum was measured on a 100 MHz spectrometer.

b) ^{1}H NMR spectrum was measured on 600 MHz spectrometer, while ^{13}C NMR spectrum was measured on a 150 MHz spectrometer.

c) The chemical shift was deduced from 2D NMR.

III.2 New Dimeric Indole Alkaloids

III.2.1 Separation and Purification

The barks of *T. macrocarpa* Jack (1520 g) were extracted with MeOH, and part of the extract (8 g) was treated with 3% tartaric acid (pH 2) and then partitioned with EtOAc. The aqueous layer was treated with saturated Na_2CO_3 (aq.) to pH 10 and extracted with $CHCl_3$ to give an alkaloidal fraction (0.8 g) and continued by a partition with butanol to give *n*-butanol fraction (1.6 g).

The antimalarial activity of all fractions was carried out by measured the growth inbihition (GI) of each fraction against *P. falciparum* laboratorium strain 3D7 by flow cytometric analysis using an automated hematology analyzer, XN-30. Fractions $CHCl_3$ (GI 122.4%) was selected for further separation by column chromatography over Sephadex LH-20 and eluted with $CHCl_3$/MeOH (1:1, v/v) to give 24 subfractions.

Among the subfractions, subfraction 17 showed promising antimalarial activity (GI 118.1%). Subfraction 17 (63 mg) was then subjected to a subsequent repeated CC by a silica gel column eluted with *n*-hexane/ethyl acetate (49:1 to 1:1, v/v) followed by $CHCl_3$/methanol (49:1 to 100%), which gave 6 subfractions and all tested for the antimalarial activity. Subfraction 4 (GI 100.9%) was selected for further separation by subjected to ODS HPLC (Cosmosil C18 MS-II, 5 µm, 10 × 250 mm; eluent 24% CH_3CN/ H_2O; 0.1% TFA aq.; flow rate, 2.5 mL/min; UV detection at 254 nm) to afford N_b-methylakuammidine (**8**, 3.2 mg, 0.00021%, tR 8.2 min), and two new bisindole alkaloids, bisnaecarpamine A (**9**, 3.2 mg, 0.00021%, tR 13.1 min), and bisnaecarpamine B (**10**, 4.1 mg, 0.00027%, tR 11.8 min). Among the two new bisindole alkaloids, **9** and **10**, bisnaecarpamine A (**9**) exhibited potent antimalarial activity against *P. falciparum* 3D7 strain with the IC_{50} value of 4.60 µM.

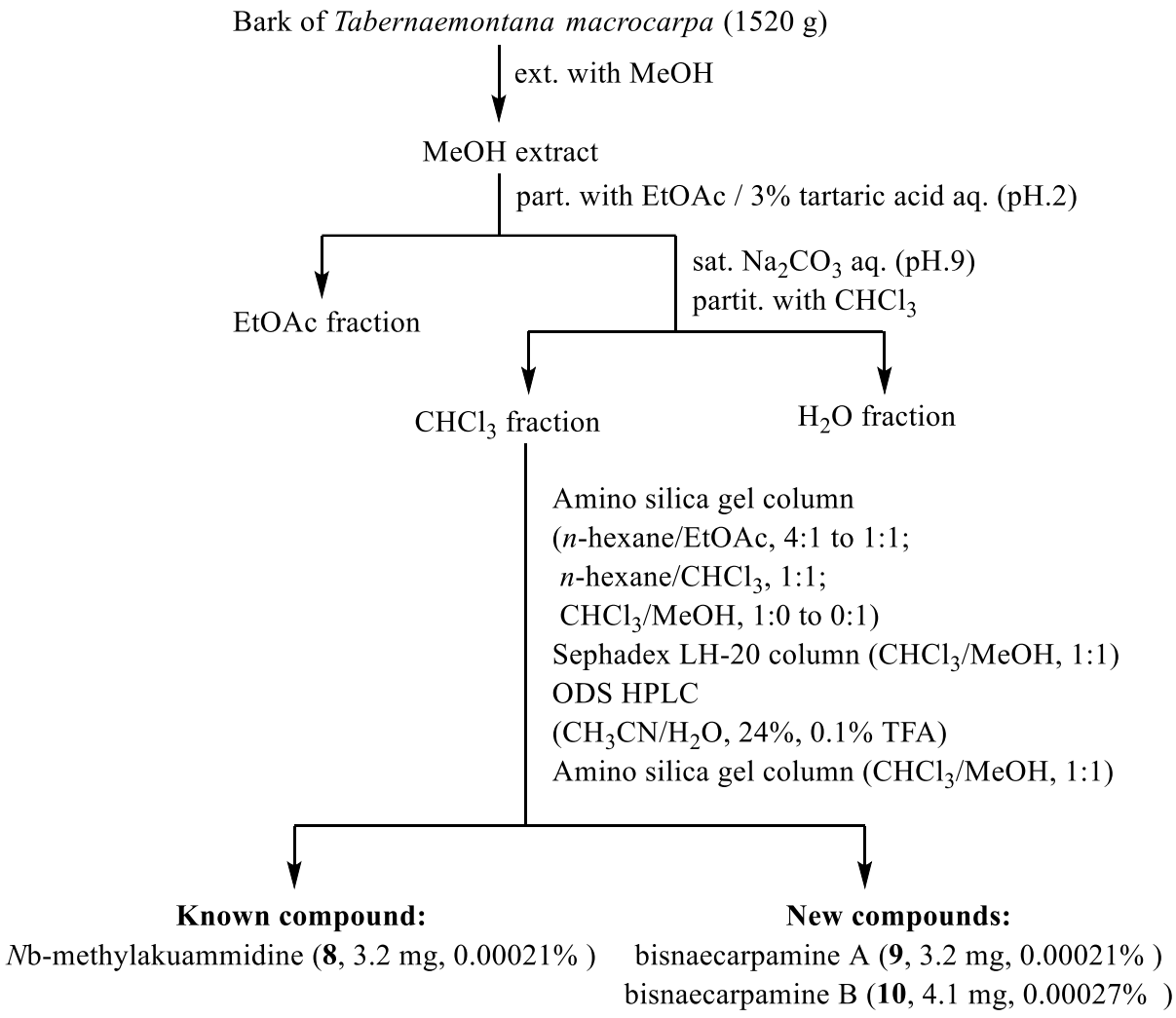

Figure III-6. Isolation scheme of **8**-**10** from *T. macrocarpa* Bark

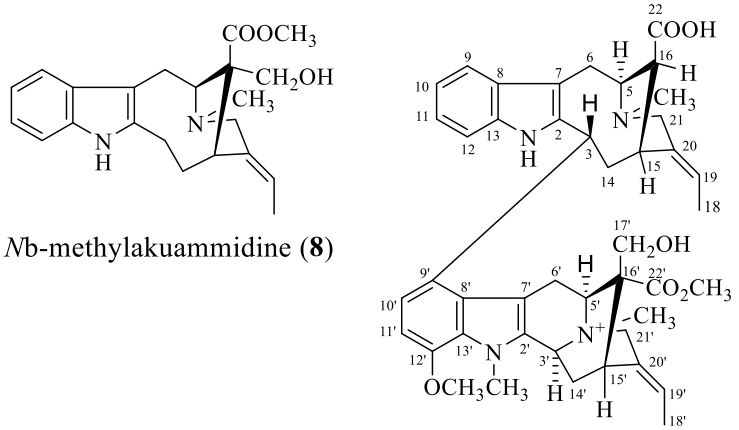

*N*b-methylakuammidine (**8**)

bisnaecarpamine A (**9**)

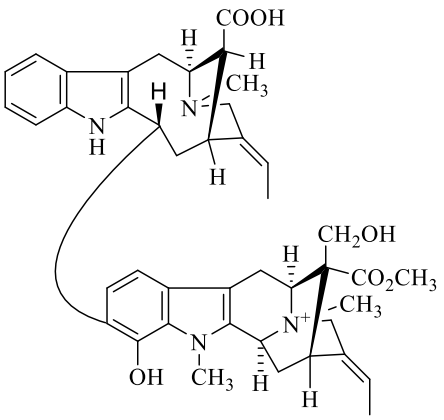

bisnaecarpamine B (**10**)

Figure III-7. Structures of **8**-**10**

III.2.2 Structure Elucidation

III.2.2.1 Bisnaecarpamine A (9)

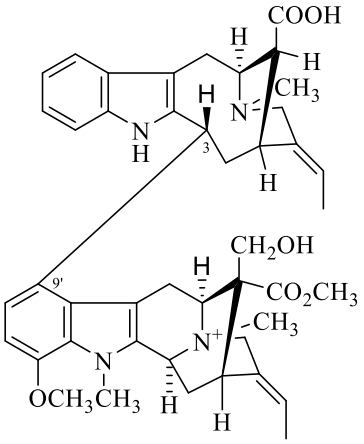

bisnaecarpamine A (**9**)

Bisnaecarpamine A (**9**) was obtained as an optically active yellowish amorphous solid, $[\alpha]^{24}_{D}$ -10 (*c* 1.0, MeOH). The IR absorptions implied the presence of hydroxy (3395 cm^{-1}) and ester carbonyl (1726 cm^{-1}) functionalities, while the UV absorption bands at λ_{max} 225 and 271 nm indicated an indole chromophore.[46] The ESIMS (pos.) of **1** showed a molecular ion peak at *m/z* 733 $[M]^+$ and the molecular formula was established as $C_{44}H_{53}N_4O_6$ from HRESIMS. Analysis of the ^1H and ^{13}C NMR data (Table 2) and the heteronuclear single-quantum correlation (HSQC) spectrum of **1** revealed the presence of seven sp^3 methines, seven sp^3 methylenes, seven methyls, eight sp^2 methines, one sp^3 quaternary carbon, and 14 sp^2 quaternary carbons.

The gross structure of **9** was deduced from analyses of the 2D NMR data, including the ^1H-^1H correlation spectroscopy (COSY), Heteronuclear single quantum coherence (HSQC), and heteronuclear multiple-bond correlation (HMBC) spectra in methanol-d_4 (Fig. III-8). The ^1H-^1H COSY and HSQC spectra revealed connectivity of seven partial structures **a** (C-9~C-12), **b** (C-3, C-14~C-16, C-5~C-6), **c** (C-18~C-19), **d** (C-10′~C-11′), **e** (C-5′~C-6′), **f** (C-3′, C-14′~C-15′), and **g** (C-18′~C-19′). These partial structures were classified into two units, A and B, as shown in Fig. III-8.

In unit A, the HMBC correlations of H-6 (δ_H 3.60) and H-12 (δ_H 7.11) to C-8 (δ_C 130.9), and H-9 (δ_H 7.54) to C-7 (δ_C 109.9) and C-13 (δ_C 137.9) revealed the attachment of partial structure as part of an indole ring, while the HMBC correlations of H-6b to C-8, C-2 (δ_C 138.3) and C-7, H-3 (δ_H 5.20) to C-2 and C-7, H-14b (δ_H 2.68) to C-2 revealed the connectivity of

partial structures **a** and **b**. In addition, the HMBC correlations of the *N*-4-methyl protons to C-5 (δ_C 54.6) and C-21 (δ_C 53.1) established the connections between C-5 and C-21 through a nitrogen atom (*N*-4). Another partial structure **c** and the presence of a carboxylate moiety at C-16 were analyzed by the HMBC correlations of H-19 (δ_H 5.44) to C-15 (δ_C 34.2) and C-21, and H-16 (δ_H 2.71) to C-22 (δ_C 172.3) as shown in Fig. III-8. These data suggested that unit A possessed a vobasine-type skeleton.[47]

In unit B, the ^{1}H and ^{13}C NMR data are highly similar to 12-methoxy-*N*b-methylvoachalotine[44], and this similarity was verified by the 2D NMR spectra analysis. The HMBC cross-peaks of H-10′ (δ_H 6.53) to C-8′ (δ_C 125.6) and C-9′ (δ_C 133.0), H-11′ (δ_H 6.59) to C-12′ (δ_C 147.8) and C-13′ (δ_C 129.5), H-5′ (δ_H 5.14) and H-6′a (δ_H 3.68) to C-7′ (δ_C 103.0) revealed the attachment of partial structures **d** and **e** to the indole moiety, and those of H-19′ (δ_H 5.54) to C-15′ (δ_C 31.4) and C-21′ (δ_C 65.5), H_3-18′ (δ_H 1.73) to C-20′ (δ_C 128.5) revealed the connectivity of partial structures **f** and **g** through C-20′. In addition, the HMBC correlations of the *N*-4′-methyl protons to C-5′ (δ_C 65.7) and C-21′ established the connections between C-5′ and C-21′ through a nitrogen atom (*N*-4′).

The presence of a methoxy group at C-12′, a methyl group at *N*-1, a methyl carboxylate, and a hydroxymethyl at C-16′ were analyzed by the HMBC correlations as shown in the Fig. III-8, revealing a sarpagine-type skeleton. Finally, the linkage between C-3 at unit A and C-9′ at unit B was provided by the HMBC correlation of H-10′ to C-3 (δ_C 41.1). Thus, the planar structure of bisnaecarpamine A was assigned as shown to be in Fig. III-8.

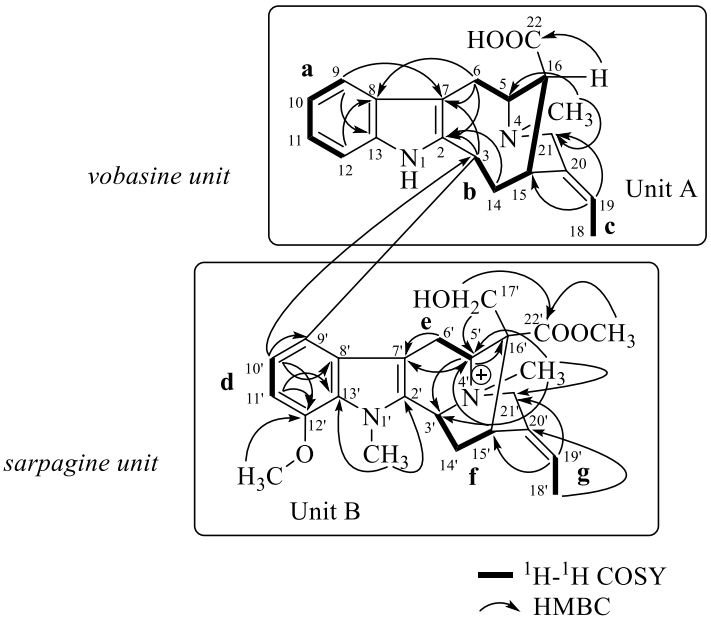

Figure III-8. 2D NMR correlations of bisnaecarpamine A (**9**)

Stereochemistry of bisnaecarpamine A (9)

The stereochemistry of each monoterpene indole unit in **9** was assigned by rotating-frame Overhauser effect spectroscopy (ROESY) correlations as shown in the computer-generated 3D drawing (Fig. III-9). In unit A, the ROESY correlations of H-3/H-15 (δ_H 3.86) and H-14a (δ_H 1.91) suggested that those three protons were in the same plane and the ROESY correlations of H-15/H_3-18 (δ_H 1.72) and H-19/H-21a (δ_H 3.10) established the *E*-configuration of the ethylidene side chain.

The relative configuration of C-16 could not assign by ROESY because there was no ROESY correlation of H-3/H-16. Treatment of **9** using trimethylsilyldiazomethane ($TMSCHN_2$) gave the methyl ester derivative of **9**. The configuration of C-16 was proven to be *S** by the highly shielded methyl chemical shift (2.62 ppm) of this derivative, which can be explained by the anisotropic effect of the indole ring.[48] While in unit B, the ROESY correlations of H-3/H-21′a (δ_H 4.39) suggested that H-3′ (δ_H 5.13) and H-21′a were in the same plane and the correlation of H-6′a to *N*-4′ suggested that H-6′a was α-oriented. Furthermore, the *E*-configuration of the ethylidene side chain was confirmed by the ROESY correlations of H-15′ (δ_H 3.45)/H_3-18′.

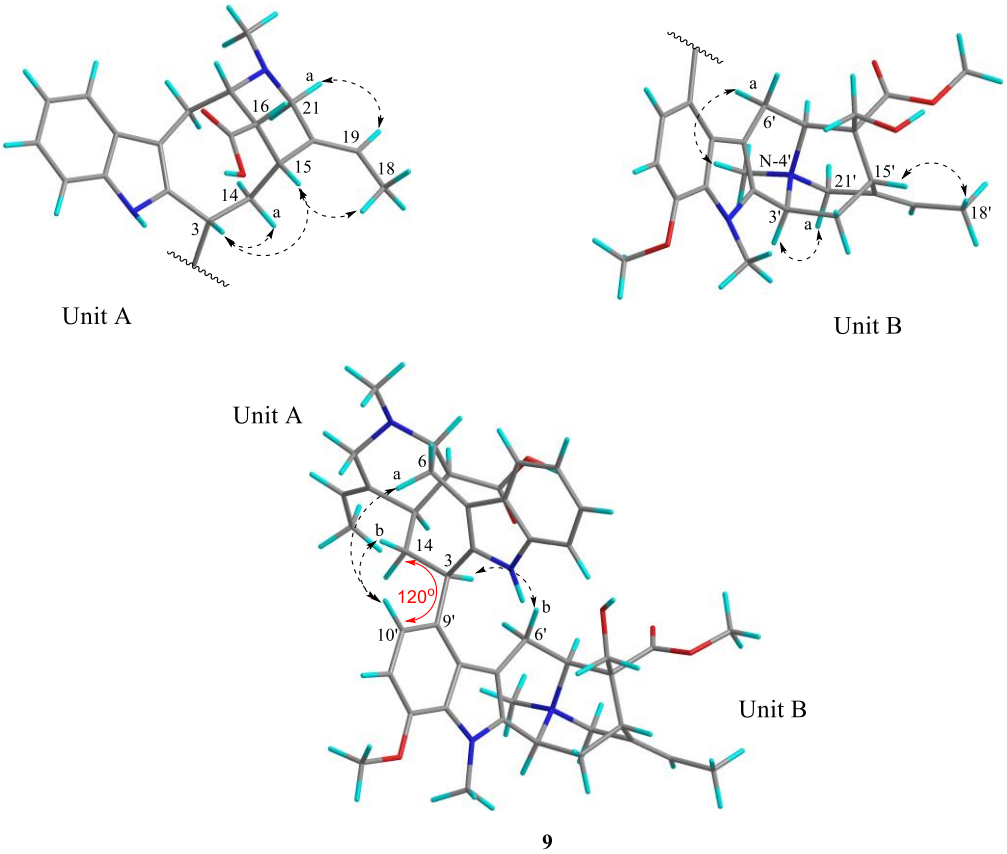

Figure III-9. Selected ROESY correlations and conformation of bisnaecarpamine A (**9**)

The relation between units A and B of **9** was deduced from the ROESY correlations of H-6a and H-14b/H-10′ (δ_H 6.53) and H-3/H-6′b (δ_H 4.59) that suggested the relative configuration of **9** was as shown in Fig III-9.

Finally, the conformation of **9** through the C-3~C-9′ bond was investigated by using molecular mechanics calculations. The global minimum obtained through Monte Carlo conformational search [49] indicated the dihedral angle of C-14~C-3~C-9′~C-10′ is ca. 120° (Fig. 3) and consistent with the conformer suggested by the observed ROESY correlations of H-6a and H-14b/H-10′ and H-3/H-6′b. Therefore, the absolute configuration of **9** was proposed as shown in Fig. III-7.

III.2.2.2 Bisnaecarpamine B (10)

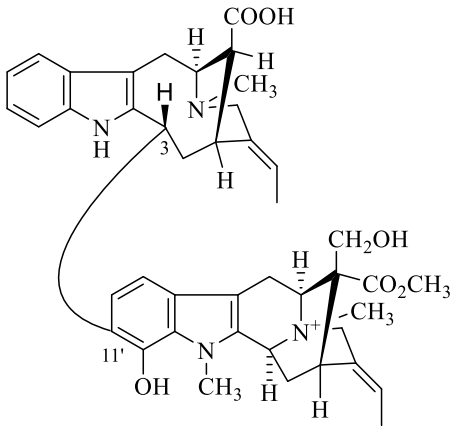

bisnaecarpamine B

Bisnaecarpamine B (**10**) was isolated as an optically active brownish amorphous solid $[\alpha]^{25}_D$ -53 (*c* 1.0, MeOH) and showed a molecular ion peak at *m*/*z* 719 $[M]^+$ in the ESIMS (pos). The IR absorptions implied the presence of hydroxy (3383 cm^{-1}) and ester carbonyl (1727 cm^{-1}) functionalities, while the UV absorption bands at λ_{max} 225 and 287 nm indicated an indole chromophore. [46] The molecular formula $C_{43}H_{51}N_4O_6$ was established by HRESIMS [*m*/*z* 719.3821 $[M]^+$, Δ +2.1 mmu]. The ^{13}C NMR data revealed the presence of seven sp^3 methines, seven sp^3 methylenes, six methyls, eight sp^2 methines, one sp^3 quaternary carbon, and 14 sp^2 quaternary carbons (Table 2).

The NMR spectra of **9** and **10** exhibited similar resonances differ in the linkage position of the two monomer units and the presence of a hydroxy group in **10** was suggested instead of a singlet methyl signal (δ_H 3.86) of a methoxy group at C-12′ in **9**. Further analysis of the two-

dimensional NMR data (^{1}H-^{1}H COSY, HSQC, and HMBC spectra in CD_3OD) of **10** revealed that it was also composed of a vobasine and sarpagine indole alkaloid as well as **9**.

The ROESY correlation of H-10′/H-3 and H-10′/H-14b in Fig. III-10, and the carbon chemical shift of C-10′ (δ_C 121.1), C-11′ (δ_C 105.5), and C-12′ (δ_C 147.8) suggested that the linkage between units A and B in **10** was C-3~C-11′ instead of C-3~C-9′ in **9** (Fig. III-7).

Stereochemistry of bisnaecarpamine B (10)

The stereochemistry of each monoterpene indole units of **10** was assigned by ROESY correlations as shown in Fig. III-10. The ROESY correlations of H-15/H_3-18 and H-15′/H_3-18′ established the *E*-configuration of both ethylidene side chains.

The β-orientation of H-3 and the α-orientation of H-3′ were elucidated by the ROESY correlations of H-3/H-15 and H-3′/H-21′a respectively. The configuration of C-16 was proven to be *S** by the ROESY correlation of H-16/H-21b. Analysis of the ROESY spectral data also suggested that **10** had a similar relative configuration as in **10** for both units A and B. Therefore, the absolute configuration of **10** was proposed as shown in Fig. III-7.

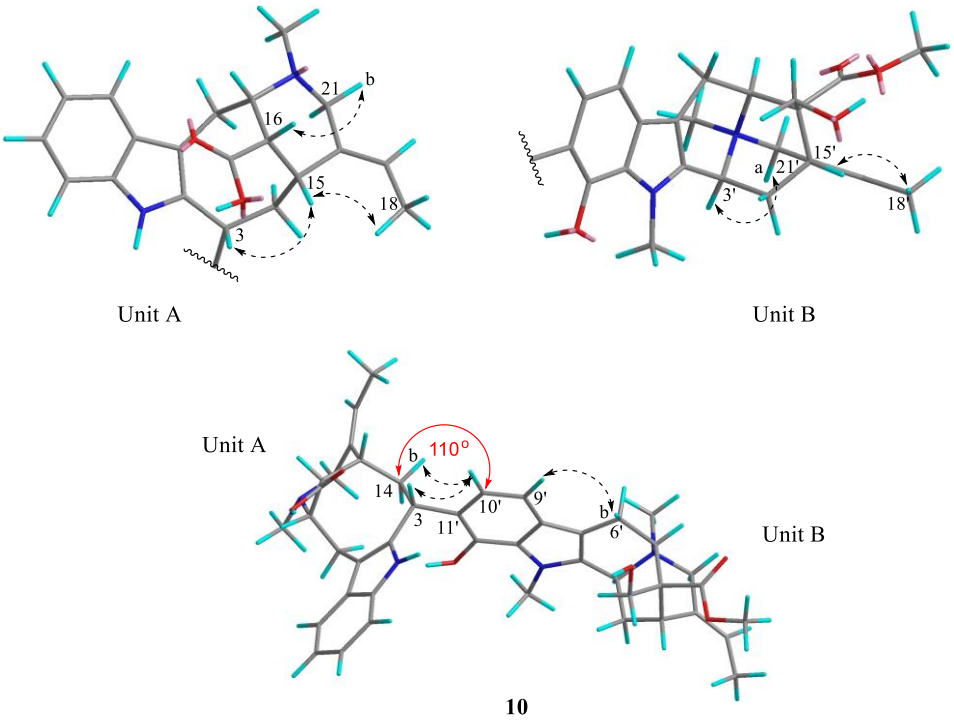

Figure III-10. Selected ROESY correlations and conformation of bisnaecarpamine B (**10**)

Table 2. ^{1}H and ^{13}C NMR data of **9** and **10** in CD_3OD[a)]

	9		**10**	
no.	δ_H (J, Hz)	δ_C	δ_H (J, Hz)	δ_C
2		138.3[b)]		133.5[b)]
3	5.20 (1H, dd, 13.1, 3.0)	41.1	5.16 (1H, br d, 10.1)	38.5
5	4.10 (1H, m)	54.6	4.00 (1H, m)	61.0
6a	3.37 (1H, dd, 11.1, 8.1)	20.5[b)]	3.31 (1H, m)	20.5[b)]
6b	3.60 (1H, br d, 11.1)		3.55 (1H, br d, 10.9)	
7		109.9[b)]		103.5[b)]
8		130.9[b)]		130.9
9	7.54 (1H, br d, 7.7)	118.4	7.52 (1H, d, 8.3)	118.3
10	7.01 (1H, t, 7.7)	119.6	6.99 (1H, m)	119.5
11	7.02 (1H, t, 7.7)	122.5[b)]	7.00 (1H, m)	122.3[b)]
12	7.11 (1H, br d, 7.7)	111.0	7.09 (1H, m)	110.0[b)]
13		137.9		138.3
14a	1.91 (1H, ddd, 15.9, 6.6, 3.0)	39.7	1.91 (1H, m)	39.4
14b	2.68 (1H, ddd, 15.9, 13.1, 11.1)		2.59 (1H, m)	
15	3.86 (1H, br d, 11.1)	34.2	3.81 (1H, m)	35.3
16	2.71 (1H, t, 3.1)	47.6	2.67 (1H, t, 3.7)	48.3
18	1.72 (3H, d, 6.9)	12.7	1.68 (3H, d, 7.2)	12.2
19	5.44 (1H, q, 6.5)	112.5[b)]	5.36 (1H, q, 7.2)	119.5[b)]
20		137.9		138.9
21a	3.10 (1H, br d, 13.5)	53.1	2.95 (1H, br d, 13.9)	53.4
21b	3.91 (1H, br d, 13.5)		3.78 (1H, m)	
22		172.3		172.2
N1-H	8.55 (1H, s)		8.55 (1H, s)	
N4-Me	2.68 (3H, s)	42.0[b)]	2.58 (3H, s)	42.3
2′		133.3[b)]		133.5[b)]
3′	5.13 (1H, br d, 10.1)	59.5[b)]	5.07 (1H, br d, 10.6)	59.4
5′	5.14 (1H, m)	65.7[b)]	4.97 (1H, m)	65.8[b)]
6′a	3.68 (1H, dd, 17.5, 6.1)	22.6	3.22 (1H, dd, 14.6, 7.1)	20.0
6′b	4.59 (1H, br d, 17.5)		3.73 (1H, br d, 14.6)	
7′		103.0[b)]		103.1[b)]
8′		125.6[b)]		125.1[b)]
9′		133.0	7.15 (1H, d, 7.1)	116.4
10′	6.53 (1H, d, 8.1)	121.1	6.68 (1H, br d, 7.1)	122.3
11′	6.59 (1H, d, 8.1)	105.5		121.7
12′		147.8[b)]		149.2[b)]
13′		129.5[b)]		129.4[b)]
14′a	2.25 (1H, br d, 13.6)	28.8	2.13 (1H, br d, 11.9)	29.3
14′b	2.55 (1H, dd, 13.6, 10.1)		2.50 (1H, m)	
15′	3.45 (1H, br s)	31.4[b)]	3.38 (1H, br s)	31.1[b)]
16′		56.8[b)]		56.8[b)]
17'a	3.78 (1H, br d, 11.5)	64.3	3.58 (1H, br d, 10.9)	63.9
17'b	3.96 (1H, d, 11.5)		3.70 (1H, br d, 10.9)	
18′	1.73 (3H, d, 6.9)	12.9	1.70 (3H, d, 7.1)	13.0
19′	5.54 (1H, q, 6.9)	121.2[b)]	5.55 (1H, q, 7.1)	121.0[b)]
20′		128.5		128.6
21'a	4.39 (1H, d, 16.7)	65.5	4.30 (1H, d, 15.3)	65.8
21'b	4.43 (1H, d, 16.7)		4.38 (1H, d, 15.3)	
22'		173.9[b)]		174.2[b)]
N1'-Me	3.98 (3H, s)	33.4	4.01 (3H, s)	32.2
N4'-Me	3.35 (3H, s)	49.9[b)]	3.17 (3H, s)	50.1[b)]
OMe-12'	3.86 (3H, s)	56.1[b)]		
OMe-22'	3.82 (3H, s)	53.6	3.75 (3H, s)	53.4[b)]

a) ^{1}H NMR spectrum was measured on a 600 MHz spectrometer, while ^{13}C NMR spectrum was measured on a 150 MHz spectrometer.
b) The chemical shift was deduced from 2D NMR.

III.2.3 Plausible Biogenetic Pathway

Monoterpenoid indole alkaloids consist of an indole moiety provided by tryptamine or tryptophan and a terpenoid component derived from the iridoid glucoside secologanin. Tryptamine and secologanin condense via the Pictete Spengler reaction to form strictosidine, the common precursor to all monoterpenoid indole alkaloids by strictosidine synthase (STR).[50] An enzymatic biosynthesis of sarpagine skeleton, as in **1** and **2**, has been reported from the *R. serpentina* cell suspensions as shown in Fig. III-11.[50]

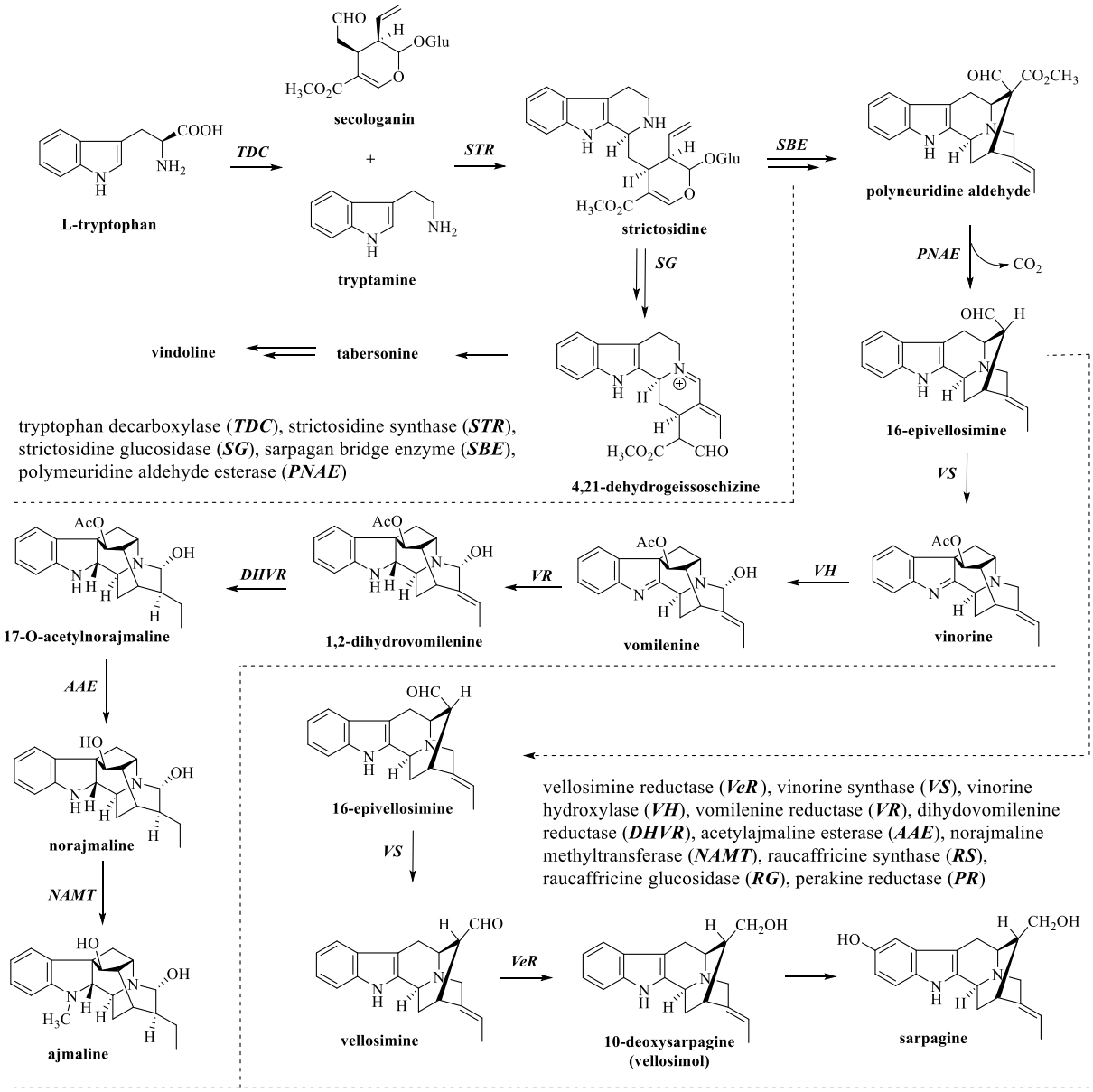

Figure III-11. Enzymatic biosynthesis of sarpagine in *R. serpentina* cell suspensions

A plausible biogenetic pathway for bisnaecarpamines A and B (**9** and **10**) is proposed as shown in Fig. III-12. Their structures consisting of a vobasine-sarpagine type skeleton might be generated through C-N bond cleavage of a quaternary sarpagine-type alkaloid [20] followed by the introduction of another sarpagine-type alkaloid as a nucleophile.

Nucleophilic attack to C-3 from C-9' in the sarpagine-type alkaloid formed bisnaecarpamine A (**9**) as shown in route **a**, while bisnaecarpamine B (**10**) might be generated by an attack from C-11' as shown in route **b**.

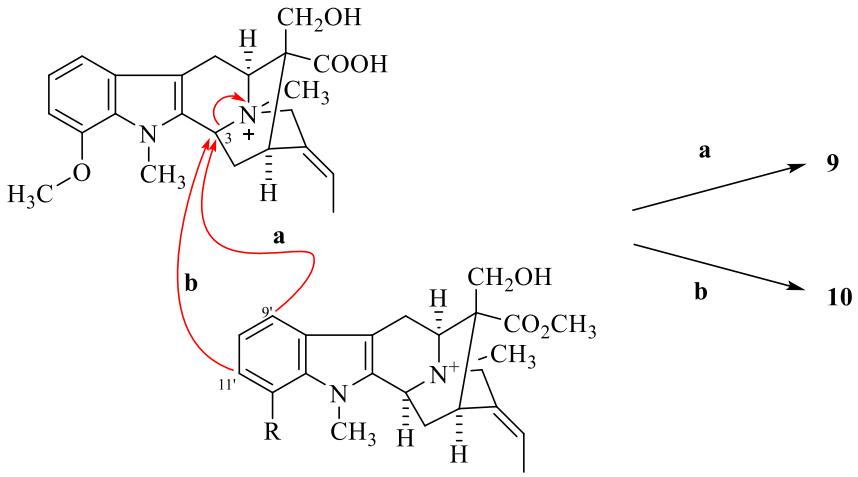

Sarpagine type
(*12-methoxy-4-methylvoachalotine) (MMV*)

9 : R = OCH_3
10: R = OH

Figure III-12. Plausible biogenetic pathway of **9** and **10**

Chapter IV Absolute Configuration

The assignment of the absolute configuration (AC) is a major challenge task to be determined when dealing with chiral molecules especially for those compounds with a relevant issue for medicinal, material, and natural products chemistry.[51] Natural products differ from synthetic compounds in several characteristics. They are highly diverse in structure, generally exhibit specific biological activities, and show astonishing spatial complexity.[52] The growing number of chiral drugs that have been developed in the field of pharmaceutical and biopharmaceuticals within the last two decades shows the important relationship between chirality and biological activity.[53]

Since the introduction of the word "chirality" by Lord Kelvin more than a hundred years ago, the determination of the exact orientation of atoms of a molecule in space, i.e., AC has been an interesting problem to be solved. Chirality is a fundamental property of (organic) molecules. A molecule is referred to as chiral if it is not superimposable to its mirror image or when a carbon atom has attached to it four different atoms or groups[54].

In the field of drug and drug development, chirality is a very important issue since the two enantiomers of a chiral drug generally possess different pharmaceutical activities. Thalidomide is considered to be the most noteworthy example of differential physiological activity between isomers in the drug, with the (*R*)-enantiomer having sedative properties, whereas the (*S*)-enantiomer is teratogenic. Thalidomide was synthesized as a racemic mixture, but purification to obtain only the (*R*)-enantiomer was not a viable solution as a liver enzyme converts the *R*-enantiomer into *S*-enantiomer.[55]

The reason for the differing biological activities is chiral recognition by drug receptors. The different enantiomers of a chiral drug can differ in their interactions with biological systems such as enzymes, proteins, and receptors and these differences can lead to differentiation in activities including efficacy, pharmacokinetics, or toxicity. Therefore, for the structural characterization of chiral natural products, the assignment of their AC is mandatory, in particular when the biological activity of the compounds has to be investigated.[51,53]

Some analytical techniques are commonly employed for AC assignments as described by Saito and Schreiner[56], including single-crystal X-ray analysis, Mosher NMR analysis, Optical Rotatory Dispersion (ORD), Electronic Circular Dichroism (ECD), Vibrational Circular Dichroism (VCD), and Raman Optical Activity (ROA).[56]

IV.1 Circular Dichroism (CD)

CD is defined as the difference between the absorption of left and right circularly polarized light. Although CD is theoretically observed for the entire spectral region, current instruments only observe CDs in the UV-Vis region (electronic circular dichroism, ECD) and IR regions (vibration circular dichroism, VCD).[49] ECD spectroscopy requires a suitable chromophore in the compound, while this is irrelevant with VCD spectroscopy. On the other hand, an ECD spectrum can be obtained from sub-μg amounts, while VCD requires much larger amounts. [49]

CD provides information on the conformation and AC of a molecule. If the CD data and the preferred conformers of a molecule are known, the AC of the molecule may be assigned. In ECD, the most common AC assignment method is by comparing the experimental CD of the compound under investigation with the experimental CD of a similar compound of known AC. The other AC assignment methods are the semi-empirical sector rules, the exciton chirality method, and comparison of the calculated CD spectra with the experimental CD.[49,52]

IV.2 *Ab initio* Calculation of ECD by Time-Dependent Density Functional Theory

CD calculations have been used for the determination of the AC of natural products for decades, as seen in the π-SCF studies of CD by Mason and co-workers.[49] However, its use has been limited until the major advancements in the CD calculations by time-dependent density functional theory (TDDFT), which resulted in a good compromise between computational costs and accuracy, in the past decade came to pass. The principle of the determination of the ACs of natural products by CD calculation is relatively simple. It is basically to compare the calculated and experimental CD spectra to assign the ACs. If the two data closely match, the assignment of higher reliability is to be obtained. [49]

CD calculations generally involve two steps, a conformational analysis to obtain the conformer(s) and the UV/CD TDDFT calculation of the conformer(s). The conformational analysis is often done by Monte Carlo methods using molecular mechanics (MMFF94, etc.) and/or semi-empirical methods (AM1, etc.) for the relative energy evaluation of the conformers. The obtained conformers are then further optimized by using the density functional theory (DFT) method before submitting it to the TDDFT calculations of the UV/CD using a program such as Gaussian, TURBOMOLE, NWChem, or Spartan.[49]

The calculated UV/CD spectra of the conformers are Boltzmann averaged to obtain the UV/CD spectra of the isomers. The averaged UV spectrum is then shifted to conform to the

experimental UV spectrum and the same shift is also applied to the calculated CD spectra before comparing the calculated CD spectra with the experimental CD of the natural product.[49]

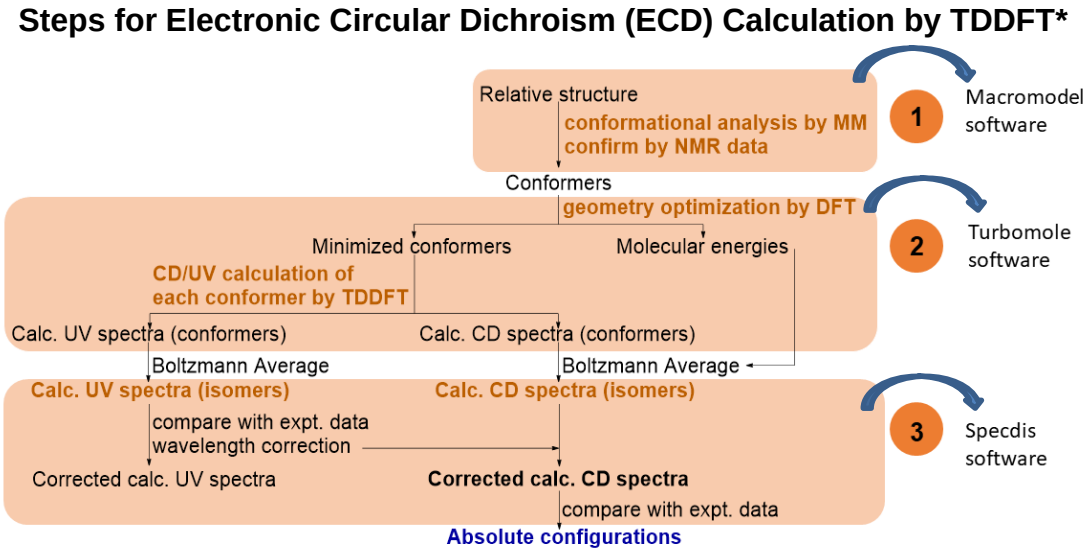

Figure IV-2. General workflow of AC assignment by TDDFT
*This figure was taken from Ref. 49 and reproduced with permission

The accuracy of the TDDFT calculations itself mainly depends on the basis set and functional used for the calculations. A larger basis set generally increases the accuracy but also increases the computational time length. In the CD calculations, basis sets with polarization and diffuse functions are commonly used, for example, 6-31G* or aug-cc-pVDZ, whereas the B3LYP functional is commonly used and performs well in general.[49]

IV.3 Absolute Configuration Assignments of New Dimers (9 and 10)

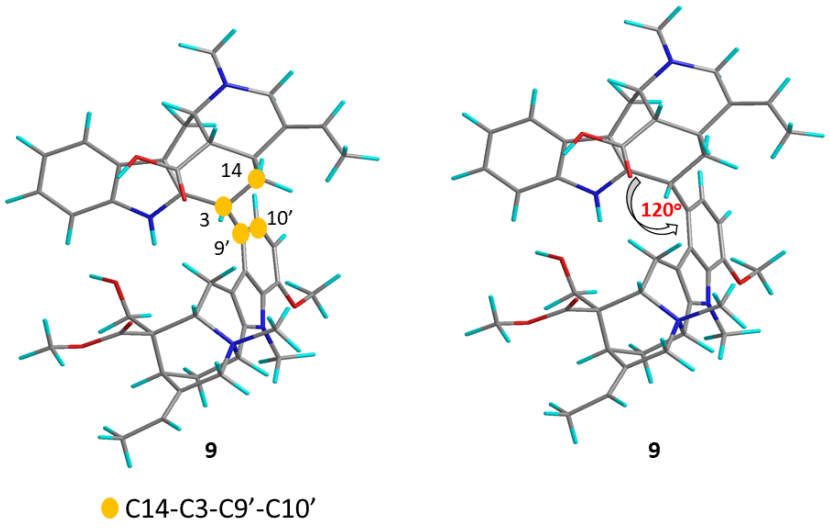

Figure IV-3. Conformational structure analysis of **9**

The conformation of **9** through the C-3~C-9′ bond was investigated by using molecular mechanics calculations [49]. The global minimum (Fig. IV-3) obtained through Monte Carlo conformational search[49] indicated the dihedral angle of C-14~C-3~C-9′~C-10′ is ca. 120° (Fig. IV-3) and consistent with the conformer suggested by the observed ROESY correlations of H-6a and H-14b/H-10′ and H-3/H-6′b.

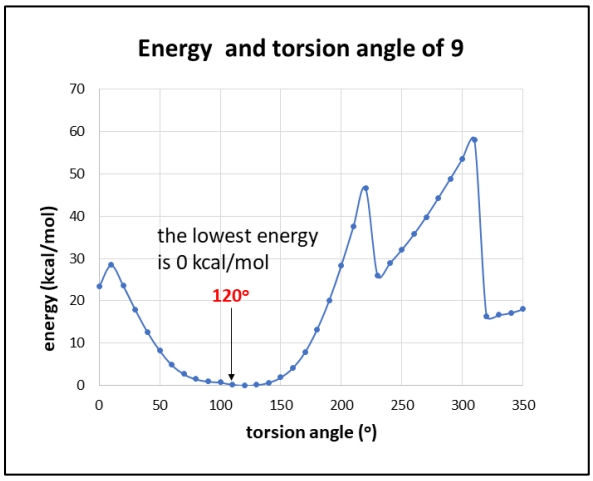

Figure IV-3. Energy and torsion angle of **9**

The absolute configuration of **9** was then assigned by comparing the experimental CD spectrum and the calculated CD spectrum as shown in Fig. IV-4. CD calculation was performed by Turbomole 7.1 [57] using RI-TD-DFT-B3LYP/SVPD level of theory on RI-DFT-B3LYP/SVP optimized geometries. The experimental CD spectrum shows a similar CD pattern compared to the calculated CD spectrum. Therefore, the absolute configuration of **9** was proposed as shown in Fig. III-7.

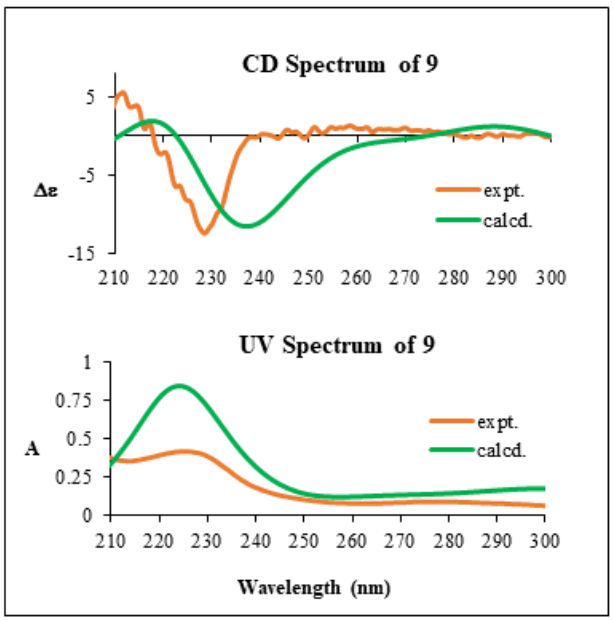

Figure IV-4. Calculated and experimental CD & UV spectra of **9**

Furthermore, the conformation of **10** through the C-3~C-11′ bond was assigned by the ROESY correlations of H-3/H-10′ and H-9′/H-6′b as shown in Fig. IIV-5. The difference in the linkage of units A and B in **9** and **10** resulted in the difference of their total conformation, *i.e.*, compound **9** possessed a twist conformation (Fig. 3), while compound **10** adopted an extended conformation with a dihedral angle of C-14~C-3~C-11′~C-10′ is ca. 110° (Fig. IV-5).

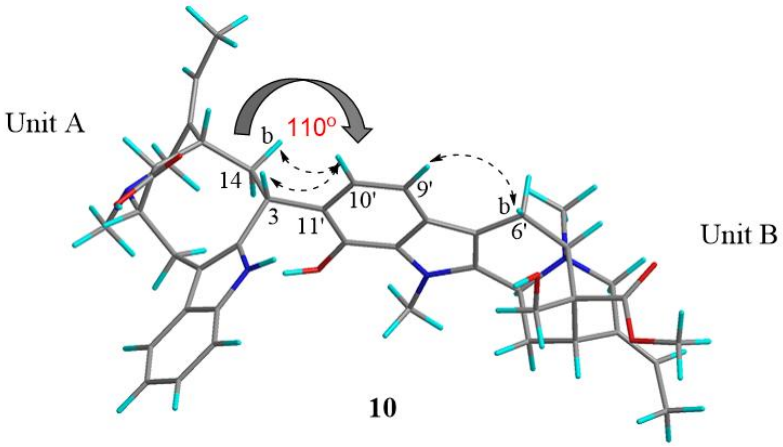

Figure IV-5. Conformational structure analysis of **10**

To define the absolute configuration of **10**, the TDDFT-ECD method was applied on the global minimum of **10**. The result showed that the calculated CD spectrum displayed a good similarity to the experimental CD spectrum of **10** as shown in Fig. IV-6. Therefore, the absolute configuration of **10** was proposed as shown in Fig. III-7.

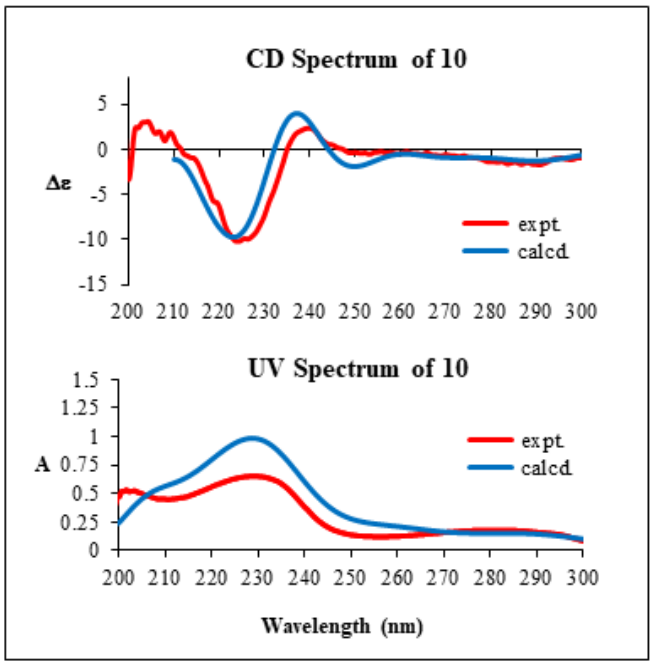

Figure IV-6. Calculated and experimental CD & UV spectra of **10**

Chapter V Antimalarial Activity

V.1 Parasites Strain Culture

P. falciparum laboratory strain 3D7 was obtained from Prof. Masatsugu Kimura (Osaka City University, Osaka, Japan). For the assessment of antimalarial activity of the compounds *in vitro*, the parasites were cultured in Roswell Park Memorial Institute (RPMI) 1640 medium supplemented with 0.5 g/L L-glutamine, 5.96 g/L HEPES, 2 g/L sodium bicarbonate ($NaHCO_3$), 50 mg/L hypoxanthine, 10 mg/L gentamicin, 10% heat-inactivated human serum, and red blood cells (RBCs) at a 3% hematocrit in an atmosphere of 5% CO_2, 5% O_2, and 90% N_2 at 37 °C as previously described [58]. Ring-form parasites were collected using the sorbitol synchronization technique [59]. Briefly, the cultured parasites were collected by centrifugation at 840 *g* for 5 min at room temperature, suspended in a 5-fold volume of 5% D-sorbitol (Nacalai Tesque, Kyoto, Japan) for 10 min at room temperature, and then they were washed twice with RPMI 1640 medium to remove the D-sorbitol. The utilization of blood samples of healthy Japanese volunteers for the parasite culture was approved by the institutional review committee of the Research Institute for Microbial Diseases (RIMD), Osaka University (approval number: 22-3).

V.2 Antiplasmodial Test Against *Plasmodium falciparum* Strain

Ring-form-synchronized parasites were cultured with compounds **1**-**10** at sequentially decreasing concentrations (50, 15, 5, 1.5, 0.5, 0.15, 0.05, and 0.015 μM) for 48 h for the flow cytometric analysis using an automated hematology analyzer, XN-30. The XN-30 analyzer was equipped with a prototype algorithm for cultured falciparum parasites (prototype; software version: 01-03, (build 16)) and used specific reagents (CELLPACK DCL, SULFOLYSER, Lysercell M, and Fluorocell M) (Sysmex, Kobe, Japan) [60,61]. Approximately 100 μL of the culture suspension diluted with 100 μL phosphate-buffered saline was added to a BD Microtainer MAP Microtube for Automated Process K_2 EDTA 1.0 mg tube (Becton Dickinson and Co., Franklin Lakes, NJ, USA) and loaded onto the XN-30 analyzer with an auto-sampler as described in the instrument manual (Sysmex). The parasitemia (MI-RBC%) was automatically reported [60]. Then 0.5% DMSO alone or containing 5 μM artemisinin used as the negative and positive controls, respectively. The growth inhibition (GI) rate was calculated from the MI-RBC% according to the following equation:

GI (%) = 100 – (test sample – positive control)/(negative control – positive control) × 100

The IC_{50} was calculated from GI (%) using GraphPad Prism version 5.0 (GraphPad Prism Software, San Diego, CA, USA) [62].

Table 3. Antimalarial activity of **1** – **10** against against *P. falciparum* 3D7 strain (IC_{50}, μM)

Compound No.	Name of compound	IC_{50} (μM)
1	22-demethyl derivative of 12-methoxy-4-methylvoachalotine (MMV) (new)	>50
2	22-deethylate of fuchsiaefoline (new)	>50
3	12-methoxy-4-methylvoachalotine	>50
4	16-demethoxycarbonylvoacamine	28.8
5	isositsirikine	>50
6	affinisine	>50
7	16-epi-affinine	>50
8	*N*b-methylakuammidine	>50
9	bisnaecarpamine A (new)	4.60
10	bisnaecarpamine B (new)	>50
	chloroquine (positive control)	0.86

Out of the 10 isolated compounds, only compounds **4** and **9** show antimalarial activity against *Plasmodium falciparum* 3D7 strain with IC_{50} value of 28.8 μM and 4.60 μM respectively. Even the two new bisindole alkaloids, bisnaecarpamines A and B (**9** and **10**) have similar structures, they possess different activity against *P. falciparum* 3D7 strain. The reason is more likely because compounds **9** and **10** have a different connection between units A and B causing them to take distinct conformations. The difference in conformations is one possible reason for the contrast in their antimalarial activity.

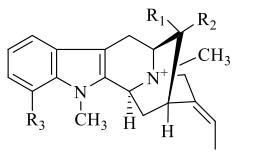

	R_1	R_2	R_3
1	CH_2OH	COOH	OCH_3
2	H	COOH	OCH_3
3	CH_2OH	CO_2CH_3	OCH_3
6	H	CH_2OH	H

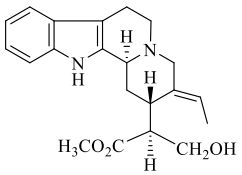

5

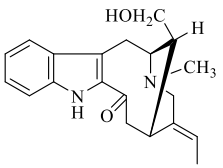

7

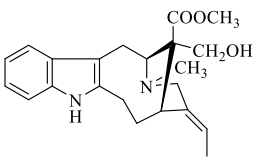

8

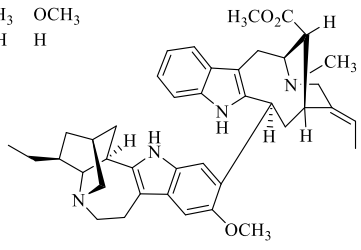

4

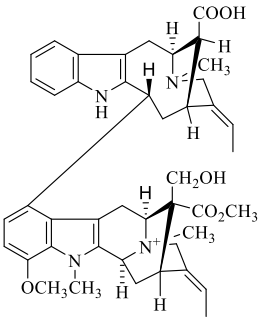

9

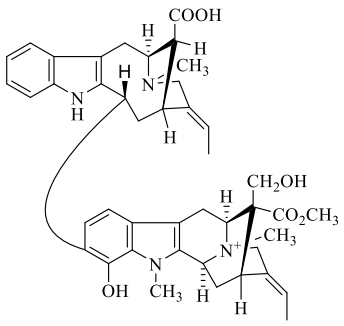

10

Chapter VI Conclusion

In the search for new antimalarial lead compounds from the bark of *T. macrocarpa* Jack (Apocynaceae), which is known to produce various skeletal of indole alkaloids, the bioassay guided and chemical investigations from this plant were conducted.

Two new monoterpene indole alkaloids (**1** and **2**) which have sarpagine-type skeleton, together with two new bisindole alkaloids, bisnaecarpamines A and B (**9** and **10**) which have vobasine-sarpagine type skeleton, were isolated. The relative structure of all compounds was deduced from 1D and 2D NMR data, and their absolute configuration was assigned by comparison of the experimental CD spectra to the TDDFT calculated CD spectra.

Six known compounds that have been isolated from this plant were identified as 12-methoxy-4-methylvoachalotine (**3**), 16-demethoxycarbonylvoacamine (**4**), isositsirikine (**5**), affinisine (**6**), 16-epi-affinine (**7**), and *N*b-methylakuammidine (**8**).

Among the 10 isolated compounds only compounds **4** and **9** showed antimalarial activity against *P. falciparum* 3D7 strain with IC_{50} value of 28.8 µM and 4.60 µM respectively. Even the two new bisindole alkaloids, bisnaecarpamines A and B (**9** and **10**) have similar structures, they possess different activity against *P. falciparum* 3D7 strain. The reason is more likely because compounds **9** and **10** have a different connection between units A and B causing them to take distinct conformations. The difference in conformations is one possible reason for the contrast in their antimalarial activity.

Experimental Section

General methods

^{1}H and 2D NMR spectra were recorded on a Bruker AV700, a JEOL ECA600, and a Bruker AV400 spectrometer. The chemical shifts were referenced to the residual solvent peaks (δ_H 3.31 and δ_C 49.0 for methanol-d_4 and δ_H 7.26 and δ_C 77.0 for chloroform-*d*). Standard pulse sequences were employed for the 1D and 2D NMR experiments.

Optical rotations were measured on a JASCO DIP-1000 polarimeter. UV spectra were recorded on a Shimadzu UVmini-1240 spectrophotometer and IR spectra on a JASCO FT/IR-4100 spectrophotometer. High-resolution ESI MS were obtained on a LTQ Orbitrap XL (Thermo Scientific). Merck silica gel 60 (40 - 63 μm), amino silica, and HP-20 were used for the column chromatography, and the separations were monitored by Merck silica gel 60 F254, or Merck amino silica gel 60 F254 TLC plates.

The conformations for the CD calculations were obtained using Monte Carlo analysis with MMFF94 force field and charges on Macromodel 9.1. Unless noted otherwise, the geometries within 3 kcal of the global minimum were further optimized by using RI-*J* approximation at the DFT BP86/SVP level of theory in Turbomole 7.1 and excited-state calculations were performed at the RI-TD-DFT-B3LYP/SVPD level of theory on RI-DFT-B3LYP/TZVP optimized geometries. The CD spectra were simulated by overlapping Gaussian functions for each transition where the width of the band at 1/*e* height is fixed at 0.3 eV or 0.25 eV, and the resulting spectra were scaled to the experimental values.

Merck silica gel 60 (40 – 63 μm), Fuji sylisia Chromatorex amino silica gel (100 – 200 mesh), nacalai tesque Cosmosil 140C_{18}-OPN, Sephadex^{TM} LH-20, and HP-20 were used for the column chromatography, and the separations were monitored by Merck silica gel 60 $F_{254,}$ Fuji sylisia Chromatorex amino silica gel, or Merck siliga gel RP C-18 F_{254} TLC plates. YMC-pack ODS Pro C18, 5 μm (10 x 250 mm) column was used for the HPLC.

Constituents of *T. macrocarpa* Bark

Barks of *T. macrocarpa* Jack were collected in June 2018 from the Centre for Plant Conservation Botanic Gardens, Bogor, Indonesia. The GPS coordinates of the field site are 6°35′59.65″S, 106°47′54.00″E. Authentication and identification of the plant were carried out by Mr. Ikar Supriatna at the Centre for Plant Conservation Botanic Gardens, Bogor, Indonesia.

In the 1st batch, the barks of *T. macrocarpa* Jack (550 g) were extracted with MeOH, and part of the extract (8 g) was partitioned between EtOAc and 3% tartaric acid. The aqueous layer was adjusted at pH 9 with saturated Na_2CO_3 (aq). and extracted with $CHCl_3$ to give $CHCl_3$ fraction (1.5g) and continued by partition with BuOH to give BuOH fraction (3.7 g). The $CHCl_3$ fraction was subjected to CC over silica gel and eluted with *n-hexane*/ethyl acetate (49:1 to 1:1, v/v) followed by $CHCl_3$/methanol (49:1 to 100%) to give 16 fractions. Fraction 9 (149 mg) was further separated by Sephadex LH-20 with $CHCl_3$/MeOH (1:1, v/v) to afford 16-demethoxycarbonylvoacamine (**4**, 3.4 mg, 0.0425%), isositsirikine (**5**, 0.6 mg, 0.0075%), affinisine (**6**, 3.1 mg, 0.0388%), and affinine (**7**, 13.0 mg, 0.1625%). Fraction 11 (160 mg) was purified by amino silica CC and eluted with $CHCl_3$/MeOH (1:1, v/v) yielded 12-methoxy-4-methylvoachalotine (**3**, 151.0 mg, 1.8875%). The butanol fraction was subjected to HP-20 Diaion CC with $CHCl_3$/MeOH (20-100%, v/v) to afford 10 fractions. Fraction 6 was further purified by silica gel CC with $CHCl_3$/MeOH (49:1 to 1:1) affording 20 fractions. Fraction 15 was then successively purified using Sephadex LH-20 with $CHCl_3$/MeOH (1:1, v/v) and HPLC (Cholester 10 x 250 mm, 50% MeOH at 2.4 mL/min, UV detection at 254 nm) to yield **1** (6.3 mg, 0.0788%, t_R 11.3 min), and **2** (3.1 mg, 0.0388%, t_R 23.2 min).

In the 2nd batch, the barks of *T. macrocarpa Jack* (1520 g) were extracted with MeOH, and part of the extract (8 g) was treated with 3% tartaric acid (pH 2) and then partitioned with EtOAc. The aqueous layer was treated with saturated Na_2CO_3 (aq) to pH 10 and extracted with $CHCl_3$ to give an alkaloidal fraction (0.8 g) and continued by a partition with BuOH to give BuOH fraction (1.6 g). The $CHCl_3$ fraction was subjected to a column chromatography over Sephadex LH-20 and eluted with $CHCl_3$/MeOH (1:1, v/v) to give 24 fractions. Separation of fraction 17 (63 mg) by a silica gel column eluted with *n*-hexane/ethyl acetate (49:1 to 1:1, v/v) continued by $CHCl_3$/methanol (49:1 to 100%), gave 6 fractions. The fourth eluted fraction was subjected to ODS HPLC (Cosmosil C_{18} MS-II, 5 µm, 10 × 250 mm; eluent 24% CH_3CN/ H_2O; 0.1% TFA aq.; flow rate, 2.5 mL/min; UV detection at 254 nm) to afford afford N_b-methylakuammidine (**8**, 3.2 mg, 0.00021%, tR 8.2 min), and two new bisindole alkaloids bisnaecarpamine A (**9**, 3.2 mg, 0.00021%, t_R 13.1 min), and bisnaecarpamine B (**10**, 4.1 mg, 0.00027%, t_R 11.8 min).

Compound **1**

Brownish amorphous solid. $[\alpha]^{25}_{D}$: -45 (*c* 1.00, MeOH). IR *V*max (KBr): 3382 and 1678 cm^{-1}. UV/Vis λ_{max} (MeOH) (log*e*) 225 (4.30), 271 (3.34) nm. CD (MeOH) λ_{max} (D*e*) 228 (-10.4) and 293 (-1.02) nm. ^{1}H and ^{13}C NMR (CD_3OD): Table 1. MS (ESI): *m*/*z*: 397 $[M]^+$. HRESIMS *m*/*z*: 397.2126 $[M]^+$ (Calcd. for $C_{23}H_{29}N_2O_4$, 397.2122).

Compound **2**

Brownish amorphous solid. $[\alpha]^{25}_{D}$: -5 (*c* 1.00, MeOH). IR *V*max (KBr): 3383 and 1685 cm^{-1}. UV/Vis λ_{max} (MeOH) (log *e*) 225 (3.91), 280 (2.91) nm. CD (MeOH) λ_{max} (D*e*) 227 (-3.78) and 291 (-0.81) nm. ^{1}H and ^{13}C NMR (CD_3OD): Table 1. MS (ESI): *m*/*z*: 367 $[M]^+$. HRESIMS *m*/*z*: 367.2143 $[M]^+$ (Calcd. for $C_{22}H_{27}N_2O_3$, 367.2152).

Bisnaecarpamine A (**9)**

Yellowish amorphous solid. $[\alpha]^{24}_{D}$: -10 (*c* 1.0, MeOH). IR V_{max} (KBr): 3395 and 1727 cm^{-1}. UV/Vis λ_{max} (MeOH) (log ε) 225 (4.30), 271 (3.34) nm. CD (MeOH) λ_{max} (Δε) 229 (-10.4) and 289 (-0.57) nm. ^{1}H and ^{13}C NMR (CD_3OD): Table 1. MS (ESI): *m*/*z*: 733 $[M]^+$. HRESIMS *m*/*z*: 733.4026 $[M]^+$ (Calcd. for $C_{44}H_{53}N_4O_6$, 733.3960).

Bisnaecarpamine B (**10):**

Brownish amorphous solid. $[\alpha]^{25}_{D}$: -53 (*c* 1.0, MeOH). IR V_{max} (KBr): 3386 and 1725 cm^{-1}. UV/Vis λ_{max} (MeOH) (log ε) 225 (4.66), 2.87 (4.12) nm. CD (MeOH) λ_{max} (Δε) 225 (-20.8) and 287 (-3.38) nm. ^{1}H and ^{13}C NMR (CD_3OD): Table 1. MS (ESI): *m*/*z*: 719 $[M]^+$. HRESIMS *m*/*z*: 719.3821 $[M]^+$ (Calcd. for $C_{43}H_{51}N_4O_6$, 719.9025).

CD calculation

The conformations were obtained using Monte Carlo analysis with MMFF94 force field and charges on Macromodel 9.1. CD calculations were performed in Turbomole 7.1 using RI-TD-DFT-B3LYP/SVPD level of theory on RI-DFT-B3LYP/TZVP optimized geometries

Antimalarial activity

Human malaria parasites were cultured according to the method of Trager and Jensen. The antimalarial activity of the isolated compounds was determined by the procedure described by Budimulya *et al.* In brief, stock solutions of the samples were prepared in DMSO (final

DMSO concentrations of < 0.5%) and were diluted to the required concentration with a complete medium (RPMI 1640 supplemented with 10% human plasma, 25 mM HEPES and 25 mM $NaHCO_3$) until the final concentrations of samples in culture plate wells were 10; 1; 0,1; 0,01; 0,001 μg/mL. The malarial parasite *P. falciparum* 3D7 clone was propagated in a 24-well culture plates. The growth of the parasite was monitored by making a blood smear fixed with MeOH and stained with Geimsa stain. The antimalarial activity of each compound was expressed as an IC_{50} value, defined as the concentration of the compound causing 50% inhibition of parasite growth relative to an untreated control.

The percentage of growth inhibition was expressed according to following equation : Growth inhibition % = 100- [(test parasitaemia/control parasitemia) × 100]. Chloroquine: IC_{50} 0.011 μM.

References

1. Jain, C.; Khatana, S.; Vijayvergia, R., *Int. J. Pharm. Sci. Res.* **2019**, *10* (2), 494–504.
2. Pagare, S.; Bhatia, M.; Tripathi, N.; Bansal, K. Y., *Curr. Trends Biotechnol. Pharm.* **2015**, *9* (3), 293–304.
3. Rungsung, W.; Ratha, K. K.; Dutta, S.; Dixit, A. K.; Hazra, J., *World J. Pharm. Res.* **2015**, *4* (07), 604–613.
4. Ahmed E, Arshad M, Khan MZ, Amjad MS, Sadaf HM, R. I. et al, *J. Pharmacogn. Phytochem.* **2017**, *6* (2), 205–214.
5. Srivastav, V. K.; Egbuna, C.; Tiwari, M., In *Phytochemicals as Lead Compounds for New Drug Discovery*, Elsevier Inc., 2019, pp 3–14.
6. Abegaz, B. M.; Kinfe, H. H., *Phys. Sci. Rev.* **2019**, *4* (6), 1–30.
7. Lahlou, M., *Pharmacol. & Pharm.* **2013**, *04* (03), 17–31.
8. Flannery, E. L.; Chatterjee, A. K.; Winzeler, E. A., *Nat. Rev. Microbiol.* **2013**, *11* (12), 849–862.
9. WHO, *World Malaria Report 2020. World Health Organization.*, 2020.
10. Tajuddeen, N.; Van Heerden, F. R., *Malar. J.* **2019**, *18* (1), 1–62.
11. Dos Santos Torres, Z. E.; Silveira, E. R.; Rocha E Silva, L. F.; Lima, E. S.; De Vasconcellos, M. C.; De Andrade Uchoa, D. E.; Filho, R. B.; Pohlit, A. M., *Molecules* **2013**, *18* (6), 6281–6297.
12. Nugroho, A. E.; Ono, Y.; Jin, E.; Hirasawa, Y.; Kaneda, T.; Rahman, A.; Kusumawati, I.; Tougan, T.; Horii, T.; Zaini, N. C.; Morita, H., *J. Nat. Med.* **2021**, *75*, 408–414.
13. Tang, Y.; Nugroho, A. E.; Hirasawa, Y.; Tougan, T.; Horii, T.; Hadi, A. H. A.; Morita, H., *J. Nat. Med.* **2019**, *73* (3), 533–540.
14. Chauhan, M.; Saxena, A.; Saha, B., *Eur. J. Med. Chem.* **2021**, *218*, 113400.
15. Widyawaruyanti, A.; Puspita Devi, A.; Fatria, N.; Tumewu, L.; Tantular, I. S.; Fuad Hafid, A., *Int. J. Pharm. Pharm. Sci.* **2014**, *6* (6), 125–128.
16. Gutiérrez-grijalva, E. P.; López-, L. X.; Contreras-angulo, L. A., In *Plant-derived Bioactives: Chemistry and Mode of Action*, 2020, pp 89–93.
17. Heinrich, M.; Barnes, J.; Garcia, J. P.; Gibbons, S.; Williamson, E., *Fundamentals of Pharmacognosy and Phytotheraphy*, 3rd ed., Elsevier, 2017.
18. Amirkia, V.; Heinrich, M., *Phytochem. Lett.* **2014**, *10*, xlviii–liii.
19. Debnath, B.; Singh, W. S.; Das, M.; Goswami, S.; Singh, M. K.; Maiti, D.; Manna, K., *Mater. Today Chem.* **2018**, *9*, 56–72.
20. Rosales, P. F.; Bordin, G. S.; Gower, A. E.; Moura, S., *Fitoterapia* **2020**, *143* (104558), 1–27.
21. Mohammed, A. E.; Abdul-Hameed, Z. H.; Alotaibi, M. O.; Bawakid, N. O.; Sobahi, T. R.; Abdel-Lateff, A.; Alarif, W. M., *Molecules* **2021**, *26* (2), 1–67.
22. Le Men, J.; Taylor, W. I., *Experientia* **1965**, *21* (9), 508–510.
23. Kisakurek, M. V; Leeuwenberg, A.; Hesse, M., In *Alkaloids: Chemical and Biological Perspectives*, 1983, pp 211–376.
24. Danieli, B.; Palmisano, G., *Alkaloids Chem. Pharmacol.* **1986**, *27* (C), 1–130.
25. Sachdeva, H.; Mathur, J.; Guleria, A., *J. Chil. Chem. Soc.* **2020**, *3* (3), 4900–4907.
26. Hamid, H. A.; Ramli, A. N. M.; Yusoff, M. M., *Front. Pharmacol.* **2017**, *8* (FEB).
27. Sachdeva, H.; Mathur, J.; Guleria, A., *J. Chil. Chem. Soc.* **2020**, *65* (3), 4900–4907.
28. Marinho, F. F.; Simões, A. O.; Barcellos, T.; Moura, S., *Fitoterapia* **2016**, *114*, 127–137.
29. Barbosa-Filho, J. M.; Piuvezam, M. R.; Moura, M. D.; Silva, M. S.; Karla Lima, V. B.; Leitão da-Cunha, E. V.; Fechine, I. M.; Takemura, O. S., *Brazilian J. Pharmacogn.* **2006**, *16* (1), 109–139.

30. Uzor, P. F., *Evidence-Based Complement. Altern. Med.* **2020**, *2020*, 8749083.
31. Nugroho, A. E.; Hirasawa, Y.; Piow, W. C.; Kaneda, T.; Hadi, A. H. A.; Shirota, O.; Ekasari, W.; Widyawaruyanti, A.; Morita, H., *J. Nat. Med.* **2012**, *66* (2), 350–353.
32. Surur, A. S.; Huluka, S. A.; Mitku, M. L.; Asres, K., *Drug Des. Devel. Ther.* **2020**, *14*, 4855–4867.
33. Dey, A.; Mukherjee, A.; Chaudhury, M., *Alkaloids From Apocynaceae: Origin, Pharmacotherapeutic Properties, and Structure-Activity Studies*, 2017, Vol. 52.
34. Ramanitrahasimbola, D.; Rasoanaivo, P.; Ratsimamanga-Urverg, S.; Federici, E.; Palazzino, G.; Galeffi, C.; Nicoletti, M., *Phyther. Res.* **2001**, *15* (1), 30–33.
35. Lichman, B. R., *Nat. Prod. Rep.* **2021**, *38* (1), 103–129.
36. Wenkert, E., *J. Am. Chem. Soc.* **1962**, *84* (1), 98–102.
37. Wong, S. K.; Lim, Y. Y.; Eric WC Chan, *Pharmacogn. Commun.* **2013**, *3* (3), 2–11.
38. Van Beek, T. A. A.; Verpoorte, R.; Svendsen, A. B. B.; Leeuwenberg, A. J. M. J. M.; Bisset, N. G. G., *J. Ethnopharmacol.* **1984**, *10* (1), 1–156.
39. Athipornchai, A., *Asian J. Pharm. Clin. Res.* **2018**, *11* (5), 45–53.
40. Kam, T. S.; Sim, K. M., *Helv. Chim. Acta* **2002**, *85* (4), 1027–1032.
41. Zaima, K.; Hirata, T.; Hosoya, T.; Hirasawa, Y.; Koyama, K.; Rahman, A.; Kusumawati, I.; Zaini, N. C.; Shiro, M.; Morita, H., *J. Nat. Prod.* **2009**, *72* (9), 1686–1690.
42. Pratiwi, D. R.; Bintang, M.; Simanjuntak, P., *J. Ilmu Kefarmasian Indonesia* **2014**, *12*, 267–272.
43. Husain, K.; Said, I. M.; Din, L. B.; Takayama, H.; Kitajima, M.; Aimi, N., *Nat. Prod. Sci.* **1997**, *3* (1), 42–48.
44. Gonçalves, M. S.; Curcino Vieira, I. J.; Oliveira, R. R.; Braz-Filho, R., *Molecules* **2011**, *16* (9), 7480–7487.
45. Braga, R. M.; Reis, F. D. A. M., *Phytochemistry* **1987**, *26* (3), 833–836.
46. Parkanyi, C.; Bouin, D.; Aaron, J.-J.; Villiers, C., *Croat. Chem. Acta* **1983**, *56* (2), 157–168.
47. Kutney, J. P., *Lloydia* **1977**, *40* (1), 107–126.
48. Nugroho, A. E.; Hirasawa, Y.; Kawahara, N.; Goda, Y.; Awang, K.; Hadi, A. H. A.; Morita, H., *J. Nat. Prod.* **2009**, *72* (8), 1502–1506.
49. Nugroho, A. E.; Morita, H., *J. Nat. Med.* **2014**, *68* (1), 1–10.
50. Namjoshi, O. A.; Cook, J. M., *Alkaloids Chem. Biol.* **2016**, *76*, 63–169.
51. Santoro, E.; Vergura, S.; Scafato, P.; Belviso, S.; Masi, M.; Evidente, A.; Superchi, S., *J. Nat. Prod.* **2020**, *83* (4), 1061–1068.
52. Krastel, P.; Petersen, F.; Roggo, S.; Schmitt, E.; Schuffenhauer, A., *Chirality Drug Res.* **2006**, *33*, 67–94.
53. Singh, J.; Hagen, T. J., *Burger's Med. Chem. Drug Discov.* **2010**.
54. Maher, T. J.; Johnson, D. A., *Drug Dev. Res.* **1991**, *24* (2), 149–156.
55. Tokunaga, E.; Yamamoto, T.; Ito, E.; Shibata, N., *Sci. Rep.* **2018**, *8* (17131), 1–7.
56. Saito, F.; Schreiner, P. R., *European J. Org. Chem.* **2020**, *2020* (40), 6328–6339.
57. TURBOMOLE V7.1, **2009**.
58. Trager, W.; Jensen, J., *Human Malaria Parasites in Continuous Culture*, 1976, Vol. 193.
59. Lambros, C.; Vanderberg, J. P., *J. Parasitol.* **1979**, *65* (3), 418–420.
60. Tougan, T.; Suzuki, Y.; Itagaki, S.; Izuka, M.; Toya, Y.; Uchihashi, K.; Horii, T., *Malar. J.* **2018**, *17* (1), 59.
61. Toya, Y.; Tougan, T.; Horii, T.; Uchihashi, K., *Parasitol. Int.* **2021**, *80* (102206), 1–6.
62. Tougan, T.; Toya, Y.; Uchihashi, K.; Horii, T., *Malar. J.* **2019**, *18* (1), 8.

Appendix

Appendix 1. ^{1}H NMR spectrum recorded for **1** (CD_3OD, 400 MHz)

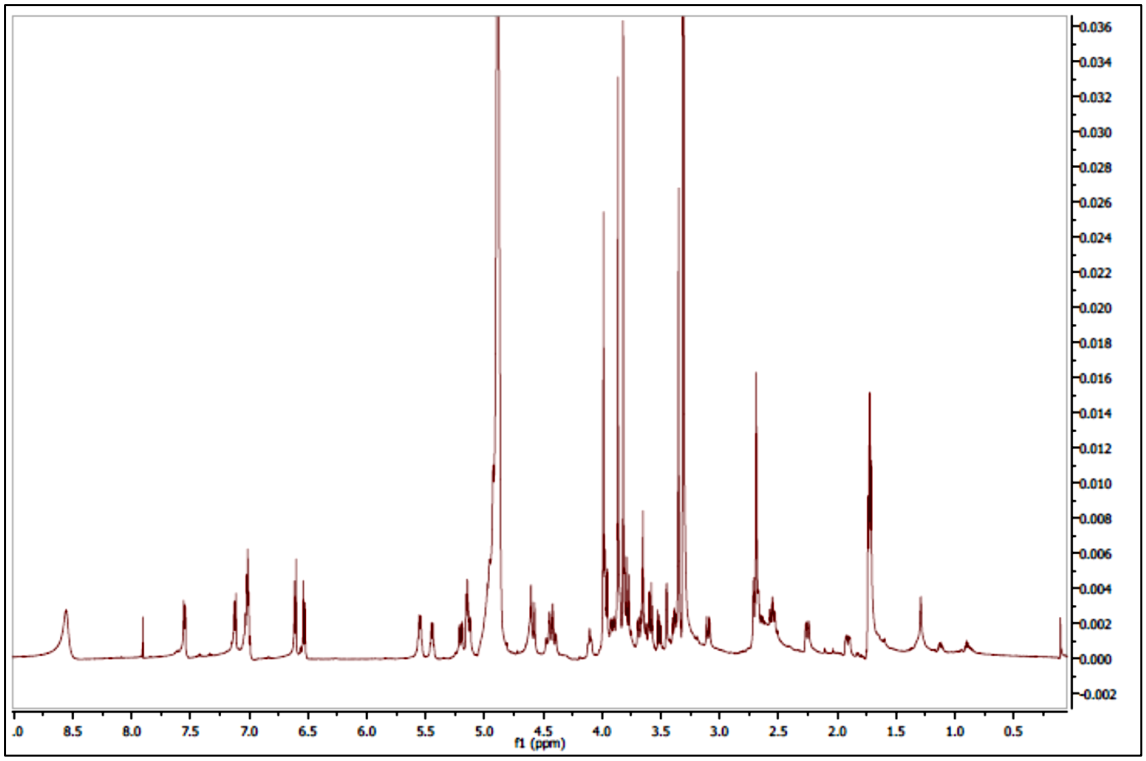

Appendix 2. ^{13}C NMR recorded for **1** (CD_3OD, 150 MHz)

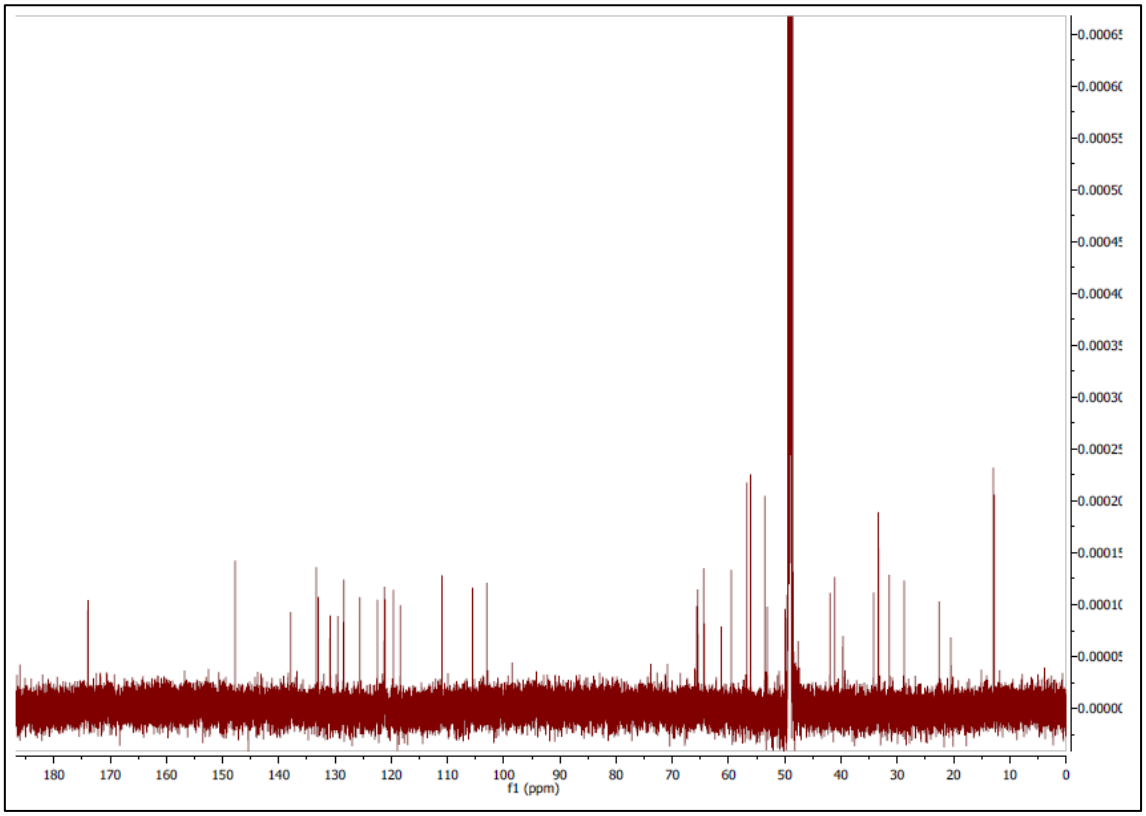

Appendix 3. ^{1}H-^{1}H COSY spectrum recorded for **1** (CD_3OD, 400 MHz)

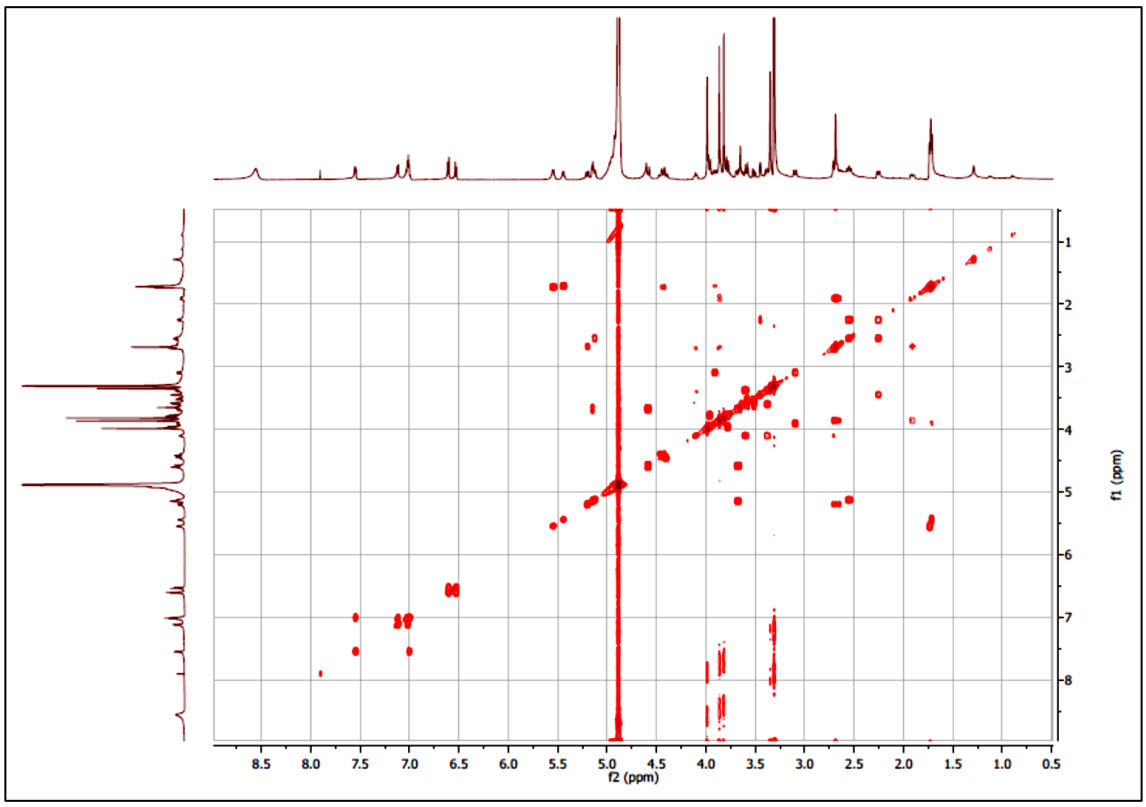

Appendix 4. HSQC spectrum recorded for **1** (CD_3OD, 400 MHz)

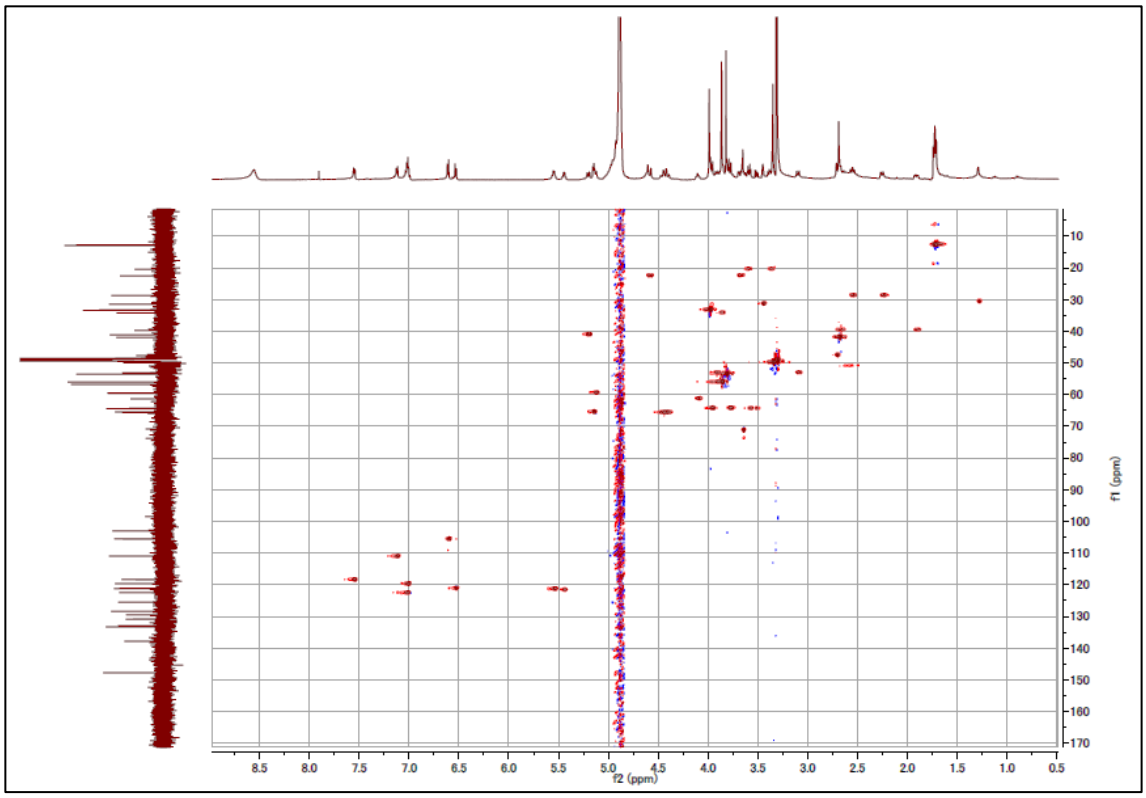

Appendix 5. HMBC spectrum recorded for **1** (CD_3OD, 400 MHz)

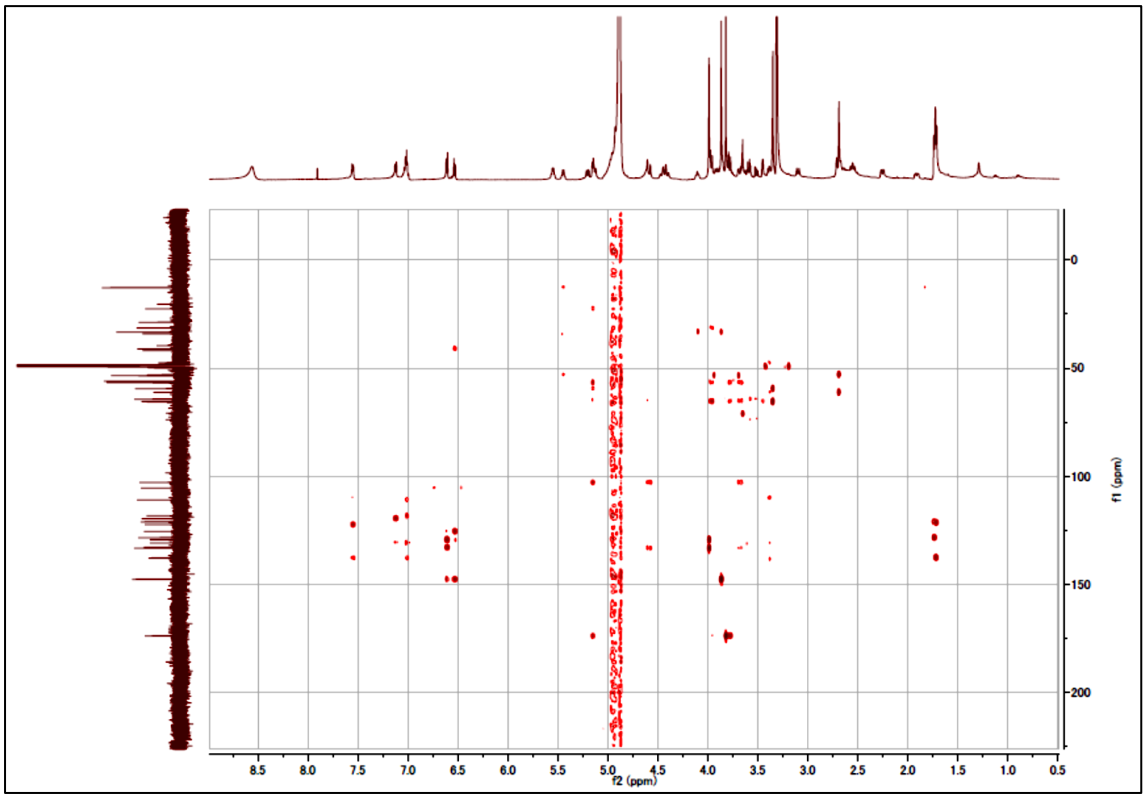

Appendix 6. NOESY spectrum recorded for **1** (CD_3OD, 400 MHz)

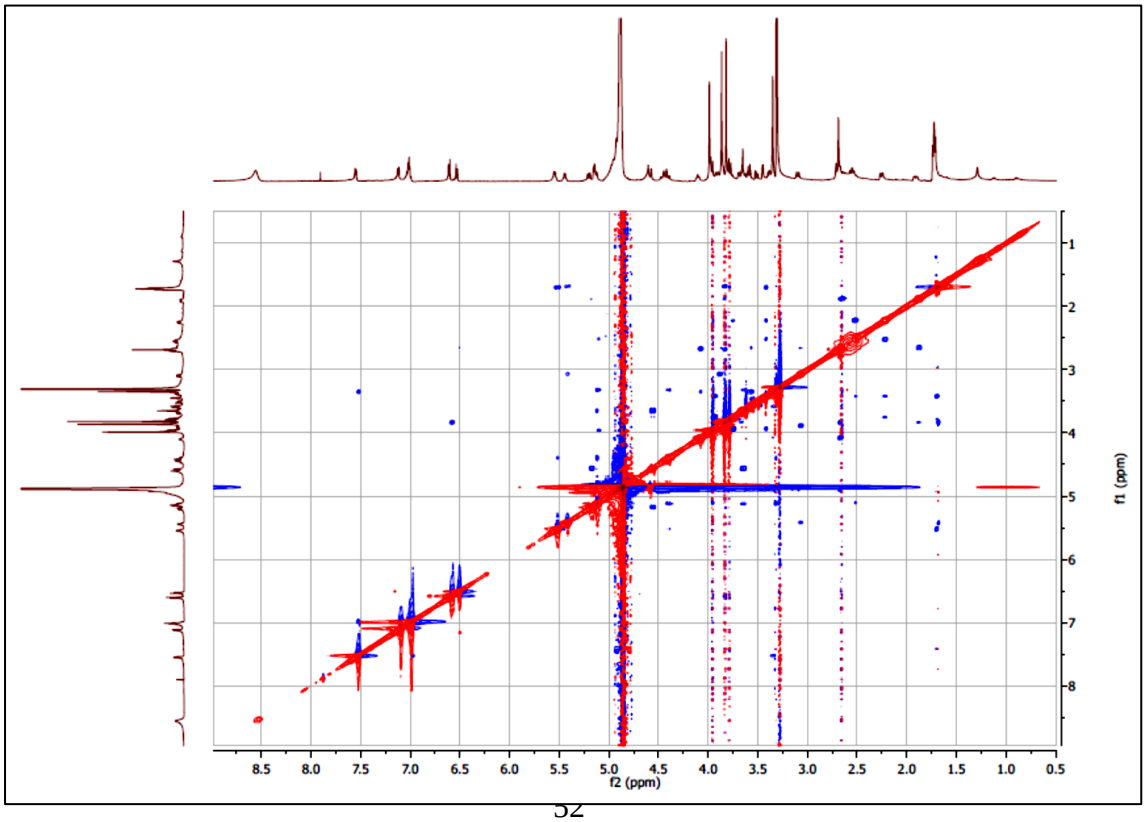

Appendix 7. ^{1}H NMR spectrum recorded for **2** (CD_3OD, 600 MHz)

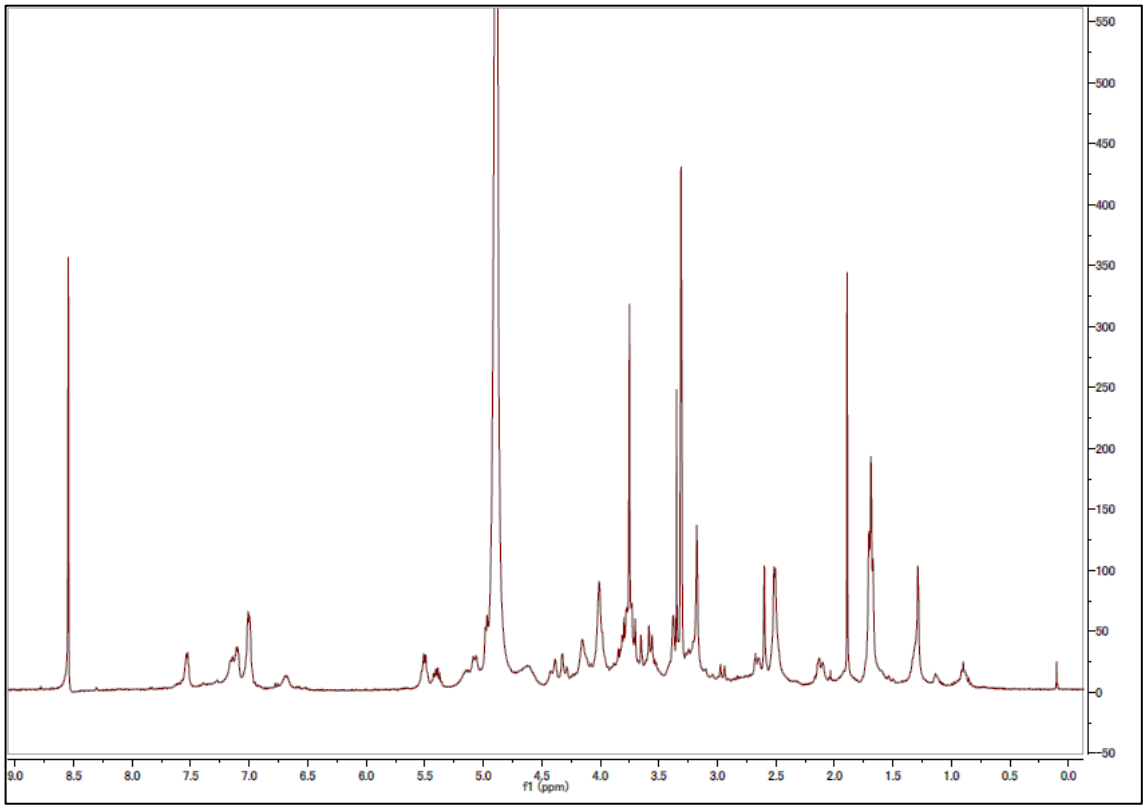

Appendix 8. ^{13}C NMR spectrum recorded for **2** (CD_3OD, 150 MHz)

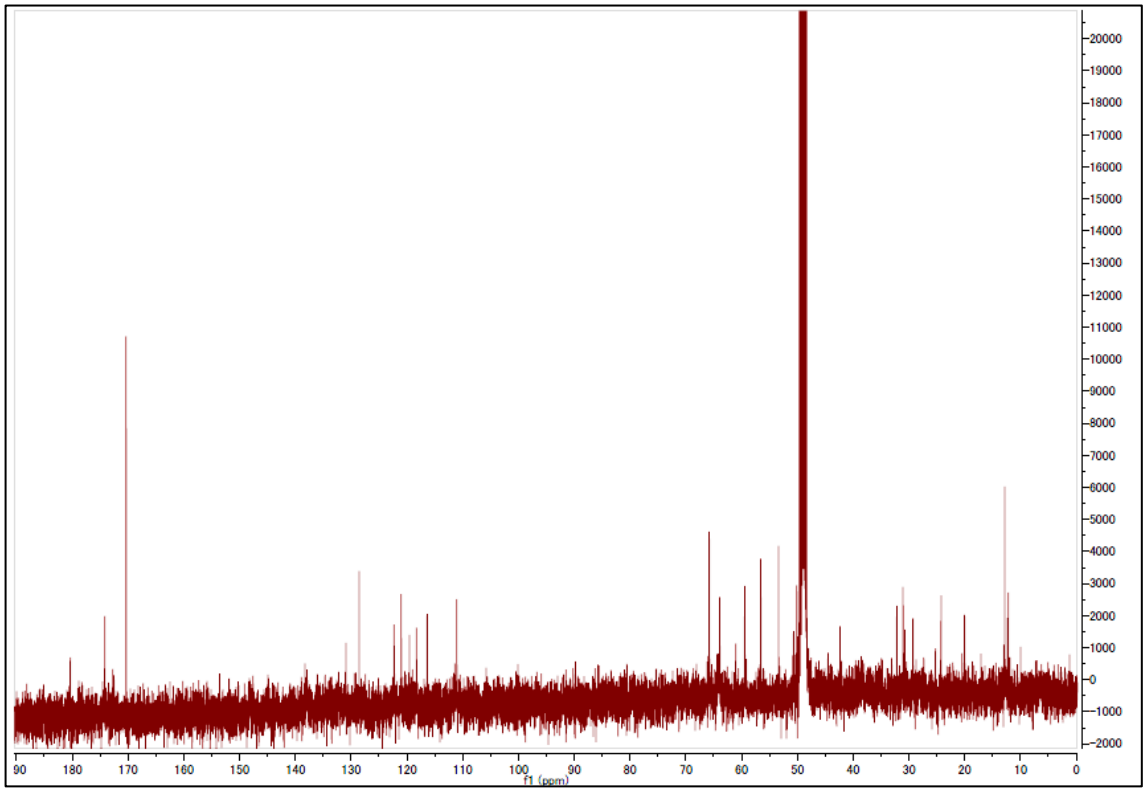

Appendix 9. ^{1}H-^{1}H COSY spectrum recorded for **2** (CD_3OD, 600 MHz)

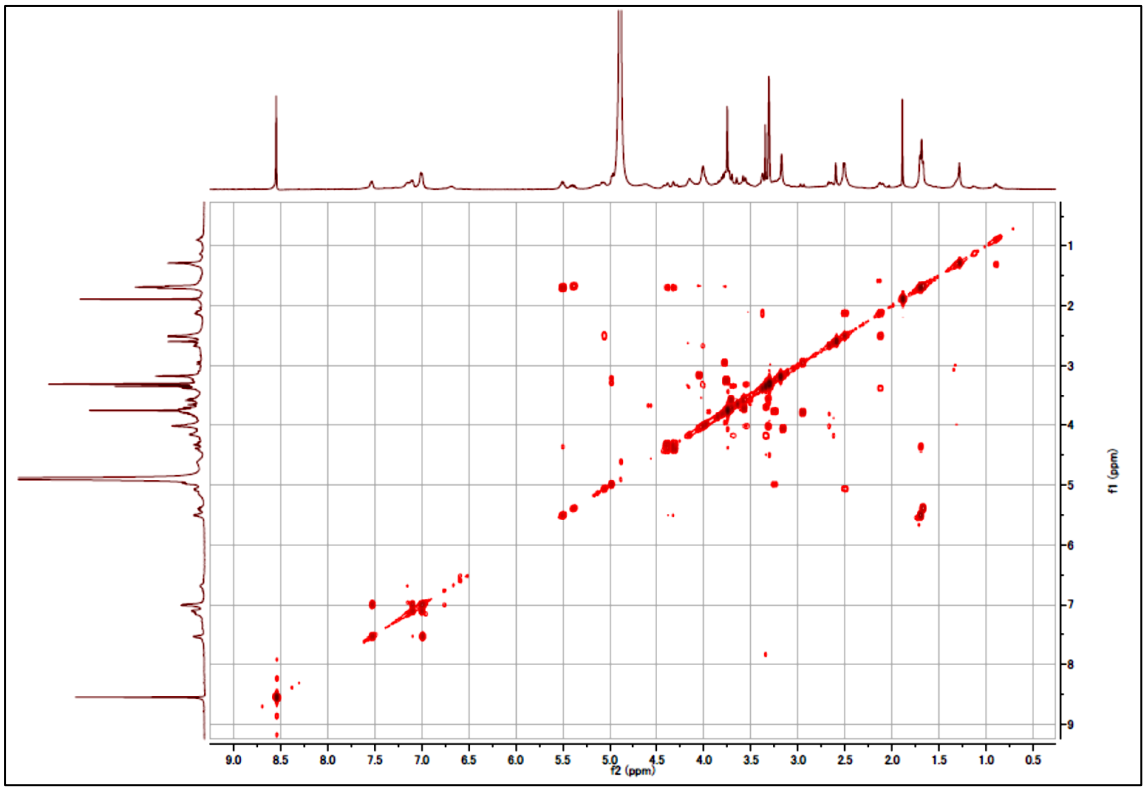

Appendix 10. HSCQ spectrum recorded for **2** (CD_3OD, 600 MHz)

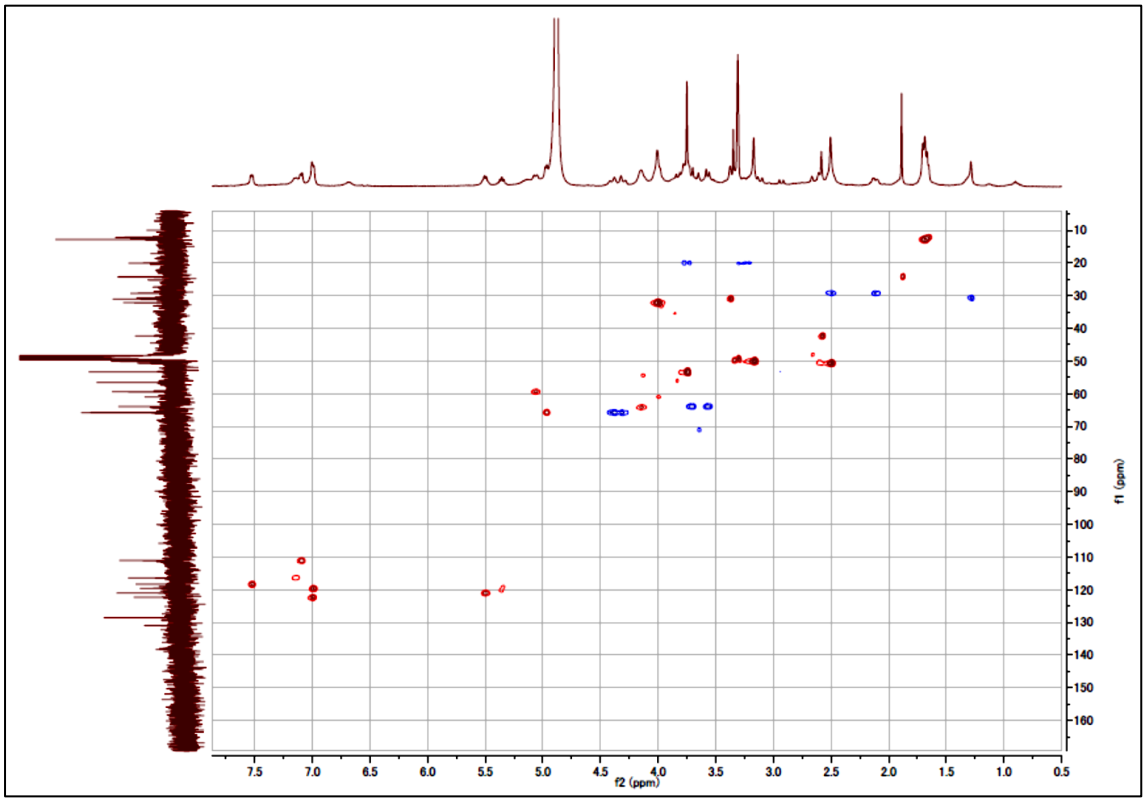

Appendix 11. HMBC spectrum recorded for **2** (CD_3OD, 600 MHz)

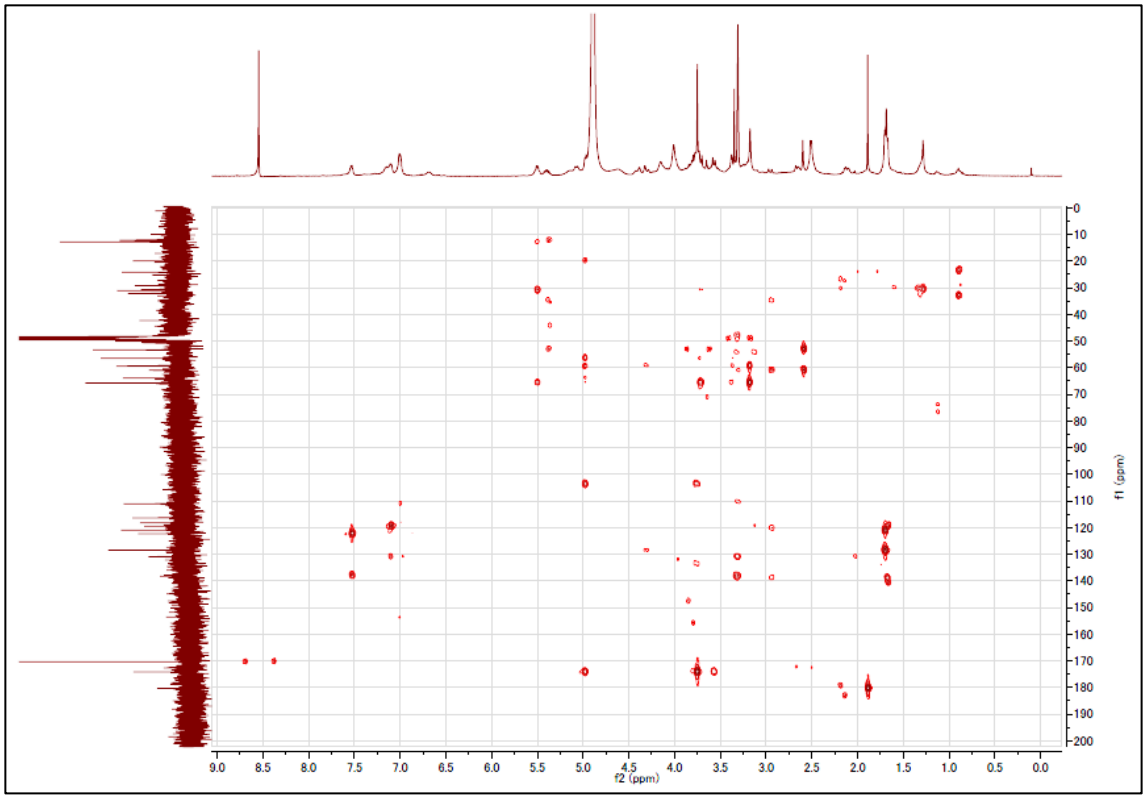

Appendix 12. NOESY spectrum recorded for **2** (CD_3OD, 600 MHz)

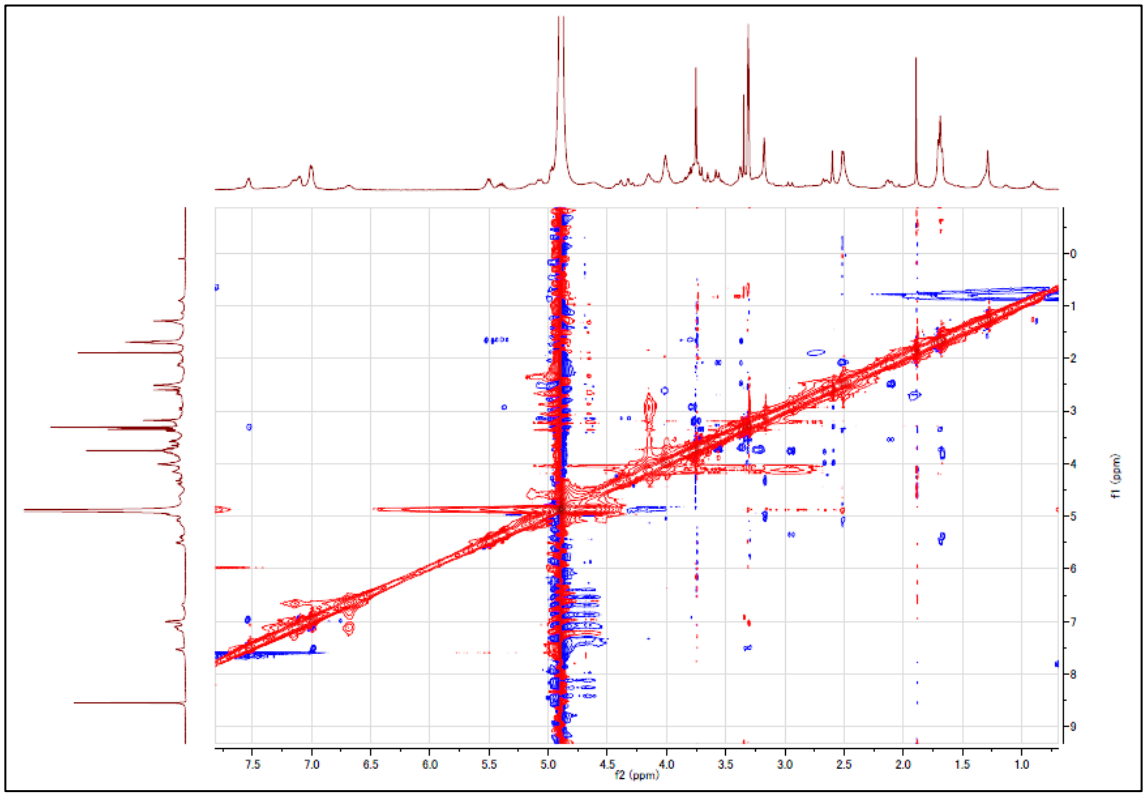

Appendix 13. ^{1}H NMR spectrum recorded for **9** (CD_3OD, 600 MHz)

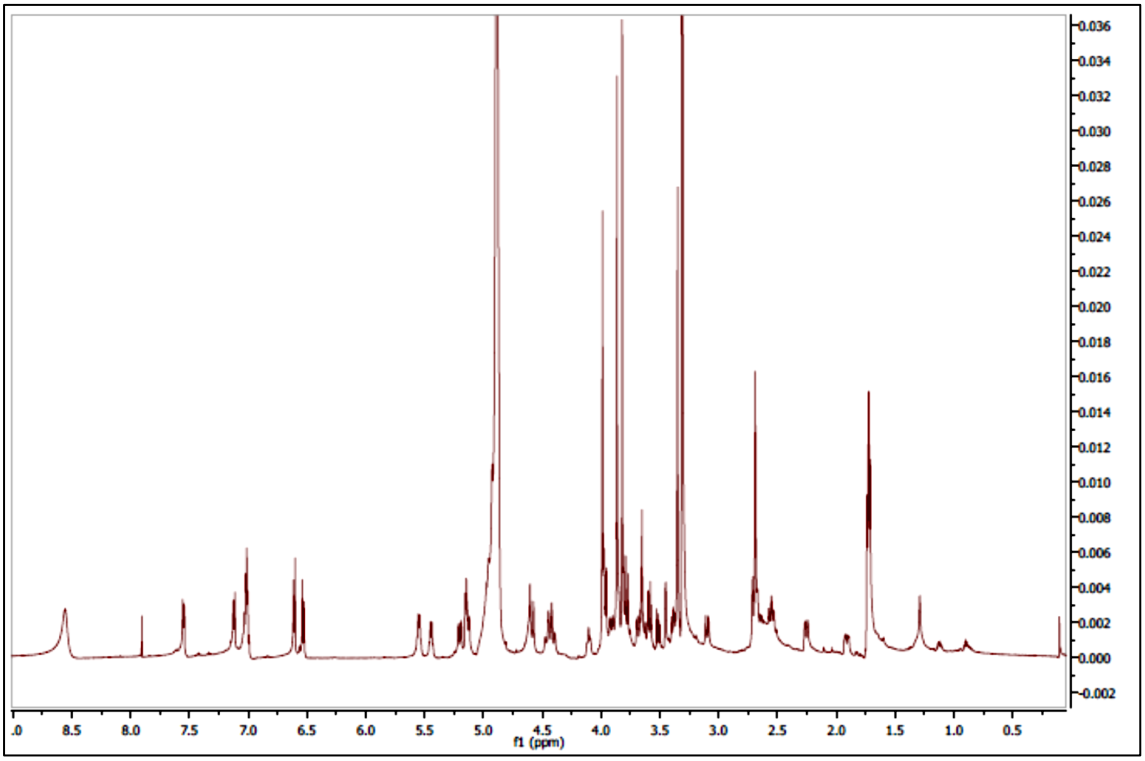

Appendix 14. ^{13}C NMR spectrum recorded for **9** (CD_3OD, 150 MHz)

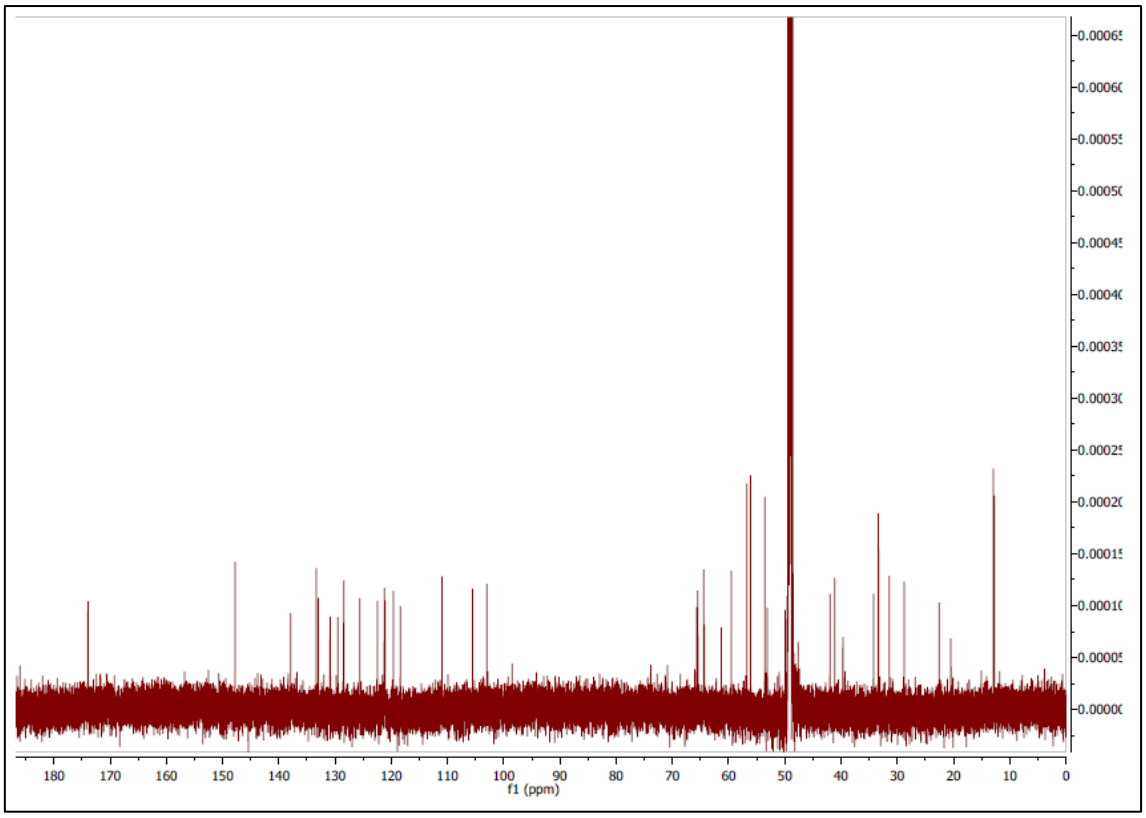

Appendix 15. ^{1}H-^{1}H COSY spectrum recorded for **9** (CD_3OD, 600 MHz)

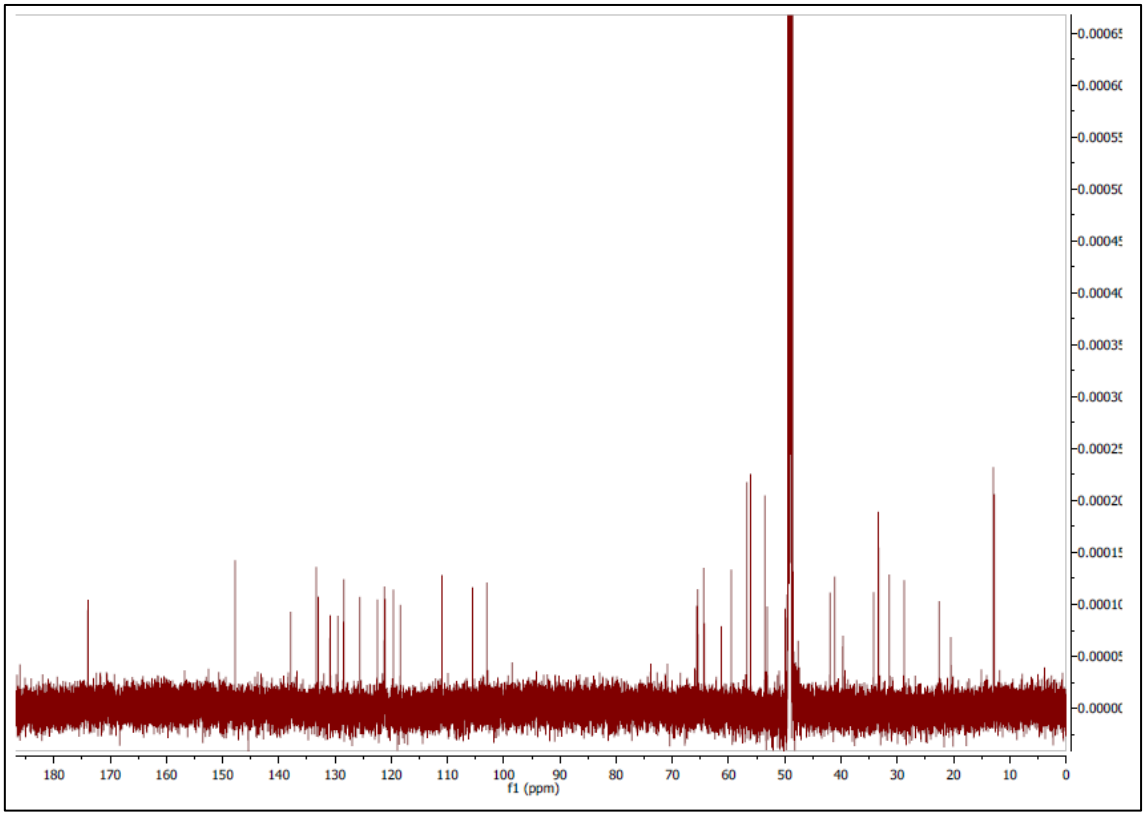

Appendix 16. HSQC spectrum recorded for **9** (CD_3OD, 600 MHz)

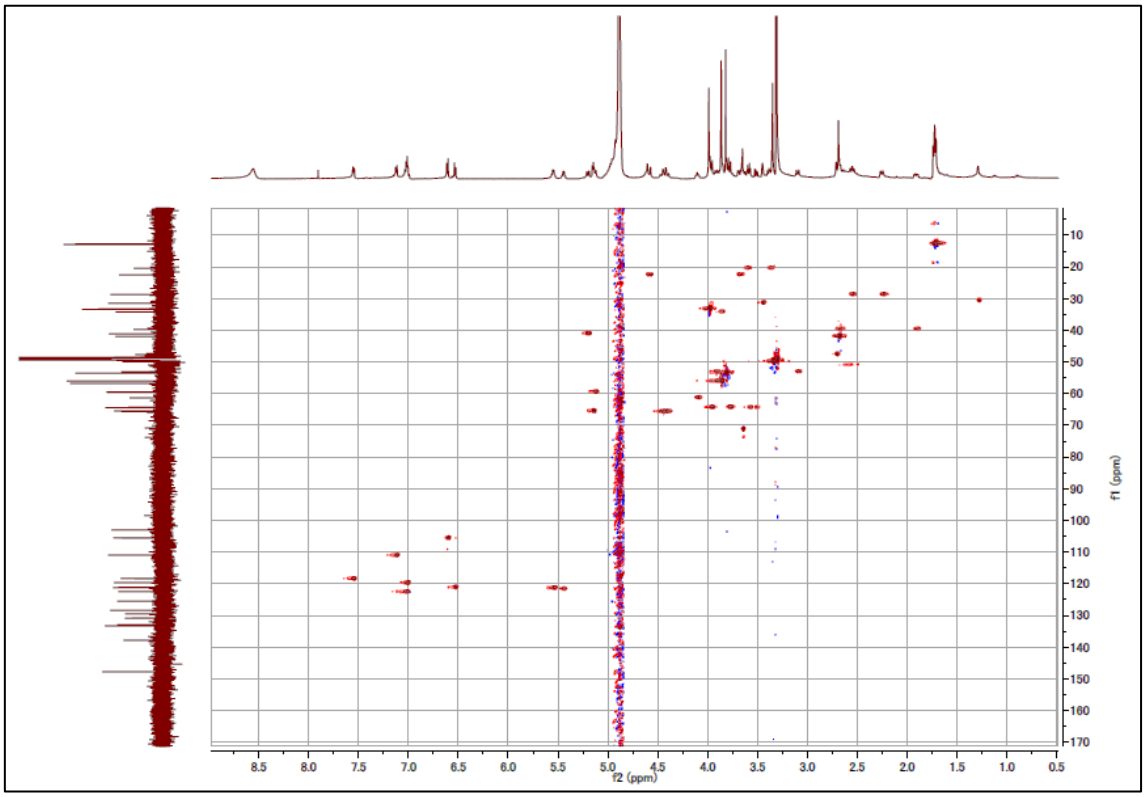

Appendix 17. HMBC spectrum recorded for **9** (CD_3OD, 600 MHz)

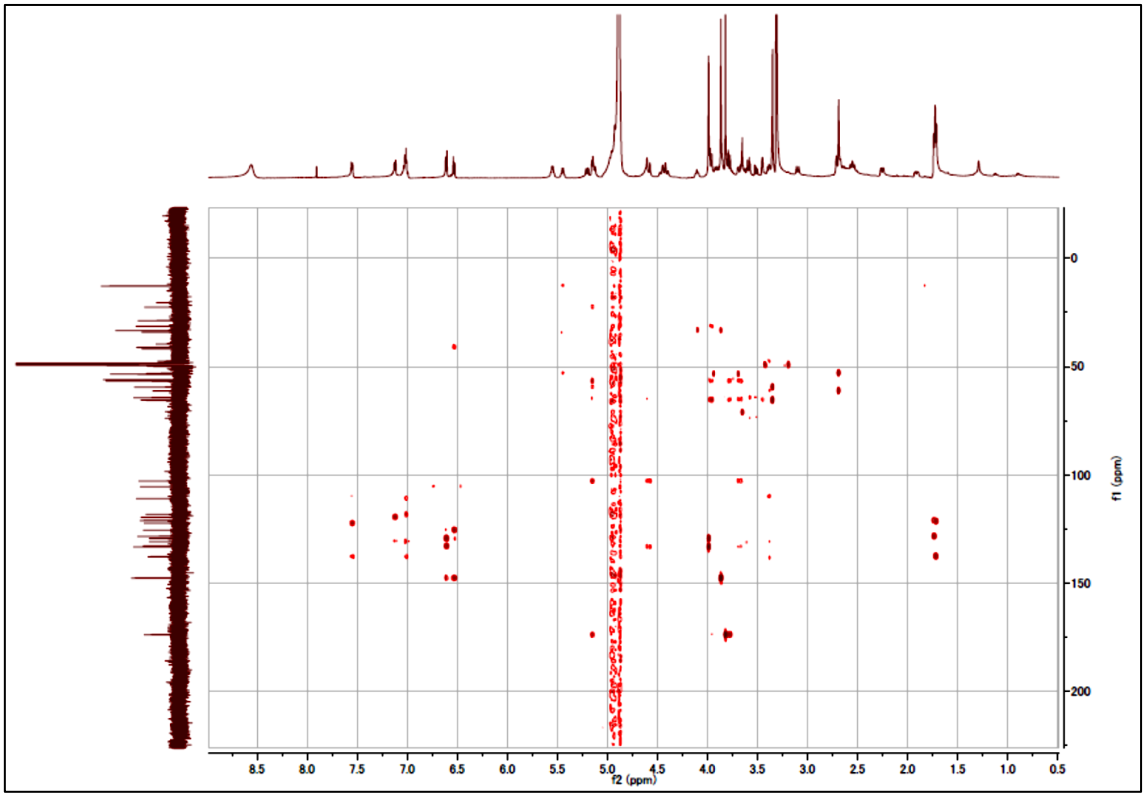

Appendix 18. ROESY spectrum recorded for **9** (CD_3OD, 600 MHz)

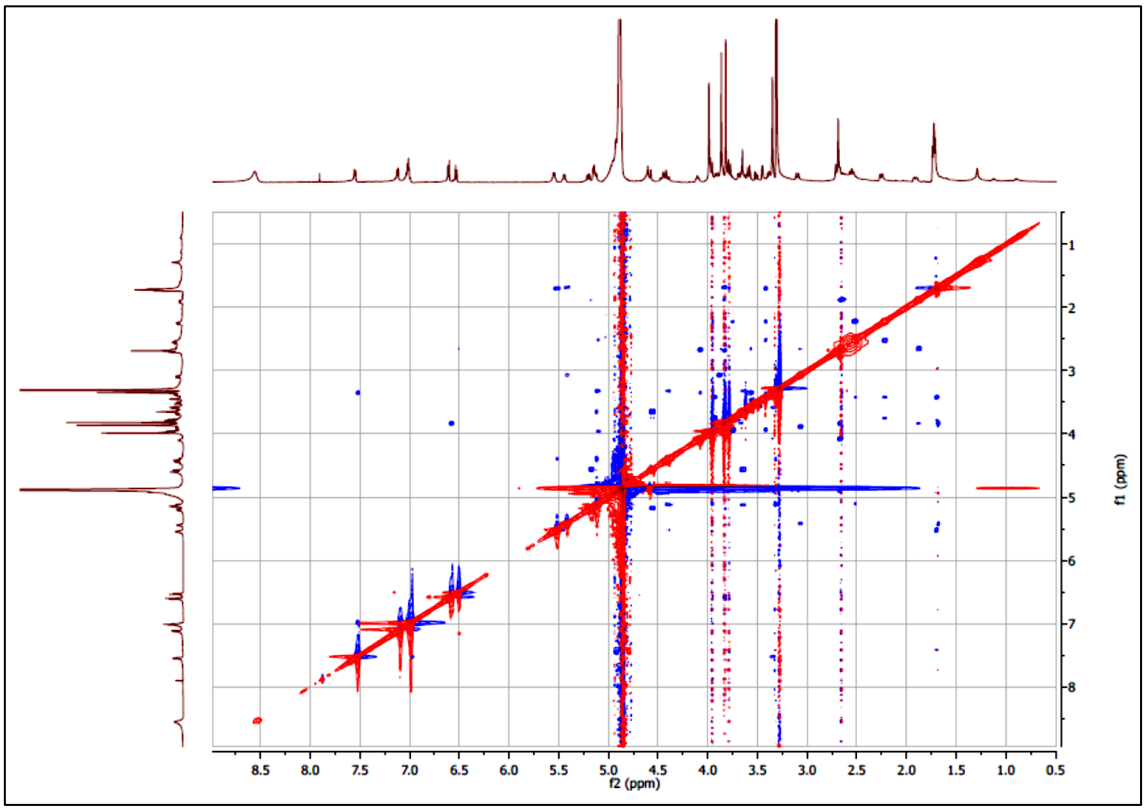

Appendix 19. ^{1}H NMR spectrum recorded for **10** (CD_3OD, 600 MHz)

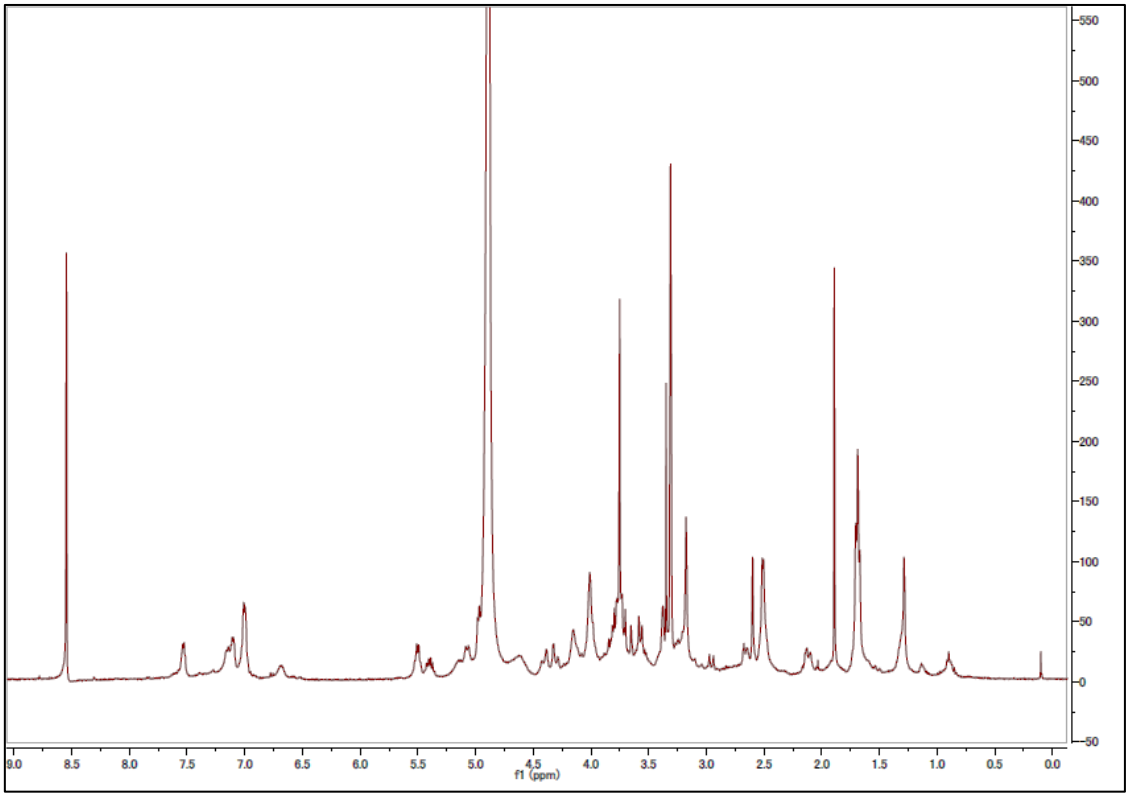

Appendix 20. ^{13}C NMR spectrum recorded for **10** (CD_3OD, 150 MHz)

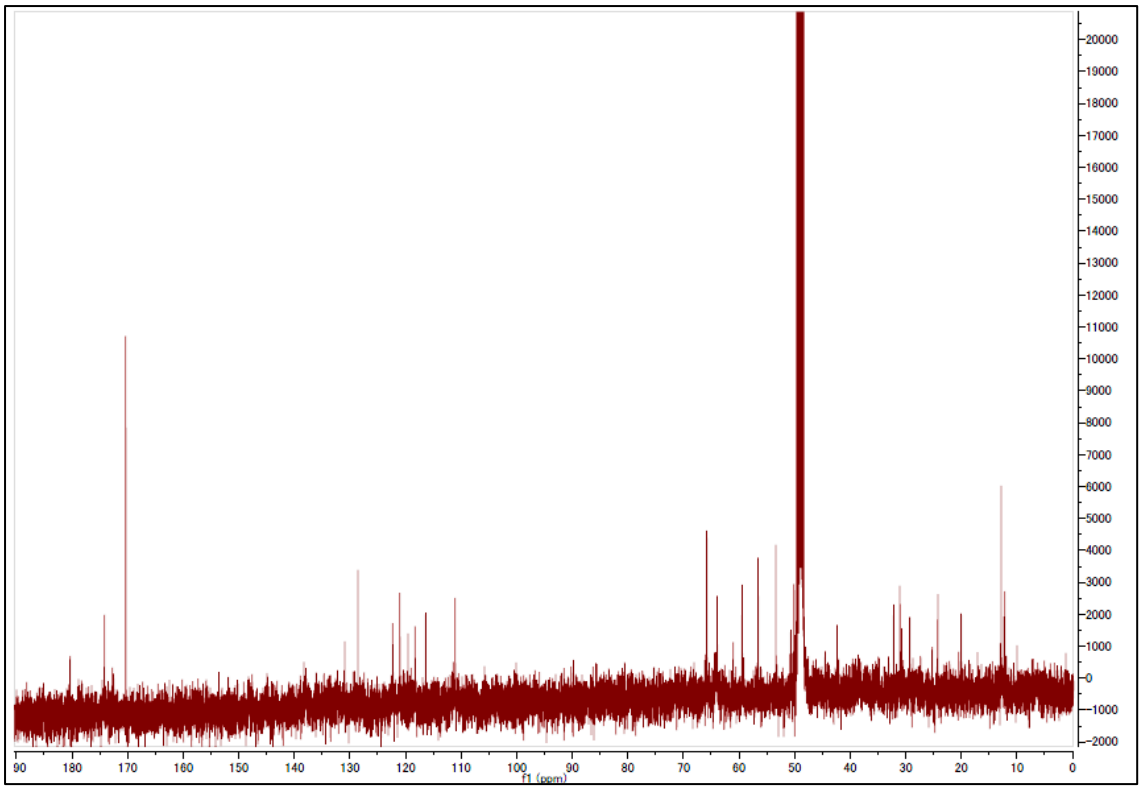

Appendix 21. ^{1}H-^{1}H COSY spectrum recorded for **10** (CD_3OD, 600 MHz)

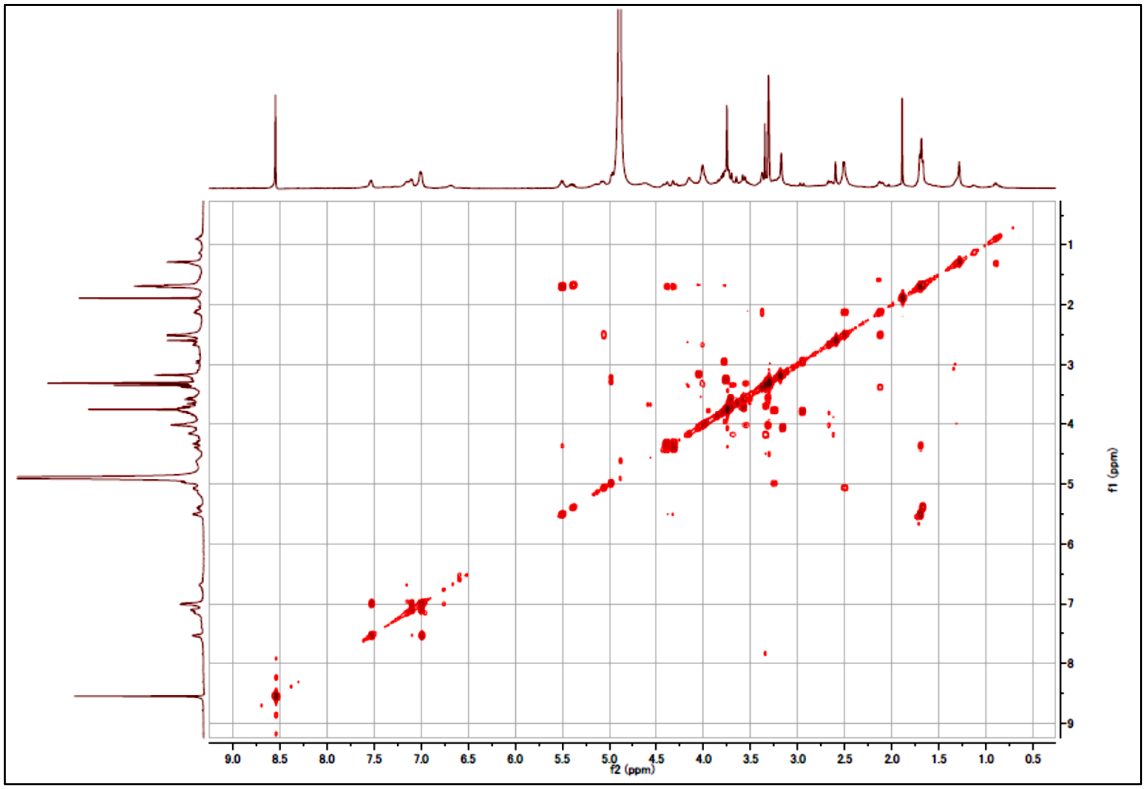

Appendix 22. HSCQ spectrum recorded for **10** (CD_3OD, 600 MHz)

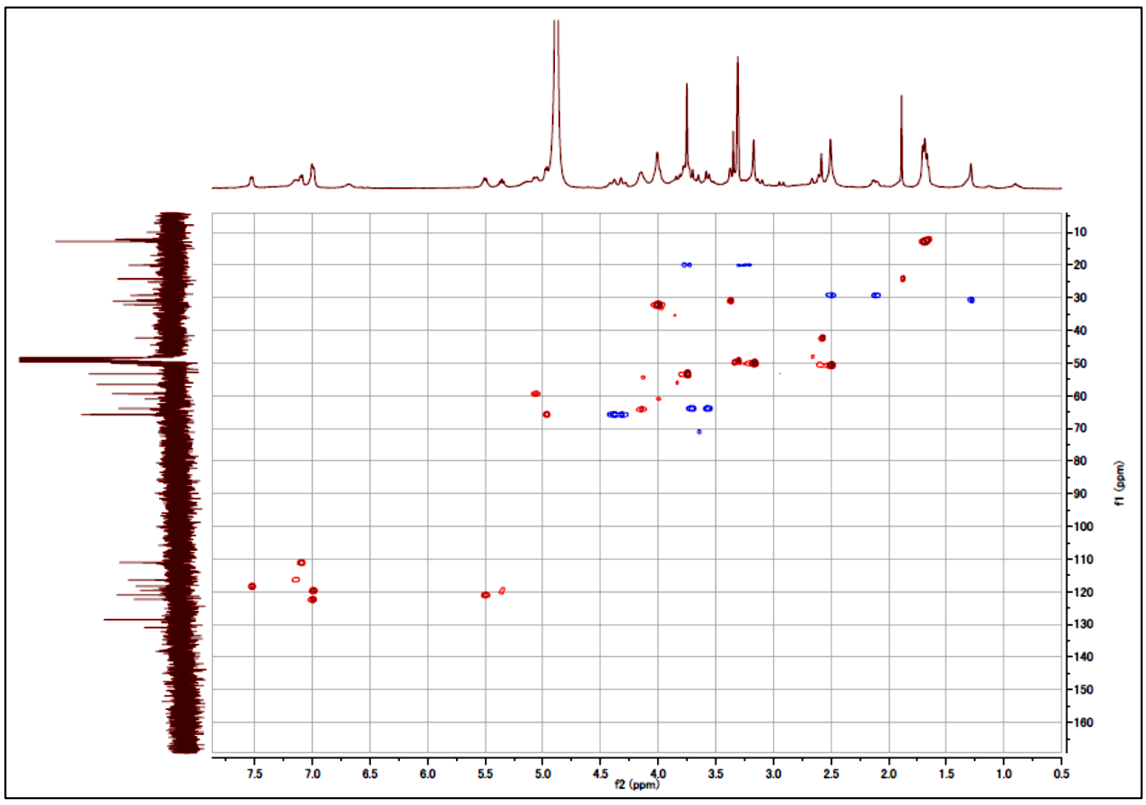

Appendix 23. HMBC spectrum recorded for **10** (CD_3OD, 600 MHz)

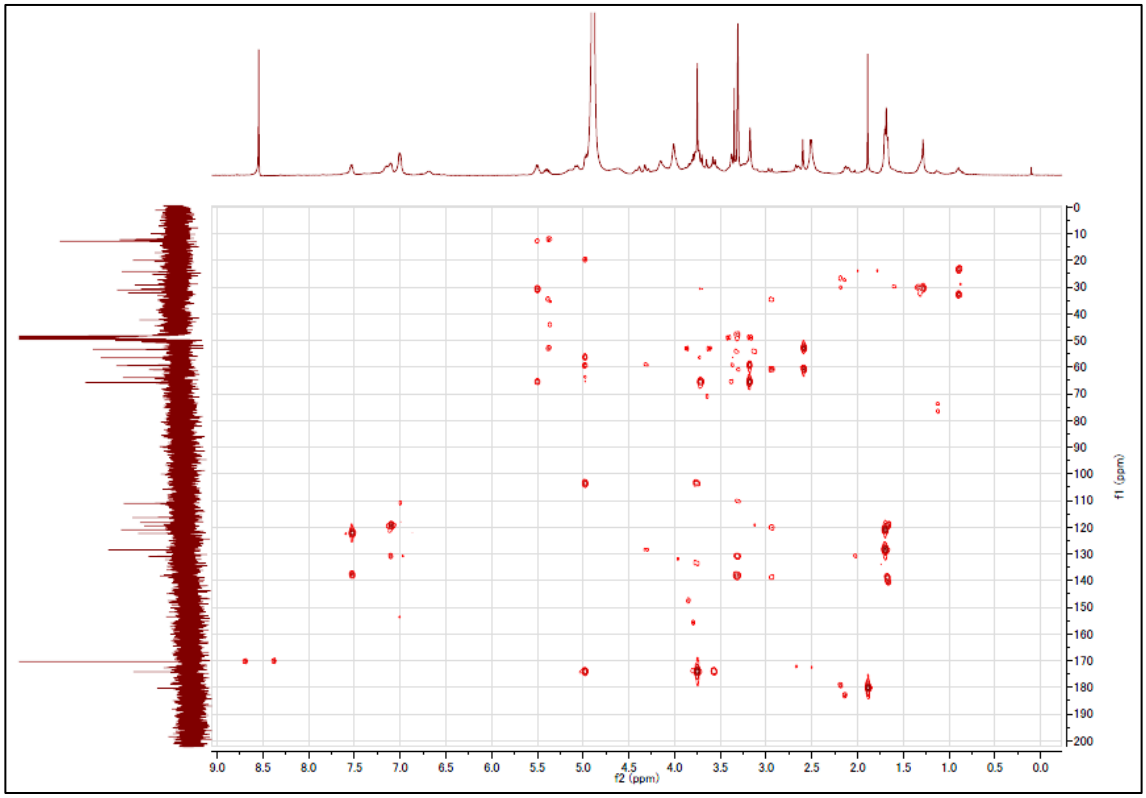

Appendix 24. ROESY spectrum recorded for **10** (CD_3OD, 600 MHz)

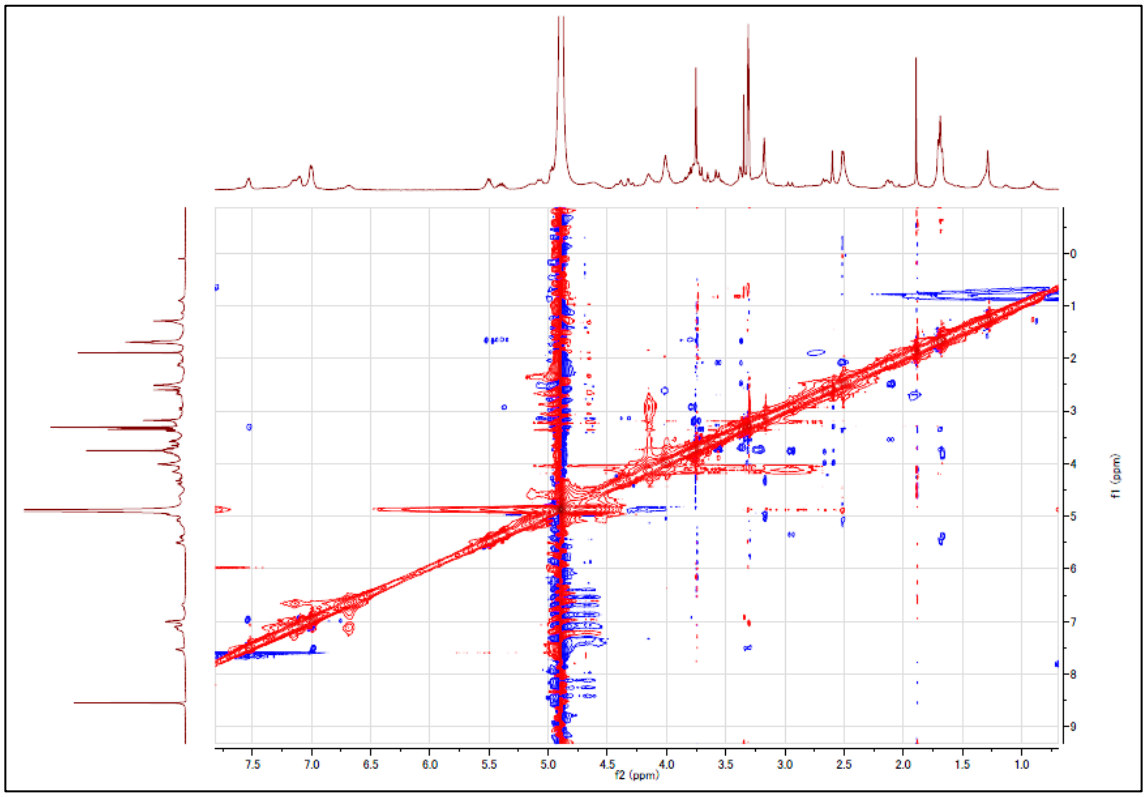

Appendix 25. ^{1}H NMR Spectrum of Methyl Esterification Product of **9**